

### 3. SITE 881<sup>1</sup>

#### Shipboard Scientific Party<sup>2</sup>

#### HOLE 881A

**Date occupied:** 29 July 1992  
**Date departed:** 29 July 1992  
**Time on hole:** 14 hr, 0 min  
**Position:** 47°6.136'N, 161°29.492'E  
**Bottom felt (rig floor; m, drill-pipe measurement):** 5542.0  
**Distance between rig floor and sea level (m):** 10.93  
**Water depth (drill-pipe measurement from sea level, m):** 5531.1  
**Total depth (rig floor; m):** 5555.5  
**Penetration (m):** 13.5  
**Number of cores (including cores with no recovery):** 1  
**Total length of cored section (m):** 9.5  
**Total core recovered (m):** 9.92  
**Core recovery (%):** 104.0  
**Oldest sediment cored:**  
Depth (mbsf): 9.5  
Nature: diatomaceous ooze  
Age: Quaternary  
**Comments:** Overshot mud line.

#### HOLE 881B

**Date occupied:** 29 July 1992  
**Date departed:** 30 July 1992  
**Time on hole:** 21 hr, 45 min  
**Position:** 47°6.136'N, 161°29.492'E  
**Bottom felt (rig floor; m, drill-pipe measurement):** 5541.7  
**Distance between rig floor and sea level (m):** 10.93  
**Water depth (drill-pipe measurement from sea level, m):** 5530.8  
**Total depth (rig floor; m):** 5708.7  
**Penetration (m):** 167.0  
**Number of cores (including cores with no recovery):** 18  
**Total length of cored section (m):** 167.0  
**Total core recovered (m):** 170.33  
**Core recovery (%):** 102.0  
**Oldest sediment cored:**  
Depth (mbsf): 167.0  
Nature: clayey diatom ooze/siliceous silty clays  
Age: late Pliocene  
Measured velocity(km/s): 1.468

#### HOLE 881C

**Date occupied:** 30 July 1992  
**Date departed:** 3 August 1992  
**Time on hole:** 3 days, 11 hr, 30 min  
**Position:** 47°6.133'N, 161°29.490'E  
**Bottom felt (rig floor; m, drill-pipe measurement):** 5541.7  
**Distance between rig floor and sea level (m):** 10.93  
**Water depth (drill-pipe measurement from sea level, m):** 5530.8  
**Total depth (rig floor; m):** 5905.5  
**Penetration (m):** 363.8  
**Number of cores (including cores with no recovery):** 39  
**Total length of cored section (m):** 363.8  
**Total core recovered (m):** 227.2  
**Core recovery (%):** 62.5  
**Oldest sediment cored:**  
Depth (mbsf): 334.8  
Nature: diatomaceous ooze  
Age: late Miocene  
Measured velocity(km/s): 1.478

#### HOLE 881D

**Date occupied:** 3 August 1992  
**Date departed:** 4 August 1992  
**Time on hole:** 1 day, 3 hr, 15 min  
**Position:** 47°6.136'N, 161°29.522'E  
**Bottom felt (rig floor; m, drill-pipe measurement):** 5542.0  
**Distance between rig floor and sea level (m):** 10.93  
**Water depth (drill-pipe measurement from sea level, m):** 5531.1  
**Total depth (rig floor; m):** 5754.0  
**Penetration (m):** 212.0  
**Number of cores (including cores with no recovery):** 6  
**Total length of cored section (m):** 57.0  
**Total core recovered (m):** 57.91  
**Core recovery (%):** 101.6  
**Oldest sediment cored:**  
Depth (mbsf): 212.2  
Nature: clayey diatom ooze  
Age: Pliocene  
Measured velocity(km/s): 1.454  
**Comments:** Washed from 0 to 155.5 mbsf.

**Principal results:** The *JOIDES Resolution* arrived at the beginning of the pre-site survey for proposed Site NW-1A (Fig. 1) on the evening of 28 July 1992, slowed to retrieve the magnetometer, and streamed out the seismic reflection profiling gear, then turned north-northeast onto the track line of

<sup>1</sup> Rea, D.K., Basov, I.A., Janecek, T.R., Palmer-Julson, A., et al., *Proc. ODP, Init. Repts.*, 145: College Station, TX (Ocean Drilling Program).

<sup>2</sup> Shipboard Scientific Party is as given in list of participants preceding the contents.

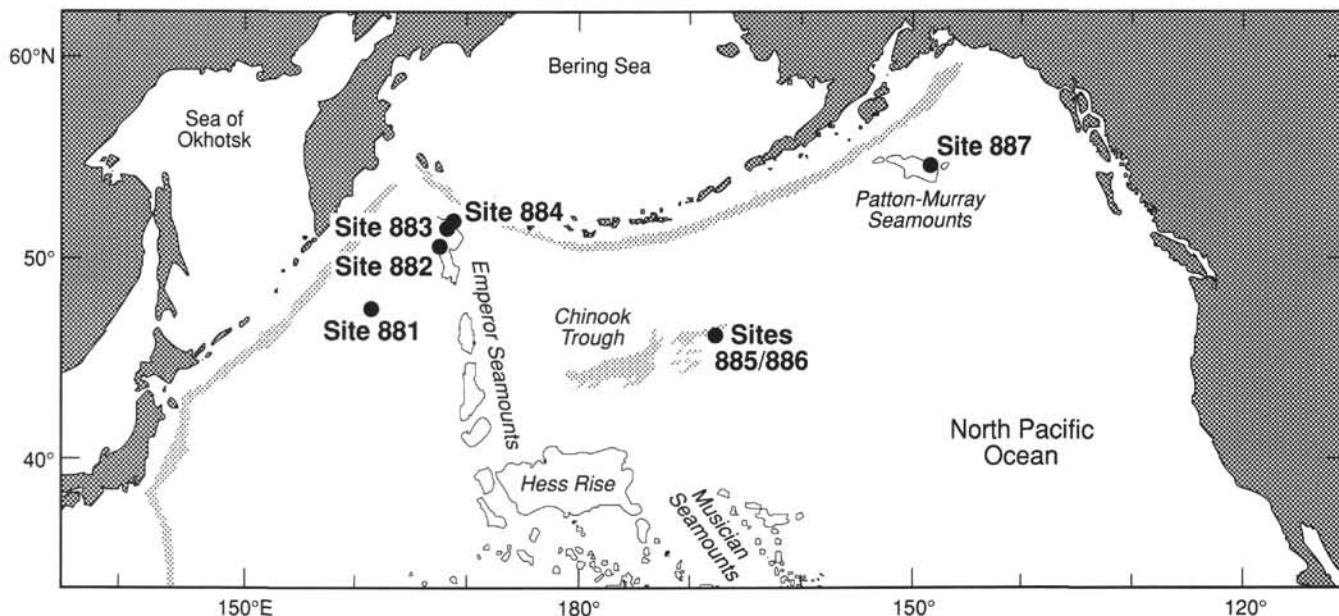


Figure 1. Index map of the North Pacific Ocean showing Leg 145 drill sites.

*Vema-21*, along which the site had been chosen. A beacon was dropped on the first pass over the site; during the survey, we continued about 6 nmi past the anticipated drilling location and eventually turned southwest to complete an orthogonal cross line.

The first APC core of Hole 881A missed the mud line by 4 m, so the drill pipe was raised, and Hole 881B was spudded with a successful mud-line core. Eighteen APC cores from Hole 881B were taken (0–167.0 mbsf), and then the ship's drilling crew pulled up the drill pipe, offset, and spudded Hole 881C. Piston-coring in Hole 881C (Cores 145-881C-1H to -17H, 0–155.8 mbsf) went well, but the ensuing XCB-coring resulted in poor recovery. Twelve of 20 XCB cores between depths of 162 and 360 mbsf were completely empty and three more were only about half full. Coring operations stopped at this point, and we began to prepare for logging. The first string of logging tools run in Hole 881C collected useful information during the third pass only; the second string could not be lowered out of the drill pipe into the hole. During the 30 hr scheduled for logging, the core recovery problems were considered and were concluded to have resulted from the soft diatom-rich oozes underlying the stiffer diatomaceous clays not being recoverable with the XCB. We decided to try to recover a complete section of depth equivalent to that in the lower portion of Hole 881C (162–360 mbsf) using the APC apparatus. Hole 881D was spudded and washed down to 155.0 mbsf, where APC-coring began. Recovery was good for six cores (145-881D-1H to 145-881D-6H, 155.0–212.0 mbsf), but the seventh core became stuck and extended out of the bit. All efforts to retract the core failed, and our final effort, to lower the drill string over the protruding core barrel, caused the APC barrel to shear off. The *JOIDES Resolution* departed Site 881 for the Detroit Seamount sites on the morning of 4 August.

A single sedimentary unit with two subunits was recovered at Site 881. Subunit IA (0–164 mbsf) is a clayey diatom ooze of late Pliocene and Pleistocene (Brunhes and Matuyama) age. Important minor lithologies include ash layers, ice-rafted debris (IRD), and dolomite as concretions, burrow fills, and discrete layers. This unit grades over a depth range of about 20 m into Subunit IB (164–364 mbsf), which is a diatom ooze and radiolarian/diatom ooze of latest Miocene to late Pliocene age. Ash layers, IRD, and dolomite are present in Subunit IB, but in much lower amounts than in the overlying unit. Calcareous nannofossils are absent or very rare and occur in only about 20% of the samples examined; twice, these markers provided useful biostratigraphic zonation information. Planktonic foraminifers occurred in one and benthic foraminifers in three of the 52 core-catcher samples. Very good age control is provided by the siliceous

microfossils and magnetic reversal stratigraphy. Sedimentation rates are 60 to 70 m/m.y. in the Pleistocene, 100 m/m.y. in the younger portion of the upper Pliocene, 35 to 55 m/m.y. in the remainder of the Pliocene, and 15 m/m.y. in the uppermost Miocene. Therefore, major increases in sedimentation rates and associated flux values occurred at the Pliocene/Miocene boundary and at the time of the onset of Northern Hemisphere glaciation during the late Pliocene. Physical properties and logging measurements also show a change in sedimentary properties at the Subunit IA/Subunit IB contact.

Seismic reflection profiles acquired during the pre-site survey were digitized, recorded, and processed on board the ship and show four acoustically defined units: (1) an upper unit characterized by flat-lying reflectors, (2) a moderately reflective unit that conforms to the underlying topography, (3) a homogeneous unit having few reflectors, and (4) acoustic basement showing hard reflecting horizons. The upper unit shows aspects of being influenced by bottom currents (thinning over highs and filling lows with horizontally bedded material) and in the lows displays onlapping relationships with the underlying pelagically draped unit. Lithologic Subunits IA and IB appear to correspond to the uppermost unit deposited under the influence of abyssal currents and the second acoustic unit, which has a purely pelagic aspect, respectively. This transition in depositional regime occurred at about 2.6 Ma, the time of onset of Northern Hemisphere glaciation (according to the time scale of Cande and Kent, 1992).

## BACKGROUND AND SCIENTIFIC OBJECTIVES

### Drilling Objectives (Site 881)

Most of the Leg 145 objectives were expected to be achieved by drilling at Site 881 (Fig. 1). Geophysical profiles in the region, including those of the *Vema-21* cruise, along which the site was chosen, indicate about 0.4 s of sediment (approximately 320 m) overlying acoustic basement. By analogy with DSDP Site 581, 350 km to the south (Heath, Burckle, et al., 1985), the unlithified sediments were presumed to consist of somewhat more than 250 m of Miocene and younger siliceous silts and clays overlying less than 70 m of pelagic clays. Sedimentation rates were expected to be highest in the Pliocene–Pleistocene sequence. As such, Site 881 was expected to provide a moderate- to high-resolution record of late Neogene age paleoceanographic events in the northwestern Pacific Ocean.

This site was to serve as a northward extension of the four-site (578, 579, 580, 581) north-south transect begun during DSDP Leg 86.

Using it, we expected to monitor the extreme northward shifts of the subarctic front during warm intervals of the Pliocene–Pleistocene. The record of Miocene siliceous sedimentation was expected to provide information about the onset of opal deposition in the North Pacific Ocean during the middle or late Miocene. One goal of Leg 145 was to determine a detailed magnetic reversal stratigraphy in these high-latitude, high-sedimentation-rate, clay-rich sediments. For Site 881, our hope was to carry this reversal stratigraphy back into or through the Pliocene. Temporal constraints provided by the diatom, radiolarian, and reversal stratigraphy were expected to provide excellent control for studies of ice-rafting and tephrochronology.

A pelagic clay section extending from the Miocene back through the middle Cretaceous was expected to underlie the younger siliceous silts and clays. This section should provide a good eolian record of both atmospheric circulation and climate of the Asian source region. Site 881 lies 1650 km north of Leg 86 Sites 576 and 578, which have good eolian records (Janecek, 1985), and together with these sites was expected to provide previously unavailable enhanced latitudinal definition of atmospheric processes. Pelagic clays also are useful recorders of ocean chemistry; thus, the paleochemistry objectives of Leg 145 were expected to be approachable at this site.

Acoustic basement in the northwestern Pacific Ocean usually consists of thin Cretaceous limestones. By comparison with other sites, about 100 m of limestone was expected at Site 881. Backtracked plots suggest that these limestones were deposited north of the high-productivity region associated with the paleoequator. Recovery of these units was expected provide information about the middle Cretaceous environment of the North Pacific Ocean. Present-day age estimates for basement at this site are lower Albian (Renkin and Sclater, 1988) to as old as Barremian (Mammerickx and Sharman, 1988). Age and paleomagnetic information obtained from igneous basement should provide a datum with which to constrain northwestern Pacific Ocean Mesozoic plate reconstructions.

To achieve these objectives, we planned to recover two APC cores to the depth of refusal (where APC-coring became no longer feasible) and to follow the second APC sequence with XCB-coring as far as lithology and time would permit. At the completion of drilling, the standard suite of logs was to be run.

## OPERATIONS

### Transit to Proposed Site NW-1A

The ship cast off the last line in Yokohama at 1100 hr, 24 July 1992, and headed north through an overcast and heavy fog to the first of six planned drill sites. The vessel traversed the 1305 nmi at an average speed of 11.5 kt and arrived at the first survey point at 2205 hr, 28 July. After the seismic equipment was deployed, a 47-nmi survey was conducted in the area of proposed Site NW-1A, at an average speed of 5.7 kt. A beacon was deployed at 0045 hr, 29 July, and was tracked by data processing control as it descended, while the ship continued with the survey. Upon our returning to the site of the beacon deployment at 0520 hr, no signal could be detected. At 0623 hr, a second beacon was deployed at a position approximately 1.5 km south-southwest of where the original beacon was dropped. After the seismic gear was retrieved, the vessel returned to location, the thrusters were lowered, and the drill pipe was run in the hole using the APC/XCB drilling assembly.

### Hole 881A

Just prior to spudding the hole and with the bit approximately 20 m above the mud line, two pipe-swabbing pigs were pumped down the drill string to remove any rust buildup within the pipe. The vessel then was offset 20 m south, where the first APC core was spudded at 2030 hr, 29 July. This first core was full (9.92 m) and thus could not be used to establish the depth of the mud line. A summary of coring operations is presented in Table 1.

### Hole 881B

Our second attempt at retrieving a mud-line core for this location recovered 5.59 m of core and established the seafloor depth at 5542.0 m below the rig floor (5531.0 m below sea level). APC-coring advanced through Core 145-881B-18H (167 mbsf), at which point 80,000 lb of overpull was required to extract the core barrel. As a result of this high overpull, this depth was considered refusal depth, and the bit was brought to the sediment surface to offset for the next hole, an APC/XCB hole to basement. Recovery for Hole 881B was 170.3 m (102% recovery).

Attempts were made to orient Cores 145-881B-4H and -5H, but the extra weight of the multishot and tensor tools apparently forced the landing shoulder of the APC into the landing saver sub in the bottom-hole assembly (BHA), which required high overpulls on the coring line winch to free the core barrel. Orientation of cores was abandoned at this site because of the risk of the core barrel sticking in the drill pipe.

### Hole 881C

After offsetting the vessel 20 m south, a third mud-line coring attempt retrieved 3.82 m of core, giving a seafloor depth of 5541.7 mbrf. APC-coring advanced to Core 145-881C-17H (155.8 mbsf), just above the Hole 881C refusal depth. Heat flow measurements were attempted for Cores 145-881C-4H (failure) and 145-881C-9H (good run). At 155.8 mbsf, coring resumed with the XCB system. Core 145-881C-18X advanced 6.5 m and had a recovery of 3.9 m, while no sediments were recovered in Cores 145-881C-19X and 20X. At this point, another APC core was attempted. After obtaining a complete stroke on the shot, the core barrel could not be freed from the formation by overpulls of up to 90,000 lb. Rather than increase the overpull, the core barrel was washed over. The recovered core contained 9.5 m of sediment. XCB-coring then resumed to 363.8 mbsf (Core 145-881C-39X). Nothing was recovered from Cores 145-881C-22X, -24X, -26X, -28X, -31X, -33X, -34X, -37X, -38X, and -39X. Coring was terminated because of time constraints after Core 145-881C-39X, and preparations for logging were begun after the last core was brought on deck. XCB recovery for this hole was 61.7 m or 31% of the cored interval. Total recovery for this hole was 62.5%.

At 2315 hr, 1 August, the top drive was set back and the hole wiped from total depth (364 mbsf) to 74 mbsf and back down to the bottom with no evidence of fill. After the hole was flushed with a highly viscous mud sweep, the pipe was pulled to logging depth (54.9 mbsf).

### Logging Operations in Hole 881C

The wireline cable and the Quad combination tool were rigged up after the wiper trip. Delays were encountered during testing, when we discovered that one of the conductor pins on the sonic tool was damaged and that the tool needed to be replaced. The Lamont-Doherty temperature tool and an aluminum go-devil were attached to the base of the tool string. Sea-state conditions were rough, so the wireline heave compensator was used. A summary of Hole 881C logging operations is presented in Table 2.

The Quad tool string was run into the hole, where we soon discovered that the SFLU resistivity channel (see "Explanatory Notes" chapter, this volume, for listing of logging tool acronyms) had failed and could not be recovered. A down-going log was recorded at 2300 ft/hr (700 m/hr) from 110 mbsf to total depth at 364 mbsf (5904.7 mbrf). The caliper was opened and indicated a borehole diameter of 11.5 in. Immediately afterward, however, the caliper began reading anomalously high diameters that exceeded 18.5 in. When the tool string was recovered, we noted that the caliper arm had been bent upward, probably the result of downward ship's heave when the arm was first extended at total depth. The first up-going log was recorded at 1800 ft/hr (550 m/hr) using the wireline heave compensator from 360 to 80

Table 1. Summary of coring operations for Site 881.

Core no.	Date (1992)	Time (UTC)	Depth (mbsf)	Length cored (m)	Length recovered (m)	Recovery (%)
145-881A-1H	29 July	1010	4.0-13.5	9.5	9.92	104.0
Coring totals				9.5	9.92	104.0
144-881B-1H	29 July	1105	0.0-5.5	5.5	5.59	11.0
2H	29 July	1200	5.5-15.0	9.5	9.92	104.0
3H	30 July	1255	15.0-24.5	9.5	9.71	102.0
4H	30 July	1530	24.5-34.0	9.5	9.96	105.0
5H	30 July	1725	34.0-43.5	9.5	9.93	104.0
6H	29 July	1840	43.5-53.0	9.5	9.94	104.0
7H	29 July	1945	53.0-62.5	9.5	9.83	103.0
8H	29 July	2050	62.5-72.0	9.5	10.1	105.3
9H	29 July	2200	72.0-81.5	9.5	9.52	100.0
10H	29 July	2300	81.5-91.0	9.5	10.02	105.5
11H	30 July	0000	91.0-100.5	9.5	9.47	99.7
12H	30 July	0050	100.5-110.0	9.5	9.96	105.0
13H	30 July	0150	110.0-119.5	9.5	8.53	89.8
14H	30 July	0250	119.5-129.0	9.5	9.05	95.2
15H	30 July	0345	129.0-138.5	9.5	9.75	102.0
16H	30 July	0440	138.5-148.0	9.5	9.81	103.0
17H	30 July	0535	148.0-157.5	9.5	9.53	100.0
18H	30 July	0620	157.5-167.0	9.5	9.80	103.0
Coring totals				167.0	170.30	102.0
145-881C-1H	30 July	0845	0.0-3.8	3.8	3.92	103.0
2H	30 July	0950	3.8-13.3	9.5	9.63	11.0
3H	30 July	1140	13.3-22.8	9.5	8.81	92.7
4H	30 July	1315	22.8-32.3	9.5	9.84	103.0
5H	30 July	1415	32.3-41.8	9.5	8.80	92.6
6H	30 July	1510	41.8-51.3	9.5	9.84	103.0
7H	30 July	1605	51.3-60.8	9.5	9.29	97.8
8H	30 July	1705	60.8-70.3	9.5	10.05	105.8
9H	30 July	1845	70.3-79.8	9.5	8.57	90.2
10H	30 July	1945	79.8-89.3	9.5	9.59	11.0
11H	30 July	2040	89.3-98.8	9.5	9.26	97.5
12H	30 July	2130	98.8-108.3	9.5	9.91	104.0
13H	30 July	2225	108.3-117.8	9.5	9.32	98.1
14H	30 July	2320	117.8-127.3	9.5	10.00	105.2
15H	31 July	0000	127.3-136.8	9.5	9.75	102.0
16H	31 July	0045	136.8-146.3	9.5	9.96	105.0
17H	31 July	0145	146.3-155.8	9.5	9.48	99.8
18X	31 July	0310	155.8-162.3	6.5	3.90	60.0
19X	31 July	0415	162.3-171.9	9.6	0.00	0.0
20X	31 July	0530	171.9-181.7	9.8	0.00	0.0
21H	31 July	0710	181.7-191.2	9.5	9.50	100.0
22X	31 July	0920	191.2-200.6	9.4	0.00	0.0
23X	31 July	1035	200.6-209.7	9.1	9.32	102.0
24X	31 July	1210	209.7-219.0	9.3	0.00	0.0
25X	31 July	1315	219.0-228.7	9.7	5.28	54.4
26X	31 July	1430	228.7-238.3	9.6	0.00	0.0
27X	31 July	1600	238.3-248.0	9.7	8.65	89.2
28X	31 July	1845	248.0-257.6	9.6	0.00	0.0
29X	31 July	2020	257.6-267.2	9.6	4.08	42.5
30X	31 July	2345	267.2-276.9	9.7	9.44	97.3
31X	1 Aug	0030	276.9-286.5	9.6	0.00	0.0
32X	1 Aug	0235	286.5-296.2	9.7	3.85	39.7
33X	1 Aug	0430	296.2-305.8	9.6	0.00	0.0
34X	1 Aug	0530	305.8-315.4	9.6	0.00	0.0
35X	1 Aug	0650	315.4-325.1	9.7	7.46	76.9
36X	1 Aug	0820	325.1-334.8	9.7	9.65	99.5
37X	1 Aug	0935	334.8-344.5	9.7	0.00	0.0
38X	1 Aug	1045	344.5-354.1	9.6	0.00	0.0
39X	1 Aug	1210	354.1-363.8	9.7	0.00	0.0
Coring totals				363.8	227.20	62.5
*****Wash/drill to 155.0 mbsf*****						
145-881D-1H	3 Aug	0230	155.0-164.5	9.5	9.35	98.4
2H	3 Aug	0335	164.5-174.0	9.5	9.87	104.0
3H	3 Aug	0500	174.0-183.5	9.5	9.81	103.0
4H	3 Aug	0610	183.5-193.0	9.5	9.70	102.0
5H	3 Aug	0700	193.0-202.5	9.5	9.63	11.0
6H	3 Aug	0800	202.5-212.0	9.5	9.55	100.0
Coring totals				57.0	57.91	101.6

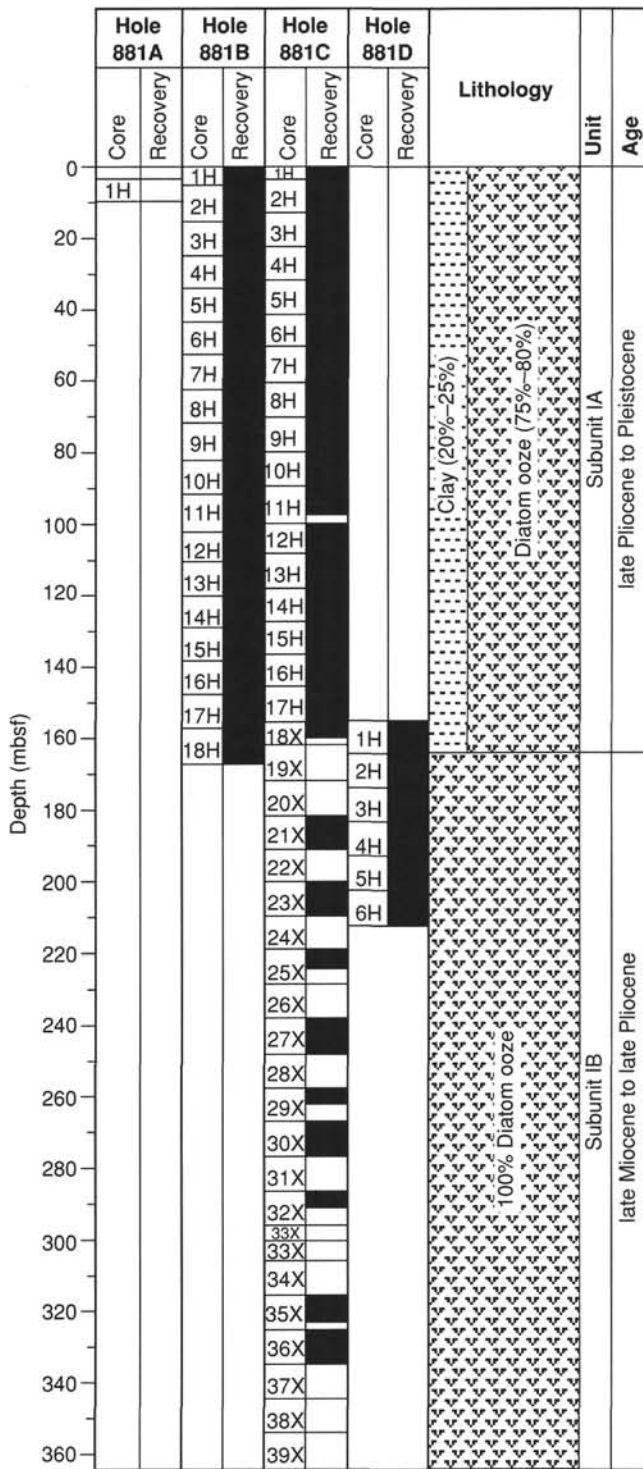


Figure 2. Lithologic summary, Site 881.

sponge spicules, whereas quartz and feldspar are accessory terrigenous components.

Dominant colors in Subunit IA are various types of gray in hues of 5Y, 10Y, 5GY, 2.5GY, and 2.5G. The uppermost 1 to 3 m of sediment are oxidized, however, as reflected by a brown color in hues of 5YR and 7.5YR. Primary depositional structures were not observed in the clayey diatom oozes of Subunit IA, but bioturbation is ubiquitous. No discrete trace fossils were observed in Subunit IA, but the extent of

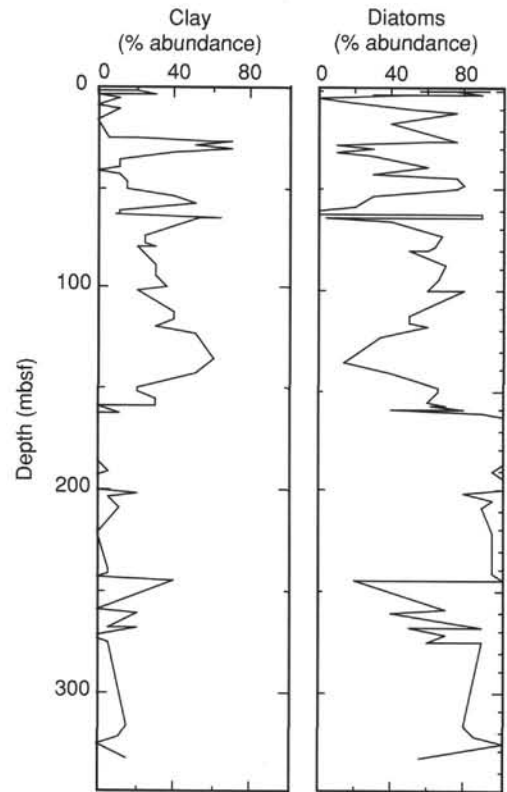


Figure 3. Diatom and clay abundances vs. depth at Site 881, compiled from smear slide analyses of dominant lithologies.

bioturbation is indicated by the presence of millimeter-scale pyritic burrow fills, of centimeter-scale burrows filled with volcanic glass and/or dolomite/rhodochrosite, and of burrowed gradational upper surfaces on decimeter-scale volcanic ash horizons (Fig. 5). Color bands, which are present to common in most of Subunit IA, range from less than 1 cm to approximately 10 cm in thickness, are more indurated than the surrounding sediments, and exhibit colors in various shades of green, purple, and red. A comparison of smear slides taken from the color bands and the adjacent sediment reveals no significant compositional difference between the two lithologies.

Dropstones are present to common in the clayey diatom ooze of Subunit IA and range in size from coarse sand to pebbles. The larger dropstones, which are most easily observed during visual description of the core, are predominantly dark and fine-grained; examination of thin sections cut from several of these dropstones reveals that they include pyroxene basalts and felsic tuffs (Fig. 6; Table 4). Other rock types are present as dropstones in lower abundances; these include volcanic pumice (Fig. 7), mineralized felsic tuff, and redeposited felsic tuff (graywacke).

Two minor lithologies occur repeatedly in Subunit IA: volcanic ash and concentrations of dolomite and/or rhodochrosite. Volcanic ash is present in a number of forms within Subunit IA; these include light-colored zones of unaltered ash that range from several centimeters to slightly less than 1 m in thickness (Fig. 5), dark-colored zones of altered ash with clay and opaque minerals, ash-filled burrows, and ash disseminated in clayey diatom ooze. The discrete ash layers generally exhibit a sharp lower boundary and a burrowed and gradational upper boundary; normal grading is common in ash layers more than 5 cm thick. The abundance of volcanic ash, measured either as the number of discrete ash layers per core or as the cumulative thickness of ash per core (Fig. 4), varies markedly within Subunit IA, but is greater on average than the abundance of volcanic ash in Subunit IB.

**Table 2. Summary of logging operations for Site 881.**

Time (local)	Depth (mbrf)	Comment
0010		Last core on deck; total depth = 5541.7 mbrf.
0200		Begin wiper trip.
0430		Rig up wire line, make up cable end, and make up Quad tool string (SDT-NGT-CNT-HLDT-DITE-LTT). Conductor pin on sonic tool damaged; tool replaced.
0540		Tool RIH.
0715	Surface	Tool in open hole.
0950	5612	SFLU fails, begin down-going log at 2300 ft/hr.
1000	5650	Tool at T/D, heave compensator turned on, HLDT caliper opened and fails, begin up-going log at 1800 ft/hr.
1020	5904.7	End first up-going log, lower tool string to begin repeat sections; driller instructed to raise pipe to 50 mbsf.
1130	5620	Begin repeat up-going log at 1800 ft/hr; WHC off.
1145	5710	Pipe not raised in time; decision to log up again from T/D to 5590 mbrf.
1205	5590	Begin third up-going log, WHC on, SFL now working.
1225	5904	WHC off to enter pipe; some trouble reentering pipe.
1305	5644	Flapper cleared.
1340	5590	W/L cable counter assembly broken; replaced.
1400	5587	Quad tool string disassembled; go-devil sheared off; HLDT caliper arm bent outward.
1700	Surface	FMS string made up with Lamont temperature tool and new aluminum go-devil, RIH.
1800	Surface	FMS cannot pass base of pipe, POOH.
2000	5612	Go-devil pumped to base of pipe.
2330	Surface	FMS still cannot pass base of pipe, POOH.
0300	5610	Rig down and end logging operations.
0515	Surface	

mbsf. A second up-going log was recorded from 170 to 70 mbsf. The SFLU log was operative following the second up-going log, so a third up-going log was recorded from 360 to 50 mbsf. The third run is considered the most complete and most reliable log for this hole. The HLDT density tool could rotate freely in the borehole because of the damaged caliper arm; thus, the logging data for density must be considered suspect over several intervals.

The formation microscanner (FMS) tool string with the Lamont temperature tool and go-devil was run into the hole after completion of logging with the Quad tool. We encountered difficulty when removing the base of the pipe, and this proved to be the end of any further logging. Several attempts were made to open the lockable flapper valve at the base of the pipe, but the tool string could not pass the obstruction. At 0300 hr, 3 August, we decided to conclude logging operations, and pulled the tool out of the hole. At 0515 hr, 3 August, our logging equipment was rigged down, and the pipe was pulled out of the hole. The bit cleared the seafloor at 0545 hr, thereby ending Hole 881C.

### Hole 881D

The vessel was offset 20 m east for coring in Hole 881D. As upper sediments were adequately recovered from Hole 881C, the pipe was washed down to 155 mbsf, at which point APC-coring resumed. Core 145-881D-1H was shot at 155 mbsf and required 90,000 lb of overpull to release. Core 145-881D-2H was shot at 164.6 mbsf and required 50,000 lb of overpull. Cores 145-881D-3H through -6H, (covering the interval from 174.0 to 212.0 mbsf) required washing over after even 100,000 lb of overpull would not release the barrels from the formation. After washing over 6 m of the core barrel for Core 145-881D-7H, the barrel stuck in the drill pipe. The core barrel appeared bent because of contact with dropstones and could not be drawn into the pipe. While slowly setting weight-on-bit to free the barrel, the tool parted at the top of the second core barrel. The upper portion of the tool was recovered unharmed, but the rest of the core barrel remained in the formation and the hole had to be abandoned. Coring was terminated, and the pipe was pulled out of the hole. The bit was on deck by 0900 hr, 4 August, at which time we began the transit to proposed Site DSM-3.

## LITHOSTRATIGRAPHY

### Introduction

Four holes were drilled at Site 881 (Fig. 1); three (Holes 881A, 881B, and 881D) were drilled using the APC-coring device, and one (Hole 881C) was drilled using a combination of APC and XCB techniques (see "Operations" section, this chapter). Recovery rate was excellent (100+%) in the APC-cored portions of the site, and the sediments recovered were essentially undisturbed. Recovery was much poorer in the XCB-cored portion of Hole 881C, averaging only 40% in that interval (Cores 145-881C-18X to -39X; 155.8–363.8 mbsf).

The cored interval is composed predominantly of diatom ooze and clayey diatom ooze (Fig. 2). Volcanic ash layers and horizons enriched in rhodochrosite and/or dolomite are present as minor lithologies. Dropstones are present throughout the cored interval, but their abundance generally decreases downhole. The dropstones recovered in place within the section are dominated by black, fine-grained lithologies, including basalt, dark pumice, volcanoclastic graywacke, and resedimented tuff. Additional rock types are present as dropstones in lower abundances, including semi-schistose felsic tuff and mineralized tuff. The diatom content of the sediments increases and the abundances of ash layers and rhodochrositic/dolomitic horizons decrease below approximately 164 mbsf (Figs. 3 and 4); on the basis of these changes, the sediments at Site 881 have been divided into two subunits (Table 3). These sediments range from Pleistocene to late Miocene in age.

### Description of Units

#### Unit I

Intervals: Core 145-881A-1H  
Cores 145-881B-1H to -18H  
Cores 145-881C-1H to -39X  
Cores 145-881D-1H to -6H  
Depth: 0–363.8 mbsf  
Age: Pleistocene–late Miocene

Unit I is composed of diatom ooze and clayey diatom ooze with varying abundances of terrigenous components and has been divided into two subunits on the basis of the increased abundance of biogenic silica in the lower part of the sedimentary section. Subunit IA (0–164.5 mbsf) comprises clayey diatom ooze and diatom ooze, with volcanic ash and zones of dolomite and/or rhodochrosite present as minor lithologies. Subunit IB (164.5–363.8 mbsf) is composed of diatom ooze with minor amounts of radiolarian diatom ooze; volcanic ash and dolomite/rhodochrosite zones are rare. Dropstones are present throughout Unit I, but the abundance of dropstones decreases downhole.

#### Subunit IA

Intervals: Core 145-881A-1H  
Cores 145-881B-1H to -18H  
Cores 145-881C-1H to -18X  
Cores 145-881D-1H  
Depth: 0–164.5 mbsf  
Age: Pleistocene–late Pliocene

Subunit IA contains 164.5 m of clayey diatom ooze, with minor amounts of diatom ooze present in Cores 145-881B-1H to -3H. Diatom abundances are high, but variable, in Subunit IA (Fig. 3) and generally range between 30% and 80%, as estimated from smear slides of the dominant lithology within each core. This range of diatom abundance reflects variation in the abundance of terrigenous clay (Fig. 3) and admixed volcanic ash; diatom abundance minima occur within decimeter- to meter-scale volcanic ash layers that form the dominant lithologies within their respective cores (Fig. 4). Accessory biogenic components in these sediments include radiolarians and

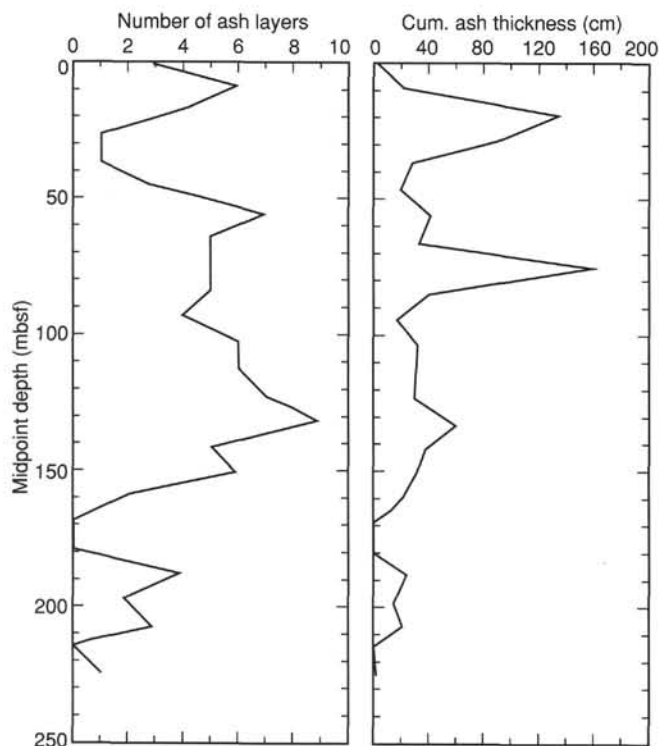


Figure 4. Ash layer frequency (number of layers/core) and cumulative ash thickness cm ash/core downcore at Hole 881C. Depth value for each point is midpoint of that core.

Concentrations of dolomite and/or rhodochrosite also occur repeatedly within Subunit IA in a variety of forms, including uncemented burrow fills, burrow-form concretions within the clayey diatom ooze, uncemented horizons overlying or underlying volcanic ash layers, and concretions overlying or underlying volcanic ash layers (Fig. 8). The mineralogy of this material has been established by a limited number of XRD analyses, and the presence of a diffraction peak at  $24.27^{\circ} 2\theta$  clearly demonstrates that this material contains rhodochrosite. The similarity of the remainder of the rhodochrosite XRD pattern and the dolomite XRD pattern, however, prevents us from concluding at this time that rhodochrosite is the only component in this material; additional geochemical data will be useful for quantifying the amounts of rhodochrosite and dolomite present in these sediments.

The uncemented concentrations of rhodochrosite/dolomite are composed almost entirely of fine silt-sized (10–20  $\mu\text{m}$ ), euhedral crystals. The burrow-form concretions range in size from several millimeters in diameter and several centimeters long to several centimeters in diameter and 5 to 10 cm long, which is much larger than any discrete burrows observed in these cores. The concretions that lie adjacent to a volcanic ash are generally subspherical in shape, with diameters of 2 to 3 cm or less. These zones of rhodochrosite and/or dolomite provide the only appreciable amounts of carbonate measured in Subunit IA (see “Organic Geochemistry” section, this chapter).

#### Subunit IB

Intervals: Cores 145-881C-19X to -39X  
Cores 145-881D-2H to -6H  
Depth: 164.5–363.8 mbsf  
Age: late Pliocene–late Miocene

The upper boundary of Subunit IB is placed at the shallowest occurrence of diatom ooze below the clayey diatom ooze of Subunit IA. According to this definition, therefore, Subunit IB begins at the top of Core 145-881D-2H, even though clayey diatom ooze was

Table 3. Lithologic summary, Site 881.

Lithologic unit	Cores	Depth (mbsf)	Age	Lithology
IA	881A-1H 881B-1H to -18H 881C-1H to -18X 881D-1H	0–164.5	Pleistocene to late Pliocene	Clayey diatom ooze
IB	881C-19X to -39X 881D-2H to -6H	164.5–363.8	late Pliocene to late Miocene	Diatom ooze

recovered at slightly greater depths in Hole 881C (i.e., Core 145-881C-21H). This variation between diatom ooze and clayey diatom ooze at equivalent depths in Holes 881C and 881D suggests that the boundary between Subunits IA and IB is gradational, as demonstrated by downhole logging results (see “Downhole Measurements” section, this chapter). Within this depth range, therefore, the boundary was chosen to provide greatest consistency with variations in physical properties (bulk density, porosity, etc.; see “Physical Properties” section, this chapter), magnetic susceptibility, and log response (natural gamma ray, sonic velocity, etc.; see “Downhole Measurements” section, this chapter).

Subunit IB contains 199.3 m of diatom ooze, with clayey diatom and radiolarian diatom oozes also present in the upper 27 m of this subunit. Diatom abundances are consistently high in Subunit IB (Fig. 3) and average greater than 80% in smear slide estimates. The biogenic silica content of Subunit IB is further enhanced by increased abundances of radiolarians, especially in Cores 145-881C-29X and -30X. This increase in biogenic silica content is accompanied by a corresponding decrease in terrigenous clay content (Fig. 3).

Dominant colors in the diatom ooze of Subunit IB are various types of brown (2.5Y, 7.5Y, 5YR, 10YR) and greenish-gray (5Y, 2.5GY, 5GY). Primary depositional structures were not observed in the diatom oozes of Subunit IB, but bioturbation effects (millimeter-scale pyritic burrow fills, color mottles, and burrowed upper surfaces of ash layers) are abundant. Green, well-indurated color bands are present to common in only a few sections within Subunit IB; overall, color bands are less common in Subunit IB than in Subunit IA.

Dropstones have two styles of distribution within the cores of Subunit IB. The first mode is clearly an in-situ distribution, with the dropstones located in the interior of a core surrounded by diatom ooze. Dropstones with this style of distribution are rare in Subunit IB and are restricted to levels above 243.5 mbsf (Section 145-881C-27X-4, 123 cm). The second style of dropstone distribution is in a concentration at the top of a core, which is attributed to downhole contamination (“wash-in”) from overlying portions of the section. As a result, the distribution of washed-in dropstones cannot be used to indicate the importance of ice-rafting at that stratigraphic interval, although the dropstones present in those concentrations can be used to gain further insight into the range of dropstone lithologies and dropstone provenance. Dropstone lithologies present in Subunit IB are similar to those observed in Subunit IA, with basalts, volcanoclastic graywackes, and redeposited tuffs most common. Felsic tuffs are less common, and a lithofeldspathic sandstone (graywacke) lithology is also present in low abundances, as identified by thin section analysis (Table 4).

Volcanic ash and concentrations of rhodochrosite/dolomite are present as minor lithologies in Subunit IB, but at lower abundances than those in Subunit IA. Both the number of ash layers per core and the cumulative ash thickness in each core decrease from Subunits IA to IB (Fig. 4), with the deepest discrete ash layer recovered at Section 145-881C-25X-2, 52 cm (221.0 mbsf). Rhodochrosite/dolomite is present as discrete layers and concretions, with the deepest occurrence at Section 145-881C-30X-5, 104–114 cm (274.2–274.3 mbsf). One particularly noteworthy occurrence is the presence of two 18-cm-thick rhodochrositic/dolomitic layers, one at Section 145-881C-18X-

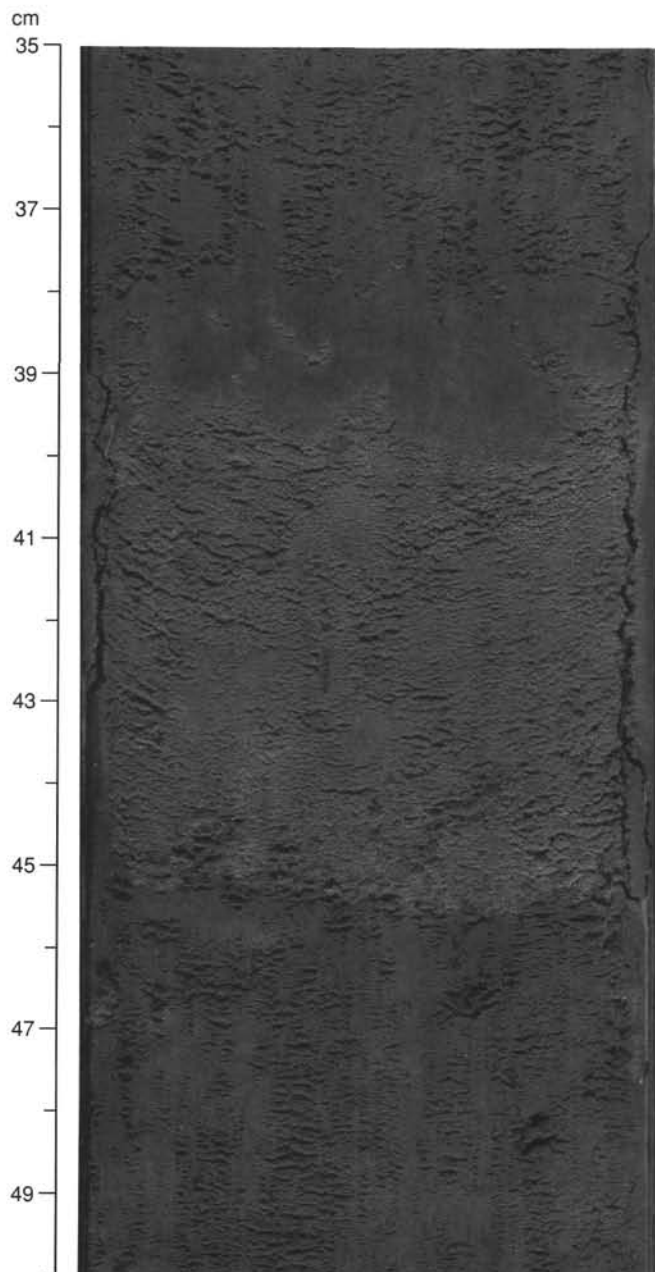


Figure 5. Photograph of ash layer in Subunit IA (Interval 145-881B-13H-5, 35–50 cm). Note sharp lower contact and burrowed, gradational upper contact.

3, 0–18 cm (158.80–158.98 mbsf), and the second at Section 145-881D-1H-3, 50–68 cm (158.50–158.68 mbsf). On the basis of their similar sub-bottom depths, these two layers may be continuous across the drill site.

### Composite Depth Sections

At Site 881, correlation of the numerous ash layers (Table 5), magnetic susceptibility measurements, and GRAPE data in Hole 881B and 881C permits identification of coring gaps in the sediment record of the past 2.6 m.y. recovered from each of the two holes (Table 6), as well as the construction of a composite depth section for the upper 166 m from Site 881 (Table 7). The upper 5.5 m of the composite section was taken from Hole 881B because visual comparison of the two cores

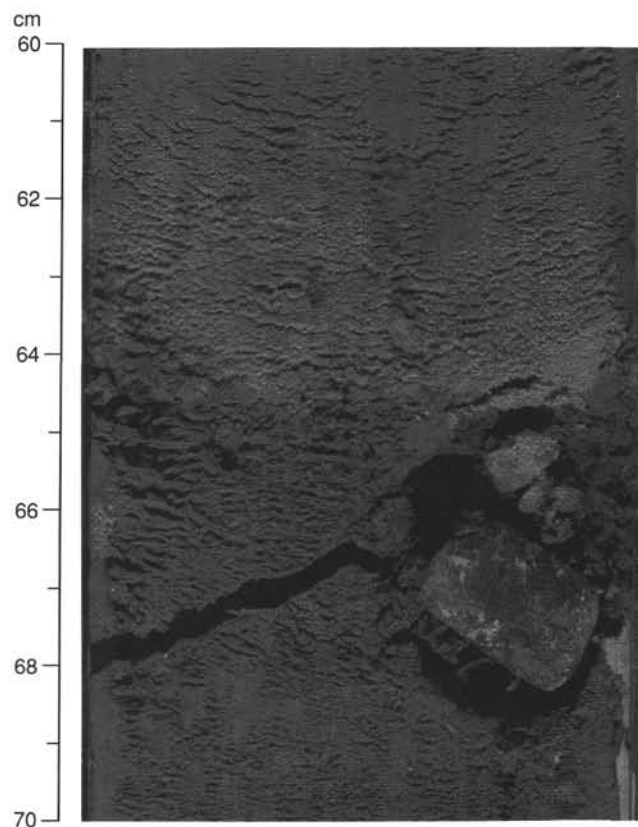


Figure 6. Photograph of common dropstone lithology, either basalt or felsic tuff (Interval 145-881B-13H-5, 60–70 cm).

indicates that a more complete sediment section was recovered in the uppermost portion of this hole.

The composite record for Site 881 is summarized in Table 7, which shows the sediment intervals combined from each hole, the thickness of each interval, and the cumulative thickness of the composite section. The composite depth record is about 4.5% longer than the sediment depth below seafloor determined at Holes 881B and 881C.

### Discussion

Sediments deposited at Site 881 since the late Miocene record interactions in the supply of biogenic silica, terrigenous clastics, and continental volcanics to the northwestern Pacific Ocean. Of these controls, however, the most important fluctuations are changes in the relative importance of biogenic silica and terrigenous clastics, which provide the data to distinguish lithologic Subunits IA and IB.

Upper Miocene through lower Pliocene sediments at Site 881 (lithologic Subunit IB) contain little terrigenous material and few volcanic ash layers and accumulated at the lowest rates calculated for any interval cored at this site (see "Sedimentation Rates and Fluxes" section, this chapter). These sediments are also enriched in biogenic opal relative to correlative deposits recovered farther to the south during DSDP Leg 86 (Heath, Burckle, et al., 1985), suggesting either that rates of biogenic supply increased toward the north or that rates of terrigenous supply decreased toward the north during the late Miocene and early Pliocene.

Dropstones first appear at Site 881 in lower Pliocene sediments (243 mbsf; approximately 4 Ma, see "Biostratigraphy" section, this chapter), significantly older than the first appearance of dropstones at DSDP Sites 579 and 580, farther to the south (Krissek et al., 1985). Dropstone abundance is low through the remainder of Subunit IB,

**Table 4. Lithologies of dropstones from Site 881 as determined from thin sections.**

Interval (cm)	Depth (mbsf)	Dropstone lithology	Comments
881B-2H-1, 56–57	6.0	Pyroxene basalt	In situ
881B-11H-1, 65–70	91.7	Tectonized felsic tuff (semi-schistose)	In situ
881C-15H-1, 1–5	127.3	Mineralized felsic tuff (sulfides present)	In situ
881C-17H-1, 1–5	146.3	Redeposited felsic tuff (unaltered graywacke)	In situ
881C-21X-1, 1–5	181.7	Lithofeldspathic sandstone (unaltered graywacke)	In situ

however, suggesting minor iceberg transport, probably the result of limited glacial extent on the surrounding landmasses.

The supplies of both terrigenous clastics and volcanic glass increased relative to the biogenic influx as the upper 50 m of Subunit IB was deposited during the end of the early Pliocene and the beginning of the late Pliocene. These changes in supply produced the interbedded diatom oozes, clayey diatom oozes, and ashy diatom clays at the top of Subunit IB. The additional influxes of material also increased sedimentation rates to approximately 70 m/m.y. through this interval. Dropstones are more abundant in this part of Subunit IB than in the underlying sediments, suggesting an increased supply of terrigenous components through ice-rafting. The relative uniformity of the dropstone lithologies suggests a common source for the icebergs, and implies an increase in glacial activity along the northeastern coast of Asia.

Upper Pliocene and Pleistocene sediments (Subunit IA) at Site 881 contain more dropstones, more fine-grained terrigenous material, and more volcanic ash than the underlying diatom oozes, which indicates an increase in the supply of both terrigenous and volcanic materials relative to the supply of biogenic silica. These relative increases contribute to an increased sedimentation rate, which reaches a maximum of 84 m/m.y. in the upper Pliocene (see "Sedimentation Rates and Fluxes" section, this chapter). These changes in lithology and sedimentation rate occurred at approximately 2.6 Ma (time scale of Cande and Kent, 1992), near the widely recognized time of the onset of continental-scale glaciation in the Northern Hemisphere. Studies from sites farther to the south in the northwestern Pacific Ocean have identified significant increases in eolian flux (Janecek and Rea, 1983; Janecek, 1985; Rea, Leinen, and Janecek, 1985) and dropstone flux (Krissek et al., 1985; Rea and Schrader, 1985) at approximately 2.5 Ma (time scale of Berggren et al., 1985), and attributed those changes to the onset of extensive Northern Hemisphere glaciation. The similarity in timing and effect suggests that the transition from Subunits IB to IA records a similar paleoenvironmental history at Site 881.

Volcanic events may have also contributed to the increased sedimentation rate and the relative decrease in biogenic relative component abundances at Site 881 since the late Pliocene. Both the number of volcanic ash layers and their cumulative thicknesses increase in Subunit IA relative to Subunit IB, suggesting an increase in the frequency and intensity of volcanic activity in the adjacent magmatic arc(s). Kennett et al. (1977) identified a correlative increase in the abundance of volcanic ash in a number of areas of the Pacific Ocean. This increase in volcanic ash (Fig. 9) influx would have increased the overall sedimentation rate, while diluting the biogenic silica component.

The only indicator of significant sediment diagenesis at Site 881 is the irregular distribution of rhodochrosite and/or dolomite through the sedimentary section. This material occurs in a variety of forms, including uncemented layers, uncemented burrow fills, cemented burrow-fill concretions, and subspherical concretions. Interstitial waters at Site 881 were not sampled in sufficient spatial detail to explain all of the occurrences of rhodochrosite/dolomite, but general trends in the composition of the interstitial waters are consistent with auth-

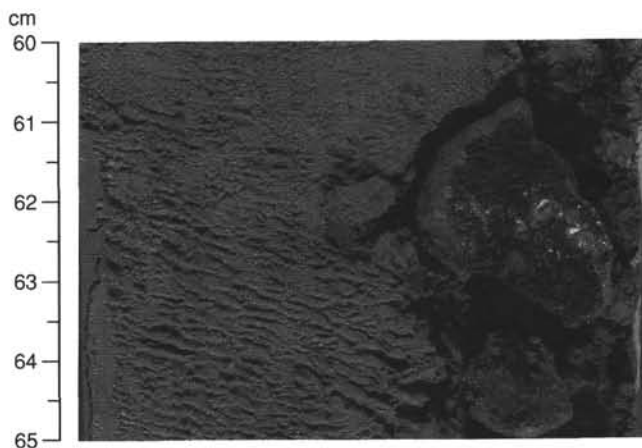


Figure 7. Photograph of pumice dropstone (Section 145-881C-16H-7, 60–65 cm).

igenic precipitation of rhodochrosite and dolomite (see "Inorganic Geochemistry" section, this chapter). Many of the thicker layers and subspherical concretions are found adjacent to layers of volcanic ash, but the burrow fills, burrow-fill concretions, and some of the layers and subspherical concretions occur independently of volcanic ash. As a result, the detailed controls on the origin of this rhodochrosite/dolomite are not understood, and should remain a challenging question for shore-based study.

## BIOSTRATIGRAPHY

An apparently continuous sequence of upper Miocene through Quaternary sediments was recovered at Site 881. The 335-m-thick section consists of diatom oozes overlain by clayey diatom ooze, with the latter containing numerous ash layers. Calcareous nannofossils and foraminifers occur at only a few intervals and at low abundances in sediments from the four holes drilled at this site. Abundant, well-preserved diatoms and radiolarians are present throughout the sequence. Figures 10 and 11 show core recovery, magnetostratigraphy, and siliceous zonations for this site. Table 8 gives the estimated ages of diatom and radiolarian datum levels recorded in sediments from Holes 881B, 881C, and 881D, the interval over which they occur, and the depth of this interval in meters below seafloor (mbsf).

Uppermost Pliocene sediments, represented by a single core, were recovered from Hole 881A. An uppermost Pliocene through Quaternary record (~2.6 Ma) was recovered from this site in both Holes 881B and 881C. Hole 881D was drilled to retrieve lowermost upper Pliocene and uppermost lower Pliocene sediments not recovered in Hole 881C. Hole 881C penetrated the oldest sediments at this site, which are late Miocene in age.

## Foraminifers

All core-catcher samples from Holes 881B, 881C, and 881D were processed and examined for foraminifers. No carbonate-rich intervals were found, although Sample 145-881C-21H-CC contains a sparse, moderately well-preserved assemblage of *Globigerina bulloides*, *Neogloboquadrina pachyderma* (dextral), *Globorotalia inflata*, and *Neogloboquadrina dutertrei* (sinistral).

Most of the samples are barren, with the exception of Sample 145-881C-21H-CC (one *Melonis sphaeroides*, four *Eggerella bradyi*), Sample 145-881C-23X-CC (one *Inaequilina* sp., six *Eggerella bradyi*), and Sample 145-881D-5H-CC (one *Pyrgo murrhina*, one *Eggerella bradyi*). Most of these forms are encrusted with pyrite. Few interpretations can be made from these sparse faunas; however, low forami-

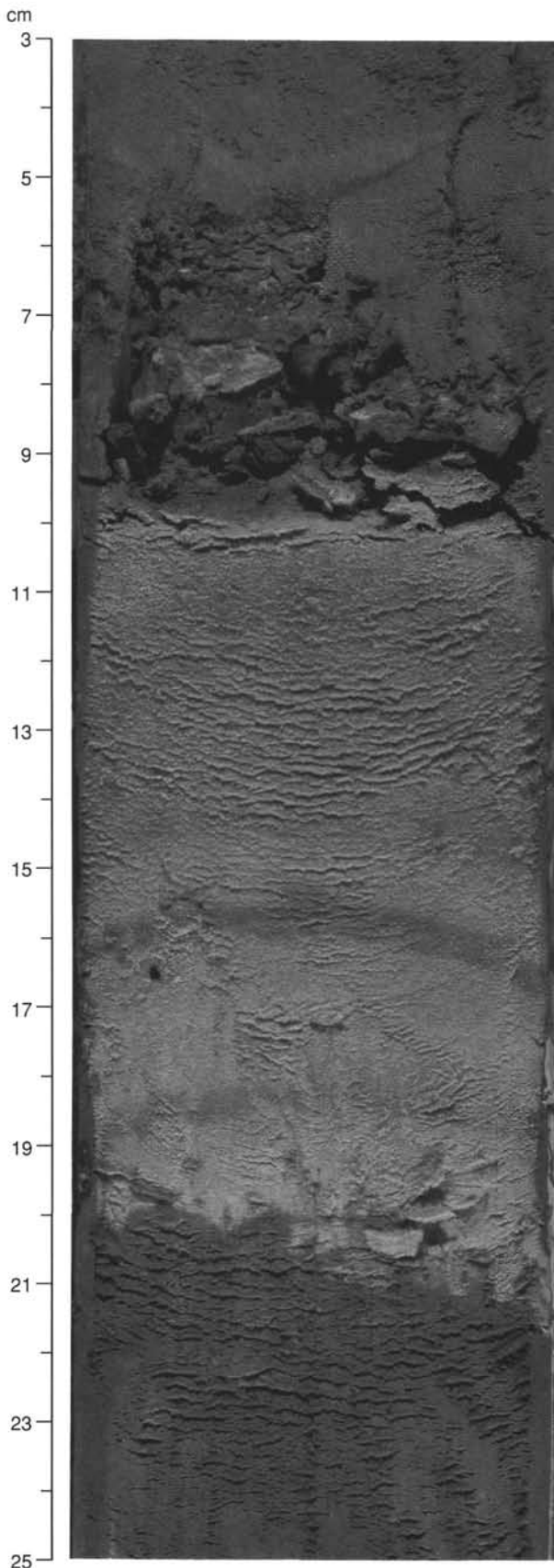


Figure 8. Photograph of volcanic ash and overlying zone of rhodochrosite and/or dolomite (Interval 145-881C-8H-3, 3–25 cm).

niferal abundances and the few species found are characteristic of abyssal depths.

### Calcareous Nannofossils

Calcareous nannofossils are either absent or rare in all core-catcher samples investigated from Site 881. Nannofossils were observed in 11 of the 55 samples examined. In Hole 881B, only one sample, Sample 145-881B-11H-CC (100.50 mbsf), contains nannofossils: rare *Coccolithus pelagicus*, and rare, probably reworked, specimens of *Reticulofenestra pseudumbilica* and *Sphenolithus* spp.

Sample 145-881C-1H-CC (3.80 mbsf) contains rare *C. pelagicus* (one specimen observed). In Sample 145-881C-17H-CC (155.80 mbsf), one reworked specimen of *Sphenolithus* spp. was observed, in addition to rare *C. pelagicus*. Sample 145-881C-21H-CC (191.20 mbsf) contains rare *C. pelagicus*, *Calcidiscus macintyrei*, *Pseudoemiliania lacunosa*, small reticulofenestrads, and small geophyrocapsids. Based on the presence of *P. lacunosa* and the absence of *Sphenolithus* spp. and *R. pseudumbilica*, the age of this sample has been identified as less than 3.6 Ma (late Pliocene). In Sample 145-881C-32X-CC (296.20 mbsf), rare specimens of *Sphenolithus abies*, *C. macintyrei*, *Triquetrorhabdulus rugosus*, *Discoaster brouweri*, and a five-armed discoaster, probably *D. quinqueramus*, were observed. The presence of *D. quinqueramus* should place this sample in Zone NN11 of the late Miocene.

Six samples from Hole 881D were examined for calcareous nannofossils. Only two samples (145-881D-5H-CC, 202.50 mbsf, and -6H-CC, 212.00 mbsf) contain rare nannofossils. Small reticulofenestrads and small geophyrocapsids were observed in the former sample, and one specimen of a five-rayed discoaster was seen in the latter.

### Radiolarians

Well-preserved late Miocene through Quaternary age radiolarians are present in all core-catcher samples from all four holes drilled at Site 881. Common-to-abundant radiolarians characteristic of the late Quaternary *Botryostrobus aquilonaris* Zone (Hays, 1970) are found in uppermost sediments from Holes 881A, 881B, and 881C (Samples 145-881A-1H-CC, 145-881B-1H-CC, and 145-881C-1H-CC through -3H-CC). *Lychnocanoma grande*, whose last occurrence (LO) has been estimated at 0.05 Ma, is present in core-catcher samples taken from the uppermost core at all three holes. The LO of *Drupptractus acquilonius* is recorded in this sediment sequence. The presence of *Stylactrus universus* and the absence of *Eucyrtidium matuyamai* in Samples 145-881B-3H-CC through -7H-CC and Samples 145-881C-4H-CC through -7H-CC place these sediments in the late Pleistocene *Stylactrus universus* Zone (Hays, 1970). Correlation with oxygen isotope stratigraphy has shown that the LO of *S. universus* is a globally synchronous event, with an estimated age of 0.45 Ma (Hays and Shackleton, 1976; Morley and Shackleton, 1978). Radiolarian abundance in samples from this interval varies from rare to abundant.

The early Quaternary *E. matuyamai* Zone (Hays, 1970; Foreman, 1975) is represented in sediments from Hole 881B in Samples 145-881B-8H-CC through -12H-CC and those from Hole 881C in Samples 145-881C-8H-CC through -13H-CC, based on the presence of the radiolarian species *E. matuyamai*. The range of this species (from the Olduvai through the base of the Jaramillo magnetic events) agrees with that of detailed studies of its presence in sediments from North Pacific Ocean piston (Hays, 1970) and DSDP (J.J. Morley, unpubl. data, 1992) cores. Abundances of radiolarians in these samples range from rare to abundant.

Sediment samples from the remainder of Hole 881B (145-881B-13H-CC through -18H-CC) and from Hole 881C for the interval between Samples 145-881C-14H-CC and -25X-CC, as well as from all of Hole 881D (145-881D-1H-CC through -6H-CC) have been tentatively assigned to the *Lamprocyrtis heteroporos* Zone (Hays,

**Table 5. Correlation of ash layers among Holes 881B, 881C, and 881D, based on magnetic susceptibility curves, barrel-sheet descriptions, and core photographs.**

Occurrence of ash layers at Site 881 during the last 2.6 Ma					
Core, section, interval (cm)	Depth (mbsf)	Core, section, interval (cm)	Depth (mbsf)	Core, section, interval (cm)	Depth (mbsf)
145-881B-		145-881C-		145-881D-	
1H-2, 72	2.22	1H-2, 52	2.02		
1H-2, 142	2.92	1H-2, 120	2.70		
1H-3, 86	3.86	1H-3, 57	3.57		
1H-3, 109	4.09	1H-3, 71	3.71		
2H-2, 57	6.07	2H-2, 34	5.64		
2H-2, 106	8.06	2H-3, 120	8.00		
2H-3, 5	8.55	2H-4, 12	8.42		
2H-4, 63	10.63	2H-5, 82	10.62		
2H-4, 100	11.00	2H-5, 121	11.01		
2H-4, 135	11.35	2H-5, 144	11.24		
2H-5, 95	12.45	2H-7, 15	12.45		
2H-5, 147	12.97	3H-1, 5	13.35		
2H-6, 144	14.44	3H-1, 125	14.55		
2H-7, 20	14.70	3H-2, 7	14.87		
3H-1, 30	15.30	3H-3, 15	16.45		
4H-1, 146	25.93	4H-2, 39	24.69		
5H-1, 114	35.14	5H-2, 118	34.98		
5H-5, 32	40.32	5H-5, 112	39.42		
5H-5, 97	40.97	5H-6, 5	39.85		
5H-6, 138	42.88	6H-1, 144	43.24		
6H-1, 75	44.25	6H-3, 113	45.93		
6H-2, 107	46.07	6H-4, 137	47.67		
6H-3, 38	46.88	6H-5, 68	48.48		
6H-6, 15	51.15	7H-1, 144	52.74		
6H-6, 106	52.06	7H-2, 131	54.11		
7H-3, 83	56.83	7H-6, 61	59.41		
8H-2, 116	65.16	8H-3, 15	63.95		
8H-6, 90	70.90	8H-6, 117	69.47		
9H-1, 43	72.43	9H-2, 59	72.39		
9H-5, 70	78.70	9H-5, 75	77.05		
9H-5, 126	79.26	9H-5, 135	77.65		
9H-6, 15	79.65	9H-6, 65	78.45		
10H-2, 21	83.21	10H-2, 29	81.59		
10H-5, 130	88.80	10H-5, 96	86.76		
10H-6, 52	89.52	10H-6, 65	87.95		
10H-6, 110	90.10	10H-6, 119	88.49		
10H-7, 18	90.68	10H-7, 9	88.89		
11H-1, 110	92.10	11H-1, 141	90.71		
11H-4, 59	96.09	11H-3, 133	93.63		
11H-6, 15	98.65	11H-5, 106	96.36		
12H-1, 34	100.84	12H-1, 110	99.90		
12H-2, 15	102.15	12H-2, 114	101.44		
13H-4, 75	105.75	12H-5, 59	105.39		
12H-6, 133	109.33	13H-1, 87	109.17		
13H-2, 117	112.67	13H-3, 147	112.77		
3H-4, 67	115.17	13H-5, 97	115.27		
14H-1, 127	120.77	14H-2, 33	119.63		
14H-4, 137	125.37	14H-5, 121	125.01		
14H-5, 46	125.96	14H-7, 9	126.89		
14H-5, 98	126.48	15H-1, 77	128.07		
14H-7, 48	128.98	15H-3, 47	130.77		
15H-3, 95	132.95	15H-4, 120	133.00		
15H-4, 130	134.80	15H-6, 15	134.95		
15H-5, 124	136.24	15H-7, 24	136.54		
15H-6, 138	137.88	16H-1, 100	137.80		
16H-1, 97	139.47	16H-2, 135	139.65		
16H-5, 9	144.59	16H-6, 100	145.30		
16H-6, 110	147.10	17H-1, 103	147.33		
16H-6, 143	147.43	17H-1, 137	147.67		
17H-3, 24	151.24	17H-4, 56	151.36		
17H-5, 107	155.07	17H-6, 85	154.65		
17H-6, 117	156.67	18X-1, 35	156.15		
18H-1, 149	158.99	18X-2, 115	158.45	1H-2, 130	157.80
18H-2, 77	159.77	18X-3, 45	159.25	1H-3, 62	158.62
18H-6, 110	166.10			2H-1, 120	165.70
18H-7, 46	166.96			2H-2, 81	166.81

1970; Foreman, 1975), on the basis of the absence of *E. matuyamai* and *Stichocorys peregrina* and the presence of *Lamprocyrtis heteroporos*. Radiolarian abundances in these samples vary from rare to abundant. Although the top of this zone, as defined from the radiolarian assemblage at Site 881, is approximately comparable to that shown in other studies (Hays, 1970; Kling, 1973; Foreman, 1975; Wolfart, 1981; Morley, 1985), the placement of the base of this zone in the early Pliocene agrees with Kling (1973), who reported the LO of *S. pere-*

**Table 6. Gaps between piston Cores 1H and 18H in Hole 881B and 1H and 18X in Hole 881C (from correlation of GRAPE data, magnetic susceptibility measurements, and volcanic ashes).**

Hole 881B coring gaps (cm)		Hole 881C coring gaps (cm)	
Between core and core	is a gap of	Between core and core	is a gap of
1H	2H 95	1H	2H 165
2H	3H 95	2H	3H 60
3H	4H no gap	3H	4H 50(?)
4H	5H 95	4H	5H no gap
5H	6H 165	5H	6H 70(?)
6H	7H 55	6H	7H 10
7H	8H no gap	7H	8H 260(?)
8H	9H 170	8H	9H no gap
9H	10H no gap	9H	10H 135
10H	11H 70(?)	10H	11H 30(?)
11H	12H 10(?)	11H	12H 30(?)
12H	13H no gap	12H	13H 30
13H	14H 130(?)	13H	14H 90(?)
14H	15H no gap	14H	15H no gap
15H	16H 20	15H	16H 40
16H	17H no gap(?)	16H	17H 45
17H	18H no gap	17H	18X 10

*grina* at this time in sediments from the eastern North Pacific Ocean. Foreman (1975), Reynolds (1980), Wolfart (1981), and Morley (1985), however, reported the LO of *S. peregrina* in younger sediments from warmer waters of the western and eastern North Pacific Ocean, placing the base of the *Lamprocyrtis heteroporos* Zone in the late Pliocene. These data indicate that the LO of *S. peregrina* occurs older (early Pliocene [ $>3.5$  Ma]) in North Pacific sites north of approximately  $45^{\circ}$ N, compared with North Pacific sites south of this latitude. As a consequence of the older LO of *S. peregrina*, the *L. heteroporos* Zone in sediments from the high North Pacific covers a longer time period, ranging over 1.5 m.y. It may be appropriate to divide the *L. heteroporos* Zone in high-latitude North Pacific sediments into upper and lower parts delineated by the FO of *Cycladophora davisiana* var. *davisiana*, which occurs at approximately 3.0 Ma.

Radiolarians are common in the next core-catcher samples from Hole 881C (145-881C-27X-CC through -30X-CC). The occurrence of both *L. heteroporos* and *S. peregrina* in these sediments places this sequence in the *Sphaeropyle langii* Zone (Foreman, 1975). The FO of this species (*Sphaeropyle langii*) defines the base of this zone. Because this species occurs at low abundances in sediments from this site, the FO of *L. heteroporos*, which falls at or just above the FO *S. langii*, was used to identify the base of this zone at this site. The placement of the base of this zone near the Miocene/Pliocene boundary agrees with other studies of North Pacific Ocean sediments (Foreman, 1975; Reynolds, 1980; Wolfart, 1981 [referred to as upper *Stichocorys peregrina* Zone]). This zone contains the LO of both *Theocorys redondoensis* and *Stichocorys delmontensis*.

Radiolarians are common in the remaining Samples 145-881C-32X-CC through -36X-CC from Hole 881C. The sediments from Samples 145-881C-32X through -35X-CC have been assigned to the *S. peregrina* Zone (Riedel and Sanfilippo, 1970, 1978). This zone is characterized by the common occurrence of both *S. peregrina* and *T. redondoensis*, the rare occurrence of *S. delmontensis*, and the absence of *L. heteroporos*. The oldest sediments from Hole 881C (Sample 145-881C-36X-CC) do not contain the characteristic fauna used to define most radiolarian sequences of late Miocene age. Rare *Cyrtocapsella tetrapera* are present in sediments from Sample 145-881C-36X-CC. Although commonly found near the top of the *Diartus petterssoni* Zone (Riedel and Sanfilippo, 1970, 1978) (i.e., Ling, 1973; Wolfart, 1981), this species has been reported in studies of Antarctic Ocean sediments as occurring earlier (i.e., Chen, 1975) and later (i.e., Abelmann, 1992). Because of the presence in this sample of *S. peregrina*, *S. delmontensis*, and *T. redondoensis*, in addition to *C. tetrapera*, this sample is probably from the transition between the *S. peregrina* and the *D. penultima* zones. It has been tentatively assigned to the *Didymocorys penultima* Zone (Riedel and Sanfilippo, 1970).

**Table 7. Composite depth model for Site 881 for the last 2.6 Ma generated by splicing sections from the offset Hole 881C across core breaks in the main hole, Hole 881B.**

Hole 881A		Hole 881B		Interval thickness (m)	Cumulative composite depth (mbsf)
Core, section, interval (cm)	Depth (mbsf)	Core, section, interval (cm)	Depth (mbsf)		
1H-1, 0	(6.00)				
1H-4, 100	(5.50)			5.50	5.50
		2H-1, 0	(3.80)		
		2H-4, 12	(8.42)	4.62	10.12
2H-3, 05	(8.55)				
2H-6, 155	(14.44)			5.89	16.09
		3H-1, 125	(14.55)		
		3H-3, 15	(16.45)	1.90	17.91
3H-1, 30	(15.30)				
3H-6, 134	(23.84)			8.54	26.45
		4H-1, 32	(23.12)		
		4H-2, 39	(24.69)	1.57	28.02
4H-1, 146	(25.96)				
4H-6, 140	(33.40)			7.44	35.46
		5H-1, 20	(32.50)		
		5H-2, 118	(34.98)	2.48	37.94
5H-1, 114	(35.14)				
5H-6, 138	(42.88)			7.74	45.68
		6H-1, 144	(43.24)		
		6H-4, 137	(47.67)	4.43	50.11
6H-2, 107	(46.07)				
6H-6, 106	(52.06)			5.99	56.10
		7H-2, 131	(54.11)		
		7H-6, 61	(59.41)	5.30	61.40
7H-3, 83	(56.83)				
8H-6, 90	(70.90)			14.07	75.47
		8H-6, 117	(68.47)		
		9H-2, 59	(72.39)	3.92	79.39
9H-1, 43	(72.43)				
9H-7, 40	(81.40)			8.97	88.36
		10H-1, 6	(79.86)		
		10H-2, 29	(81.56)	1.70	90.06
10H-2, 21	(83.21)				
10H-7, 18	(90.68)			7.47	97.53
		10H-7, 9	(88.89)		
		11H-1, 141	(90.71)	1.82	99.35
11H-1, 110	(92.10)				
11H-6, 147	(109.33)			7.87	107.22
		12H-1, 29	(99.09)		
		12H-1, 110	(99.90)	0.81	108.03
12H-1, 34	(100.84)				
12H-6, 133	(109.33)			8.49	116.52
		13H-1, 87	(109.17)		
		15H-6, 15	(134.95)	25.78	142.30
15H-4, 130	(134.80)				
15H-6, 138	(137.88)			3.08	145.38
		16H-1, 100	(137.80)		
		16H-6, 100	(145.30)	7.50	152.88
16H-5, 9	(144.59)				
16H-6, 110	(147.10)			2.51	155.39
		17H-1, 103	(147.33)		
		17H-6, 85	(154.65)	7.32	162.71
17H-5, 107	(155.07)				
17H-6, 117	(156.67)			1.60	164.31
		18H-1, 35	(156.15)		
		18H-2, 115	(158.45)	2.30	166.61

## Diatoms

Diatoms are generally common to abundant and moderately well to well preserved throughout the upper Miocene through Quaternary section recovered at Site 881. In parts of the upper Pliocene and Quaternary section, however, diatoms are few because of increases in clay and other detrital materials. Assemblages are commonly dominated by *Coscinodiscus marginatus*, a large, robust diatom that is resistant to dissolution and fragmentation.

A complete sequence from the *Neodenticula seminae* Zone into the *Thalassionema schraderi* Zone was recovered from the four holes cored at Site 881 (Figs. 10 and 11). The single core taken from Hole 881A contains rare *Simonseniella curvirostris* and has been assigned to the *S. curvirostris* zone. However, comparison with the diatom stratigraphy of Cores 145-881B-1H and 145-881C-1H suggests that these specimens of *S. curvirostris* have been reworked and that Core 145-881A-1H is more likely equivalent to the *Neodenticula seminae* Zone.

In Holes 881B and 881C, the same Quaternary to upper Pliocene interval was cored between the seafloor and about 165 mbsf. The boundary between the late Quaternary *N. seminae* and *S. curvirostris* Zones can be recognized by the LO of *S. curvirostris* in Samples 145-881B-1H-CC and -145-881C-4H-CC (Table 8). It is possible that this boundary has been placed two cores too high in Hole 881B, because *S. curvirostris* becomes common only in Sample 145-881B-4H-CC. The last consistent occurrence of *Actinocyclus oculatus* in Samples 145-881B-8H-CC and 145-881C-8H-CC has been used to place the boundary between the *S. curvirostris* and *A. oculatus* zones in these holes. A rare occurrence of *Rhizosolenia matuyamai* in Sample 145-881C-8H-CC indicates correlation with a short interval spanning the Jaramillo normal-polarity subchron and is supportive of this correlation.

Following Koizumi (1992), the base of the *A. oculatus* Zone and top of the underlying *Neodenticula koizumi* Zone is defined by the LO of *N. koizumi*. This latest Pliocene event falls between Samples

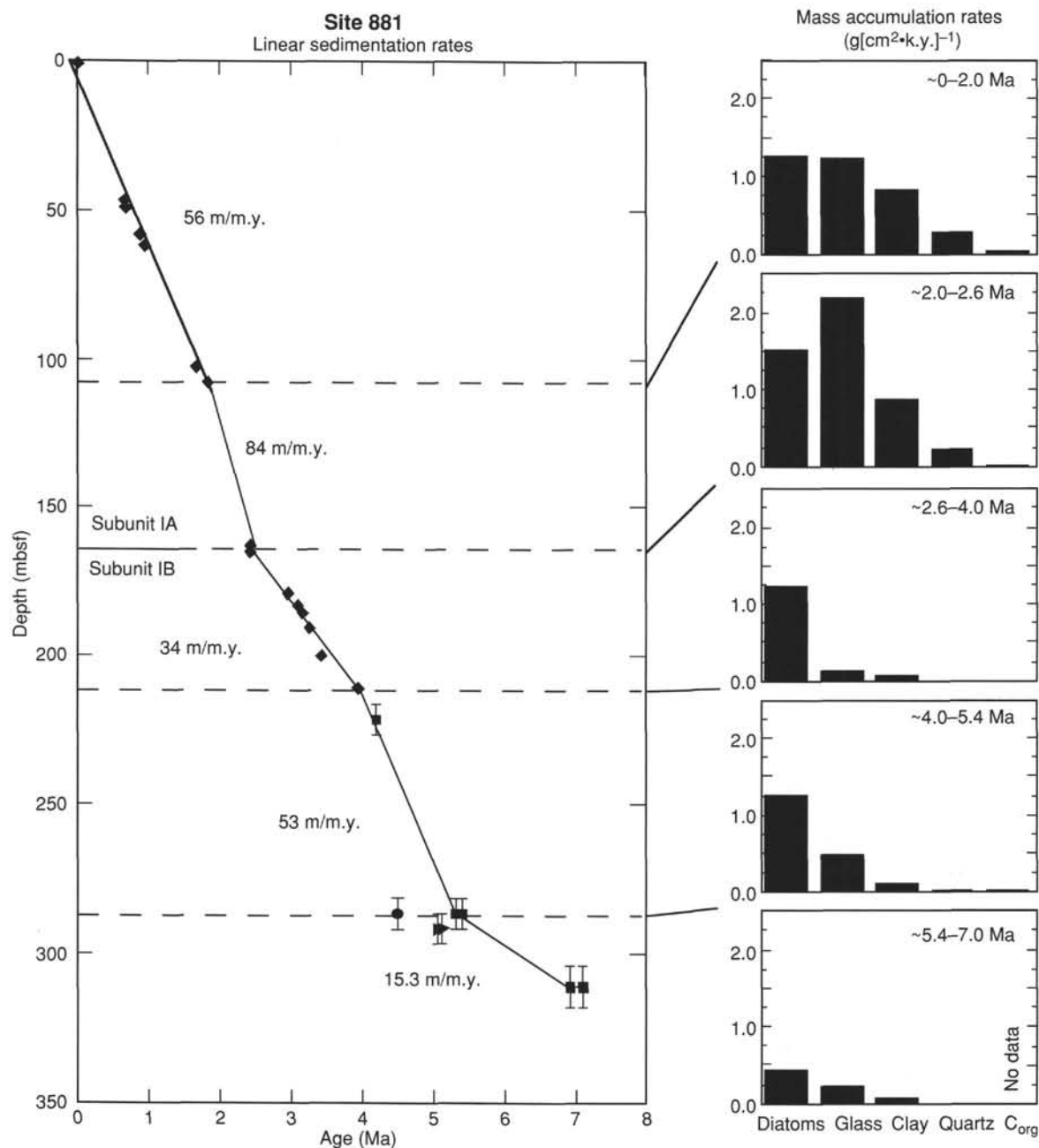


Figure 9. Plot of composite sedimentation rate for Holes 881A to 881C of Site 881 (left) using magnetostratigraphy above ~210 mbsf (diamonds) and biostratigraphy below 210 mbsf (squares, circles, and triangles = diatom, radiolarian, and nannofossil datum levels, respectively). Dashed lines mark significant changes in the linear rate of sedimentation. On the right, histograms show the average flux (mass accumulation rate, in g[cm<sup>2</sup>·k.y.]<sup>-1</sup>) of sedimentary components for each of the five time-stratigraphic intervals delimited by the dashed lines. It is evident that the major lithological break at this site (at ~164 mbsf) resulted from a dramatic increase in fluxes of glass, clay, and quartz that began 2.6 m.y. ago.

145-881B-11H-CC and -12H-CC and between Samples 145-881C-11H-CC and -12H-CC in Holes 881B and 881C, respectively.

The top of the underlying *Neodenticula koizumii*-*N. kamschatkana* Zone has been placed at the last common occurrence of *N. kamschatkana*, between Samples 145-881C-18X-CC and -21H-CC. This horizon falls below Core 145-881B-18H, the last core taken at Hole 881B; however, it occurs between Samples 145-881D-1H-CC and -2H-CC. According to Koizumi (1992), the FO of *Neodenticula seminiae* should fall immediately below this datum level. The lowest record of *N. seminiae* in Samples 145-881C-18X-CC and 145-881D-1H-CC

thus are supportive of this placement of the top of the *N. koizumii*-*N. kamschatkana* Zone, in Holes 881C and 881D, respectively.

The FO of *Neodenticula koizumii* in Sample 145-881C-23X-CC marks the boundary between the *N. koizumii*-*N. kamschatkana* Zone and the underlying *N. kamschatkana* Zone. The rare occurrence of *N. koizumii* in the core-catcher sample of Core 145-881D-6H indicates that the lowest horizon cored in Hole 881D falls within the *N. koizumii*-*N. kamschatkana* Zone.

The boundary between subzone a and subzone interval b-c of the *N. kamschatkana* Zone can be recognized by the LO of *Rouxia cali-*

**Table 8. Age and stratigraphic position of radiolarian (R) and diatom (D) datum levels in Holes 881B, 881C, and 881D.**

Sample no.		Datum	CK92 (Ma)	Hole 881B	Depth (mbsf)	Hole 881C	Depth (mbsf)
R1	LO	<i>Lychnocanoma grande</i>	0.05	/1H-CC	/5.5	/1H-CC	/3.8
D2	LO	<i>Simonseniella curvirostris</i>	0.30	1H-CC/2H-CC	5.5/15.0	3H-CC/4H-CC	22.8/32.3
R2	LO	<i>Drupptractus acquiloniis</i>	0.35	2H-CC/3H-CC	15.0/24.5	3H-CC/4H-CC	22.8/32.3
R3	LO	<i>Stylatractus univertus</i>	0.45	2H-CC/3H-CC	15.0/24.5	3H-CC/4H-CC	22.8/32.3
R4	LO	<i>Lamprocyrtis neoheteroporos</i>	0.78	7H-CC/8H-CC	62.5/72.0	7H-CC/8H-CC	60.8/70.3
D3	LO	<i>Rhizosolenia matuyamai</i>	1.04-0.91			7H-CC/8H-CC	60.8/70.3
R5	LO	<i>Eucyrtidium matuyamai</i>	1.05	7H-CC/8H-CC	62.5/72.0	7H-CC/8H-CC	60.8/70.3
D4	FO	<i>Rhizosolenia matuyamai</i>	1.12-0.98			8H-CC/9H-CC	70.3/79.8
D5	LCO	<i>Actinocyclus oculatus</i>	1.00	7H-CC/8H-CC	62.5/72.0	7H-CC/8H-CC	60.8/70.3
D6	FO	<i>Simonseniella curvirostris</i>	1.58	10H-CC/11H-CC	91.0/100.5	11H-CC/12H-CC	98.8/108.3
D7	LO	<i>Coccinodiscus pustulatus</i>	1.8	10H-CC/11H-CC	91.0/100.5	11H-CC/12H-CC	98.8/108.3
R7	FO	<i>Eucyrtidium matuyamai</i>	1.9	12H-CC/13H-CC	110.0/119.5	13H-CC/14H-CC	117.8/127.3
D9	LO	<i>Neodenticula koizumii</i>	2.0	11H-CC/12H-CC	100.5/110.0	11H-CC/12H-CC	98.9/108.3
D11	LO	<i>Thalassiosira convexa</i>	2.4	15H-CC/16H-CC?	138.5/148.0		
				Hole 881D		Hole 881D	
D12	LCO	<i>Neodenticula kamtschatica</i>	2.63-2.7	1H-CC/2H-CC	164.75/174.0	18X-CC/21H-CC	162.3/191.2
D13	FO	<i>Neodenticula seminae</i>	2.7			18X-CC/21H-CC	162.3/191.2
R8	FO	<i>Cycladophora davistiana</i>	2.8	2H-CC/3H-CC	174.0/183.5	18X-CC/21H-CC	162.3/191.2
R9	LO	<i>Stichocorys peregrina</i>	2.9			25X-CC/27X-CC	228.7/248.0
D14	LO	<i>Thalassiosira marujamica</i>	3.2	3H-CC/4H-CC	183.5/193.0	18X-CC/21H-CC	162.3/191.2
D15	LO	<i>Thalassiosira jacksonii</i>	3.3	3H-CC/4H-CC	183.5/193.0	18X-CC/21H-CC	162.3/191.2
R10	LO	<i>Stichocorys delmontensis</i>	3.55			27X-CC/29X-CC	248.0/267.2
D17	FO	<i>Neodenticula koizumii</i>	3.75	>6H-CC		23X-CC/25X-CC	209.7/228.7
R11	LO	<i>Theocorys redondoensis</i>				29X-CC/30X-CC	267.2/276.9
R12	FO	<i>Lamprocyrtis heteroporos</i>	4.6			30X-CC/32X-CC	276.9/296.2
D18A	LO	<i>Thalassiosira plicata</i>	4.6			27X-CC/29X-CC	248.0/267.2
D19	FO	<i>Thalassiosira latimarginata</i>	5.05			29X-CC/30X-CC	267.2/276.9
D21	FO	<i>Thalassiosira oestrupii</i>	5.4			30X-CC/32X-1, 46	276.9/286.96
D22	LO	<i>Rouxia californica</i>	6.3			32X-3, 46/32X-CC	288.46/296.20
D24C	FO	<i>Thalassiosira jacksonii</i>	6.8	32X-CC/35X-CC	296.2/325.10		
D24D	FO	<i>Nitzschia reinholdii</i>	6.9			35X-CC/36X-CC	325.1/334.8
D25	FO	<i>Neodenticula kamtschatica</i>	7.25			35X-CC/36X-CC	325.1/334.8
D26	LO	<i>Thalassionema schraderi</i>	7.45			35X-CC/36X-CC	325.1/334.8

Notes: Samples constraining each datum level are separated by a slash (/) as is the meters below seafloor depths (mbsf) of these samples. LO = last occurrence; LCO = last common occurrence; FO = first occurrence. CK92 refers to the Cande and Kent (1992) geomagnetic polarity time scale.

*formica* between Samples 145-881C-32X-3, 46 cm, and -32X-CC. The FO of *Thalassiosira oestrupii* between Samples 145-881C-30X-CC and -32X-1, 46 cm, appears to be slightly younger than this event, as has been suggested by Barron (1992). Within subzone interval b-c, the FO of *Thalassiosira latimarginata* between Samples 145-881C-29X-CC and -30X-CC, may be a more useful datum level in the open ocean for dividing subzones b and c of the *N. kamtschatica* Zone than the LO of *Coccinodiscus insignis* (Barron, 1980), which appears to be restricted to marginal sequences.

The FO of *N. kamtschatica* and the last common occurrence of *Thalassionema schraderi* between Samples 145-881C-35X-CC and -36X-CC mark the base of the *N. kamtschatica* Zone and the top of the underlying *T. schraderi* Zone at approximately 7.25 Ma. The presence of *Nitzschia reinholdii* in Sample 145-881C-36X-CC, however, indicates that the base of the cored section at Site 881 may be younger than 6.9 Ma, an assignment that is more consistent with that of the radiolarians.

### Placement of Epoch Boundaries

The epoch and subepoch boundaries have been placed based on the biostratigraphy and the interpretation of magnetostratigraphy shown in Figures 10 and 11, as follows:

1. Pliocene/Quaternary = 103 mbsf in Hole 881B; approximately 101 mbsf in Hole 881C;
2. lower Pliocene/upper Pliocene = 198 mbsf in Hole 881D; and
3. Miocene/Pliocene = 265 mbsf in Hole 881C.

## PALEOMAGNETISM

### Procedures

Pass-through measurements were performed on all APC and XCB cores from Site 881. Both the natural remanent magnetization (NRM)

and the remanence after alternating field (AF) demagnetization at 15 mT were measured at a sample spacing of 10 cm. Discrete samples were measured using both the Molspin and the Japanese spinner magnetometers. Approximately three 7-cm<sup>3</sup> samples from each section of Hole 881B were demagnetized in five steps up to 30 mT. From one of these samples, the Japanese instrument also provided susceptibility and anhysteretic remanent magnetization (ARM) data. Automated susceptibility ( $\chi$ ) measurements were performed at 5-cm intervals in whole cores, in conjunction with other measurements performed using the multisensor track (MST). Although the multishot orientation devices were not deployed at this site, at this latitude, the remanent inclination data provide unambiguous polarity information, so that a magnetostratigraphy can easily be constructed. In principle, the mean declinations of the cores could be used to orient them should this be necessary at a future date.

## Results

Pass-through measurements of NRM and whole-core susceptibility are shown in Figure 12 for Hole 881B. In general, remanence intensities are high (5–50 mA/m), with scattered extremely high (>100 mA/m) readings, usually coinciding with the presence of dropstones or black ash layers. However, the NRM intensity, in fact, represents a low-field isothermal remanent magnetization (IRM) acquired in the field of the core barrel. This field apparently was directed vertically up the core barrel because the NRM was almost invariably steeply reversed. Discrete-sample measurements demonstrate that this coring overprint was easily removed with AF demagnetization fields as low as 5 to 10 mT (Fig. 13). The remanent intensity decreases by almost an order of magnitude below about 160 mbsf (Fig. 12). This NRM transition coincides with changes in many other physical property measurements and with downhole logging results. This transition also coincides with a decrease in clay content and

percentage of ash layers to represent the boundary between lithologic Subunits IA and IB.

Whole-core susceptibility measurements show numerous discrete peaks superimposed on a background value. These peaks appear to coincide with IRD (dropstones and gravels) and the many ash layers, especially the black ash layers. Large peaks in Hole 881D correspond with accumulations of gravels that occurred at the top of each core. In a fashion similar to the NRM signal, the background susceptibility signal shows a considerable decrease at approximately 160 mbsf. Roughly coincident with this decrease is a drop-off in the frequency and amplitude of discrete susceptibility peaks associated with ash layers and dropstones.

Measurements of ARM and low-field susceptibility were performed with the Japanese spinner magnetometer and the Bartington susceptibility meter for discrete samples from each section of Hole 881B. Results for 0 to 80 mbsf are shown in Figure 14. Both the ARM and  $\chi$  values show variations similar to those of the NRM intensity (Fig. 14). The ARM/ $\chi$  ratio indicates a fairly consistent magnetic grain size with depth in this depth interval. However, this ratio does indicate that magnetic grain sizes change (toward coarser values) and are associated with some of the low values in NRM intensity (Fig. 14).

With the exception of a few apparently disturbed regions of the cores, the sediments may record stable normal and reversed-field directions (axial dipole field inclination is about  $\pm 65.8^\circ$  at a latitude of  $47^\circ 06'N$ ). For the most part, the discrete sample demagnetizations show a straight line to the origin on Zijderveld plots after removal of the coring overprint between 5 and 10 mT. Therefore, the whole-core measurements after 15 mT demagnetization have been used for magnetostratigraphic interpretations at this site. The discrete sample directions after demagnetization at 30 mT show almost perfect agreement with this whole-core result (Fig. 15).

## Discussion

A magnetostratigraphic interpretation of the whole-core inclination records (Figs. 15 and 16) was done with the aid of the biostratigraphic framework established for this site. The magnetic record contains more events than those listed in the Cande and Kent (1992) time scale, and in Hole 881B, an extra polarity interval can be seen. Identification of the Brunhes/Matuyama reversal and the Jaramillo and Olduvai chrons is straightforward in Hole 881B. However, below the Olduvai, two periods of normal polarity can be seen that would have to be assigned to Reunion events 1 and 2, although these polarity intervals are much thicker than expected for these events. The Matuyama/Gauss boundary then would coincide with the reversal at the base of Hole 881B (approximately 165 mbsf). Correlation of these results with those from Hole 881C (Fig. 16) becomes difficult at the presumed location of the Olduvai Chron, which does not appear to be recorded in Hole 881C. This is not the result of a depth offset between the two holes because their whole-core susceptibility and GRAPE records clearly correlate and indicate not more than a 1-m offset at these depths (130–150 m). Thus, either an extra event is found in Hole 881B or an event is missing in Hole 881C. Anomalously shallow reversed directions do occur at the depths where the Olduvai Chron would be expected in Hole 881C. Therefore, a possible explanation for the missing chron lies in the extreme tilt (as much as  $60^\circ$ ) and disturbance of layers observed at these depths in Hole 881C. Untilting the anomalously shallow reversed directions in Hole 881C might easily restore directions to normal polarity in this zone. The restored Olduvai Chron, however, would be short and would cover only about 4 m. Unfortunately, we do not have any means to calculate the real dip value and direction of the layers within the core; the value from the surface of the core halves represents a minimum estimate. Another explanation for the missing Olduvai event is suggested by data from the bottom few meters of Core 2H in Hole 881D, where an influx of sediment occurs. The data illustrate that any coring disturbance that results in remobilization of the sediment will produce a reversed remagnetization (in the core barrel field),

which cannot be removed with demagnetization. This result implies that while one would find it very difficult to create normal polarity inclinations artificially by coring disturbance, one could certainly eliminate normal polarity and replace it with reversed inclinations.

Directional data from the XCB cores taken below 160 mbsf in Hole 881C were not sufficiently consistent to interpret in terms of magnetostratigraphy. However, the APC core data from Hole 881D (155–212 mbsf) were of excellent quality (Fig. 17) and provided clear determination of the Matuyama/Gauss and Gauss/Gilbert boundaries, and the Kaena and Mammoth subchrons. This means that a continuous magnetostratigraphy is available for this site from the present to the top of the Cochiti subchron, in the Gilbert at 4.033 Ma (depths to boundaries are given in Table 9).

## SEDIMENTATION RATES AND FLUXES

### Sedimentation Rates

Rates of sedimentation at Site 881 have been calculated using magnetostratigraphy for the past 4 m.y. and biostratigraphy for older sediments. In general, for the past 4 m.y., biostratigraphy and magnetostratigraphy are in excellent agreement; thus, for clarity in Figure 9, only paleomagnetic datum levels (for Holes 881B, 881C, and 881D) have been plotted for the younger part of the section. The slight depth offset among Site 881 holes was not corrected. The excellent paleomagnetic age control for the past 4 m.y. shows significant variability in the linear rates of sedimentation at Site 881, with breaks in the curve marked by dashed lines (Fig. 9). Sedimentation varied by more than a factor of two at this site during the past 4.0 m.y., from 34 m/m.y. during the "pre-Northern Hemisphere glaciation" interval (~2.6–4.0 Ma) to 84 m/m.y. during the late Pliocene (~2.0–2.6 Ma).

Where age control has been limited to biostratigraphy, it is evident that rates of sedimentation were as high during the early Pliocene as during the Pleistocene, but reached minimum values older than 5.4 Ma during the latest Miocene. This important change appears robust, despite some scatter in the biostratigraphic datum levels near the Miocene/Pliocene boundary (Fig. 9).

### Sediment Fluxes

Sediment fluxes, or mass accumulation rates, were determined in the conventional way, by taking the product of the sedimentation rate, the dry-bulk density, and the concentration of the sediment component. Calculations were performed for each of the five intervals where obvious differences in linear sedimentation rates occurred. Dry-bulk density values were taken from pycnometer measurements, and sedimentary component data come from smear slide estimates, with the exception of organic carbon data ( $C_{org}$ ), which were measured analytically and found to be uniformly low (Table 10). Flux results (in  $g/cm^2 \cdot k.y.$ )<sup>-1</sup> for diatoms, glass, clay, quartz, and  $C_{org}$  are listed in Table 10 and are shown as histograms along the right axis of Figure 9 for each of the five time-stratigraphic intervals. These results are only semiquantitative, with the greatest source of error probably resulting from estimates of smear-slide abundances. Additional errors may stem from the necessity to assume that the abundance estimates are directly proportional to the weight percentage of each sedimentary component. Thus, taking the 0- to 2-Ma interval for example, we assume that an average of 33% diatoms translates directly to 0.33 g diatoms per gram of bulk sediment. The resulting diatom (opal) flux for that interval,  $\sim 1.25 g/cm^2 \cdot k.y.$ <sup>-1</sup>, is close to the glacial and interglacial opal fluxes (0.5 and 1.5  $g/cm^2 \cdot k.y.$ <sup>-1</sup>, respectively) measured by Keigwin, Jones, and Froelich (1992) to the northeast on Meiji Seamount.

Even with the uncertainties in our flux calculations, it appears that important flux changes may have taken place in Site 881. As noted in the lithological description of this site, significant change occurred at about 164 mbsf (~2.6 Ma). In lithologic Subunit IA, the volcanic ash-bearing diatom ooze and clayey diatom ooze, both the 0- to 2-Ma and the 2- to 2.6-Ma intervals have been marked by high (and

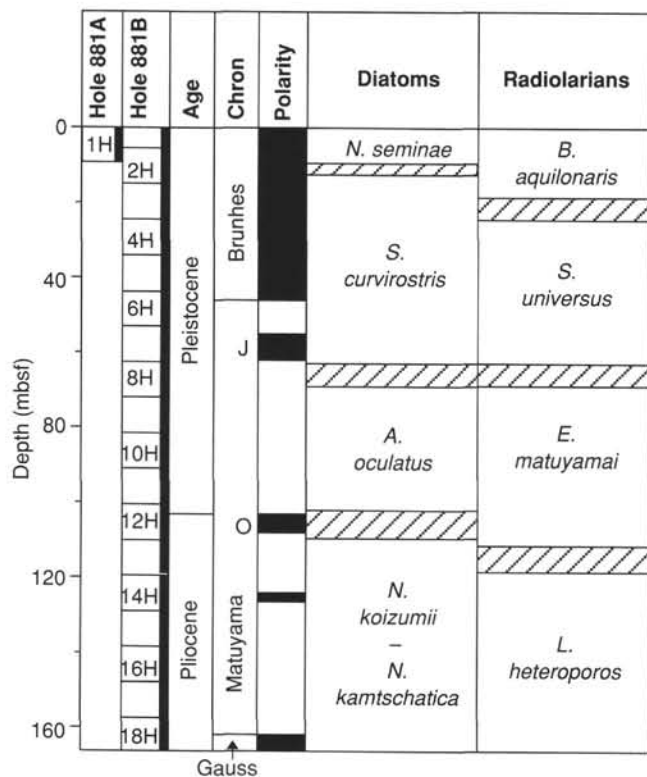


Figure 10. Stratigraphic position of cores, recovery (black), placement of magnetostratigraphic chrons and subchrons, and placement of diatom and radiolarian zones in Holes 881A and 881B. Intervals filled by slanted lines indicate uncertainty in the placement of magnetostratigraphic and biostratigraphic boundaries.

comparable) fluxes of diatoms, glass, clay, and quartz. Older than 2.6 Ma, in Subunit IB (radiolarian-bearing diatom ooze), a dramatic decrease is seen in glass, clay, and quartz fluxes, with minimum diatom flux during the late Miocene (older than ~5.4 Ma).

We judge the major break in flux patterns at ~2.6 Ma to be significant because it is driven by decreased rates of sedimentation, decreased dry-bulk densities, and decreased concentrations of glass, clay, and quartz before that time. In other words, no single term in the flux calculation dominates the results. Although these results are still preliminary, the increased fluxes of clay and quartz beginning at ~2.6 Ma in the northwestern Pacific Ocean most likely resulted from increased glaciation at that time. Rea and Schrader (1985) reported that the onset of significant ice rafting was coincident with the onset of glaciation in the North Atlantic Ocean. Should further research at Site 881 support our flux calculations, then the onset of glaciation in Siberia and Kamchatka was synchronous with the onset of Laurentide and Fennoscandian glaciation, as seen from cores in the North Atlantic Ocean (Shackleton et al., 1984). The abrupt increase in the flux of glass at Site 881 at ~2.6 Ma may signal an increase in explosive volcanism associated with increased glaciation, a pattern observed at many other locations during late Cenozoic time (Kennett and Thunell, 1975).

## INORGANIC GEOCHEMISTRY

Twenty interstitial water samples were collected at Site 881: three from Hole 881A at depths ranging from 4.0 to 13.0 mbsf and 17 from Hole 881C at depths ranging from 1.5 to 321.4 mbsf. Analytical results have been plotted separately for the two sets of samples in all graphs in this section. Concentrations of most parameters in the two sets are comparable for similar sub-bottom depths, with the exceptions of dissolved silicate, potassium, magnesium, and chloride, as

noted below. All data are listed in Table 11. The pore water samples span nearly the entire depth range of the sediments drilled at this site, including the volcanic-ash-bearing diatom and clayey diatom oozes of lithologic Subunit IA (0–164.5 mbsf) and the radiolarian-bearing diatom ooze of Subunit IB (164.5–363.8 mbsf). Volcanic ash is rare in the latter (see “Lithostratigraphy” section, this chapter). Carbonate-rich layers and concretions are minor but frequently appearing components in Subunit IA. Dolomite has been identified by X-ray diffractometry in at least some of the concretions and layers and may be the principal authigenic carbonate at this site.

Chloride concentrations in interstitial waters at Site 881 range from near the Pacific Ocean Deep Water value (554 mM) in the shallow sample of Hole 881A (4.0 mbsf) to a maximum of ~576 mM at 38.3 mbsf in Hole 881C (Fig. 18A). The 1- $\sigma$  standard deviation of the measurements at the levels shown is about  $\pm 3$  mM; thus, the small-scale variations in the profile are most probably attributable to analytical scatter. The broader trend of an increasing concentration with depth in the upper 50 m and a gradual, slight decrease in the underlying deposits probably reflects the ongoing adjustment of the  $\text{Cl}^-$  concentration in pore waters to variations in the mean salinity of the ocean, which has increased over the last few million years as continental ice volume expanded (McDuff, 1985).

The bacterially catalyzed degradation of organic matter in marine sediments is accomplished through progressive utilization of a suite of terminal electron acceptors, including, in order of free energy yield,  $\text{O}_2$ ,  $\text{NO}_3^-$ ,  $\text{MnO}_2$ ,  $\text{FeOOH}$ , and  $\text{SO}_4^{2-}$  (Froelich et al., 1979). Where demand exceeds supply, for example through downward diffusion, the oxidants will be sequentially depleted in the order listed, yielding reaction products such as  $\text{Mn}^{2+}$ ,  $\text{Fe}^{2+}$ , and  $\text{H}_2\text{S}$ . To assess the nature of such early diagenetic reactivity at Site 881, the concentrations in interstitial waters of the redox-sensitive species  $\text{Mn}^{2+}$  and  $\text{NO}_2^-$  were measured. An attempt to measure the nitrate concentration was unsuccessful owing to the poor performance of a trio of nitrate reduction columns that were packed aboard the ship. In lieu of shipboard measurements, subsamples of pore waters were frozen and will be analyzed for  $\text{NO}_3^-$  onshore.

Although sedimentary organic carbon concentrations in Site 881 sediments are low (see “Organic Geochemistry” section, this chapter), the organic carbon accumulation rate is moderate, reflecting high rates of sedimentation in this area (see “Accumulation Rates and Fluxes” section, this chapter). The oxidant demand associated with the organic carbon burial flux is sufficient to deplete oxygen at shallow depths at Site 881, as evidenced by the significant enrichment of  $\text{Mn}^{2+}$  in the shallowest pore water sample (1.5 mbsf) collected at the site (Hole 881C; Table 11). Nitrite was undetectable ( $<0.5 \mu\text{M}$ ) in the top several samples, suggesting that nitrate reduction is essentially complete at shallow depths. Manganese is depleted at depth (Fig. 18B), probably because of the precipitation of authigenic manganese carbonate. A subtle increase in the concentration of dissolved manganese in the deepest sample may indicate upward diffusion of  $\text{Mn}^{2+}$ , produced by the reductive dissolution of  $\text{MnO}_2$  in the pelagic brown clay facies that is presumed to underlie the siliceous ooze deposits at this site.

Titration alkalinity increases steadily from ~3 mM at the top of the section to a maximum of ~8 mM at about 120 mbsf (Fig. 18C). Significant upward convexity in the profile between 25 and 100 mbsf indicates that the highest rate of production of alkalinity (mostly bicarbonate ion at the pH measured in the samples; Table 11) is occurring in this zone. This suggestion is supported by the sulfate profile, which shows downward concavity in the same depth interval, indicating maximum rates of sulfate reduction in this zone (Fig. 18D). Below the maximum at 120 mbsf, alkalinity decreases approximately linearly to ~250 mbsf, beneath which slight downward concavity implies that dissolved carbonate species are being consumed from solution. The approximate linearity in the sulfate profile between 1.5 and 25 mbsf and between ~100 and 350 mbsf indicates control by diffusion and the absence of significant sulfate reduction in these zones, as shown in Figure 18D.

**Table 9. Depths of polarity of chron boundaries in Holes 881B, 881C, and 881 D.**

Polarity chron	Depth (mbsf)			Age (Ma) (CK92)
	Hole 881B	Hole 881C	Hole 881D	
Brunhes/Matuyama	46.50 (6H-3, 0 cm)	48.10 (6H-5, 30 cm)		0.780
Termination Jaramillo	55.05-58.1 (7H-2, 55 cm– 7H-4, 60 cm)	57.60 (7H-5, 30 cm)		0.984
Onset Jaramillo	61.70 (7H-6, 120)	62.5 or 66.7 (8H-2, 20 cm or 8H-4, 140 cm)		1.049
Termination Olduvai	103.60 (12H-3, 10 cm)	105(?) (12H-5, 20 cm?)		1.757
Onset Olduvai	108.95 (12H-6, 95 cm)	109.9? (13H-2, 10 cm?)		1.983
Termination Réunion	117.8–119.8 (13H-6, 30 cm)	123.05 (14H-4, 75 cm)		2.197
Onset Réunion	121.5(?) (14H-2, 50 cm)	127.50 (14H-7, 70 cm)		2.229
Matuyama/Gauss	164.80 (18H-2, 130 cm)		163.0-164.5 (1H-6, 5 cm– 2H-1, 0 cm)	2.600
Termination Kaena			178.20 (3H-3, 120 cm)	3.054
Onset Kaena			181.50 (3H-5, 150 cm)	3.127
Termination Mammoth			184.20 (4H-1, 70 cm)	3.221
Onset Mammoth			186.20 (4H-2, 120 cm)	3.325
Gauss/Gilbert			197.9-201.5 (5H-4, 40 cm– 5H-6, 100 cm)	3.553
Termination Cochiti			210.80 (6H-6, 80 cm)	4.033

Note: CK92 = Cande and Kent, 1992.

**Table 10. Listing of averaged sediment data and flux results for five time-stratigraphic intervals at Site 881.**

Depth (mbsf)	Age (Ma)	LSR (m/m.y.)	DBD (g/cm <sup>3</sup> )	Diatoms		Glass		Clay		Quartz		C <sub>org</sub>	
				(%)	(flux)	(%)	(flux)	(%)	(flux)	(%)	(flux)	(%)	(flux)
0–108	0–2.0	56	0.68	33	1.26	32	1.22	21	0.80	0.7	0.27	0.2	0.01
108–164	2.0–2.6	84	0.68	26	1.49	38	2.17	15	0.86	0.4	0.22	0.2	0.01
164–211	2.6–4.0	34	0.39	92	1.22	8	0.11	4	0.05	0.2	0.00	0.3	0.00
211–287	4.0–5.4	53	0.43	55	1.25	21	0.48	5	0.11	0.4	0.01	0.3	0.01
287–335	5.4–7.0	15	0.48	59	0.43	30	0.22	10	0.07	0.1	0.00	—	—

LSR = linear sedimentation rate; DBD = dry-bulk density.

Note: Flux is in units of g(cm<sup>2</sup>·k.y.)<sup>-1</sup>.

No ammonium was detected in the topmost sample (1.5 mbsf), suggesting that sulfate reduction commences at Site 881 at a greater depth. The ammonium profile is similar to that of alkalinity (Fig. 19A), indicating that NH<sub>3</sub> is being produced as a result of anaerobic degradation of organic matter, particularly between ~30 and 130 mbsf, where the profile exhibits upward convexity. The concentration of NH<sub>4</sub><sup>+</sup> decreases in a linear fashion below the maximum value at ~140 mbsf. This indicates that no ammonium is being produced between ~140 and ~330 mbsf, which further implies that the rate of degradation of organic matter is extremely low in the Pliocene to upper Miocene diatomaceous oozes in this section. This insinuation is consistent with an absence of reactivity, evinced by the sulfate distribution in this depth interval.

Dissolved calcium and magnesium tend to be distributed oppositely in Site 881 pore waters (Fig. 19B). The upward convexity of the calcium and downward concavity of the Mg<sup>2+</sup> profiles in the upper 100 m are indicative of alteration of volcanic ash, which is most abundant in the upper 160 m of the sedimentary section (see "Lithostratigraphy" section, this chapter). Such alteration releases calcium to solution, presumably from feldspars or volcanic glass, while consuming magnesium during authigenesis of magnesian smectites or

sepiolite (see McDuff and Gieskes, 1976). A minimum value in the magnesium concentration at 142 mbsf (Fig. 19A) may be a reflection of dolomite formation, as suggested by the presence of dolomitic concretions and layers (see "Lithostratigraphy" section, this chapter), particularly an obvious layer at ~150 mbsf. Dolomite formation might also explain the consumption of Ca<sup>2+</sup> between 100 and 190 mbsf, which is implied by the slight downward concavity in the calcium profile in this depth interval. Approximately constant concentrations of magnesium and calcium below 200 mbsf obviate any influence of exchange with the underlying crustal basalts on the pore water distributions of these elements in the sampled section (Fig. 19A).

The concentration of dissolved silicate in the topmost pore water sample (~690 μM) is sharply higher than that in the overlying North Pacific Bottom Water (~160 μM), reflecting dissolution of opaline skeletons near the sediment water interface (Fig. 19C). The concentration increases progressively to ~1200 μM at 200 mbsf and remains approximately constant below this horizon. Hurd and Theyer (1975) determined that the saturation concentration of dissolved silicate in equilibrium with biogenic silica was ~1100 μM, suggesting that pore waters in the lower half of the section sampled at Site 881C are saturated with respect to opal.

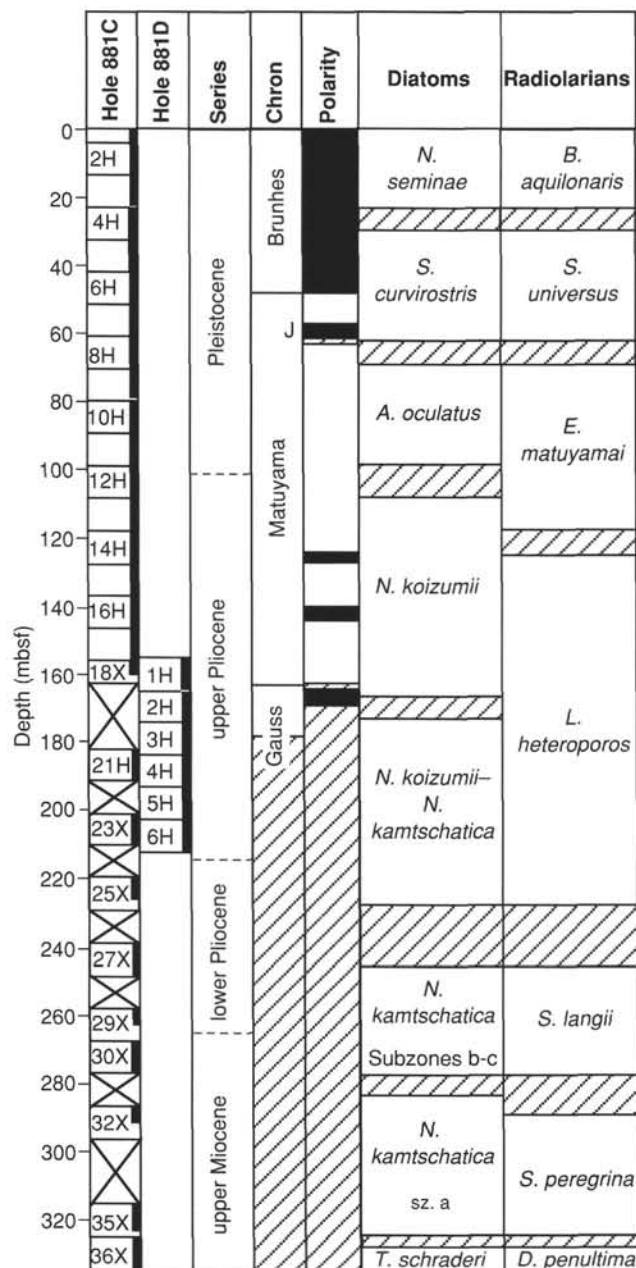


Figure 11. Stratigraphic position of cores, recovery (black), placement of magnetostratigraphic chrons and subchrons, and placement of diatom and radiolarian zones in Holes 881C and 881D. Intervals filled by slanted lines indicate uncertainty in the placement of magnetostratigraphic and biostratigraphic boundaries.

Sodium and potassium show little variation in the pore waters downcore, with concentrations being near those in seawater (sodium at 476 mM and potassium at 10.35 mM; Fig. 19D). A slight depletion of  $K^+$  between about 30 and 130 mbsf may reflect alteration of volcanic ash in this interval. The constant concentrations of sodium and potassium toward the base of the core are consistent with the calcium and magnesium data, indicating the absence of exchange with basaltic basement.

Reactive silica, potassium, and to a slight extent, sodium are slightly enriched in the trio of samples from Hole 881A relative to samples collected from similar sub-bottom depths in Hole 881C. The contrast, which is most obvious in the  $H_4SiO_4$  data, may be related to

a "temperature of squeezing" artifact (Mangelsdorf et al., 1969; Bischoff et al., 1970) if the squeezing temperatures of the two sets of samples were different. The closely spaced trio of samples from Section 145-881A-1H-1 was collected simultaneously from this one core and may have been squeezed at a higher temperature than any samples from Hole 881C. This postulate is consistent with the higher values that were measured in the samples from Hole 881A.

The concentration of strontium in the uppermost pore water samples from Hole 881A and 881C is the same as that in modern seawater (87  $\mu M$ ; Fig. 20). Like the concentration of silicate, the  $Sr^{2+}$  content generally increases downcore to 110  $\mu M$  at 330 m, possibly reflecting the alteration of volcanic ash and diagenesis of siliceous microfossils and clays. Two concentration minima of strontium occur at 50 and 130–190 m, coincident with the highest abundance of the dolomitic layers in the cores and with the highest number of ash layers (see "Lithostratigraphy" section, this chapter). This decrease of strontium in the pore fluids would be expected to accompany the precipitation of authigenic dolomite resulting from the partitioning of strontium in that phase (~1000–2000 ppm).

The concentration of lithium in the uppermost sample of Hole 881C is the same as that in modern seawater at 27  $\mu M$  (Fig. 20). In general, the lithium profile is similar to that of strontium. Between 0 and about 20 mbsf, the content of lithium decreases to about 17  $\mu M$ , followed by a monotonic increase to about 80  $\mu M$  between 20 and 330 m. This trend contrasts with that seen in some deep-sea sediments (e.g., Sites 845 through 854), where lithium and strontium show opposite distributions, but is consistent with results obtained at a large number of other sites, where the lithium content generally increases with depth (see Gieskes, 1981). The process(es) that control this phenomenon are not well understood, but apparently include uptake of lithium by clays and zeolites and release to solution in reactions involving biogenic silica and alteration of volcanic ash (Gieskes, 1981). As noted above, alteration of basement basalts is not thought to have influenced the pore water chemistry in the sampled section.

## ORGANIC GEOCHEMISTRY

### Volatile Hydrocarbons

As dictated by safety and pollution requirements, hydrocarbon gases were monitored in the sediments of Site 881 by using the head-space technique and a Carle gas chromatograph to determine the concentrations of  $C_1$  (methane),  $C_2$  (ethane), and  $C_3$  (propane). The results of 52 headspace analyses are presented in Table 12. The amount of methane ranges between 2 and 28 ppm, whereas ethane and propane were not detected in the samples analyzed. The very low concentration of volatile hydrocarbons is probably an indication that conditions in the sediment column were unfavorable for methanogenesis.

### Carbonate Carbon

No samples were taken from Hole 881A; from Holes 881B and 881C, 106 and 51 samples, respectively, were analyzed for inorganic carbon (IC) using the Coulometrics carbon dioxide coulometer. At Hole 881D, which was drilled to fill the gaps of the previous hole, 12 measurements were performed. The results are reported as weight percentage in Table 13.

Carbonate content is near zero in almost all of the samples, because the site is well below the carbonate compensation depth (CCD). As shown in Figure 21, some single spikes having carbonate contents up to 60 wt% occur. According to the core description in the "Lithostratigraphy" section (this chapter), these carbonate-rich samples are from intercalated, light brown to yellowish, aragonite-bearing layers. Samples having lower carbonate contents, between 5 and 10 wt% (145-881B-17H-5, 122 cm, and 145-881C-23X-1, 98 cm) were taken from the transition zones between the aragonite layer and the surrounding sediment.

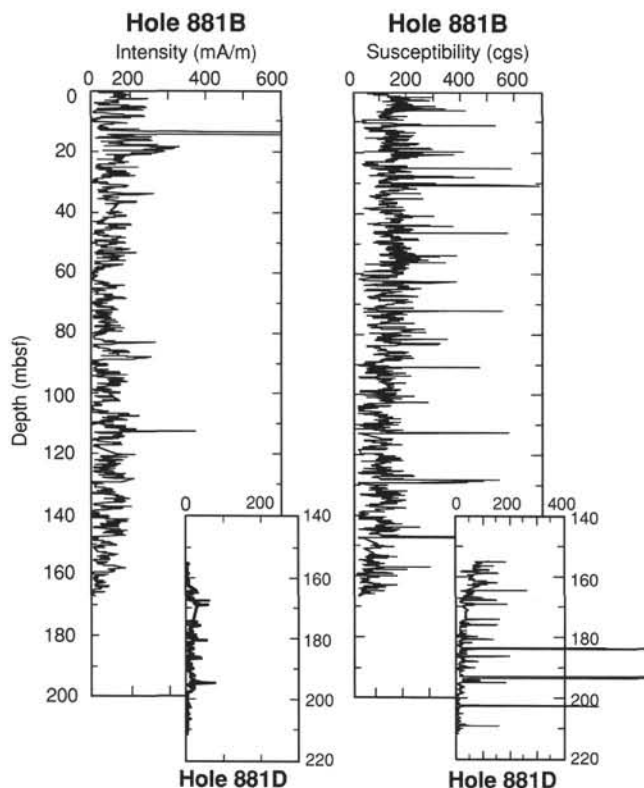


Figure 12. NRM intensities from Holes 881B and 881D, compared to whole-core susceptibility.

### Organic Carbon

The amount of total organic carbon in samples from Holes 881B, 881C, and 881D was calculated as the difference between the total carbon (TC), determined with the NCS analyzer, and inorganic carbon (IC), determined by coulometry. The results are reported in Table 13.

Organic carbon contents are very low in Site 881 sediments. Values fluctuate between 0.1 and 0.5 wt%, and no depth-related trend is visible (Fig. 22). This result reflects the remarkably uniform lithology of the sediment column throughout the sampled interval. The organic matter was probably subjected to aerobic oxidation during or subsequent to deposition, as suggested by the presence of brown, oxidized sediments in the uppermost few meters of the first core (see "Lithostratigraphy" section, this chapter), and further degradation by sulfate-reducing bacteria within the sediment column (gray sediments of lithologic Subunits IA and IB).

Total nitrogen and total sulfur contents are commonly near or below the detection limit of the NCS analyzer, precluding discussion of the TOC/TN-ratios regarding the composition and provenance of the organic matter.

### PHYSICAL PROPERTIES

Physical properties measurements at Site 881 were performed using standard ODP methods (Boyce, 1976; "Explanatory Notes" chapter, this volume). Table 14 summarizes the physical properties measured on cores from Holes 881A, 881B, 881C, and 881D. Index property (density, porosity, water content, and void ratio), digital sediment velocimeter (DSV), and shear strength measurements were taken at approximately 75-cm intervals from cores in Hole 881B, 1.5-m intervals from cores in Hole 881C, and 3-m intervals from cores in Hole 881D. Thermal conductivity was measured at 1.5-m intervals in cores from Hole 881B and at 3-m intervals from cores in Hole 881C. No thermal conductivity measurements were performed in

Holes 881A or 881D. Continuous measurements of GRAPE bulk density, *P*-wave velocities, and magnetic susceptibility were performed in all four holes. Tables containing the compressional wave velocity, shear strength, and thermal conductivity data from Holes 881A, 881B, 881C, and 881D are included here, as are tables of index property data from Holes 881B, 881C, and 881D (Tables 14 through 20). Index property data from Hole 881A were not included because of their limited nature. GRAPE density data have been smoothed using a 29-point moving average, and data from the *P*-wave logger data have been filtered to remove points associated with weak signal strength (<30) and then smoothed using a 29-point moving average. A 29-point data window was chosen to produce useable plots, while reducing resolution as little as possible. The rest of the data have not been subjected to any form of filtering or smoothing.

Profiles of sediment shear strength, wet-bulk density, dry-bulk density, dry water content, and void ratio values for Holes 881B, 881C, and 881D are presented in Figures 23 through 26. The wet-bulk density, dry-bulk density, dry water content, and wet porosity values in the upper 150 mbsf remain fairly constant, ranging from 1.38 to 1.48 g/cm<sup>3</sup>, 0.7 to 0.45 g/cm<sup>3</sup>, 90% to 125%, and 69% to 72%, respectively, while shear strength increases downward from roughly 10 to 125 kPa. Below 150 mbsf in Holes 881C and 881D, a sharp decrease in both wet-bulk density (averaging 1.28 g/cm<sup>3</sup>) and shear strength (averaging 60 kPa) can be seen that corresponds to an increase in wet porosity and dry water content of 78% and 200%, respectively can be seen (Figs. 24 and 25). This sharp break occurs at approximately 164 mbsf, which corresponds to a change in sediment type from a clayey diatom ooze above 164 mbsf to a diatom ooze below this point (see "Lithostratigraphy" section, this chapter). The increased biogenic silica content might easily account for these changes in index properties. A second, less distinct, slope break at approximately 245 mbsf. At this point, the variation lithology and a decrease in biogenic silica/increase in terrigenous clay.

The grain density profiles (Fig. 27) display trends similar to those seen in the wet-bulk density profiles. Above 160 mbsf, the grain density is a fairly constant (2.58 g/cm<sup>3</sup>), while below 160 mbsf, the grain density decreases to approximately 2.30 g/cm<sup>3</sup>, probably the result of the previously mentioned decrease in terrigenous clay and increase in biogenic opal content. Figure 28 shows a profile of the GRAPE bulk density for each of Holes 881A, 881B, 881C, and 881D. Although in all four cases the GRAPE bulk density trends paralleled those obtained with the pycnometer, the GRAPE data were consistently higher than those produced by pycnometer analysis. This may be attributed to the GRAPE analysis being performed on sealed whole-core sections, while the pycnometer analyses were performed using discrete samples that may have experienced some expansion/relocation when splitting the core. Figures 29 and 30 show profiles of *P*-wave velocity and thermal conductivity data, respectively. The *P*-wave profiles include data from both the *P*-wave logger (PWL) and the DSV. The data from both *P*-wave tools reveal an average *P*-wave velocity of 1520 m/s throughout the section cored. The spiky nature of the PWL data may be attributed to the presence of IRD in the form of basalt pebbles (see "Lithostratigraphy" section, this chapter). The inclusion of data associated with weak signal strengths. The DSV profiles do not reflect the abundance of the IRD pebbles because of the bias inherent in the discontinuous sampling for DSV data.

Thermal conductivity profiles reveal a fairly constant thermal conductivity of approximately 1.0 W/(m · °C) above 160 mbsf and a slight decrease to an average value of approximately 0.8 W/(m · °C) below 160 mbsf. Again, this is probably in response to the change in sediment type that occurs at 164 mbsf.

### DOWNHOLE MEASUREMENTS

#### Quality of Logs

Logging operations were conducted for about 30 hr at Site 881 (Table 2). The sonic, resistivity, density, and natural gamma-ray logs

**Table 11. Interstitial water data for Holes 881A and 881C.**

Core, section, interval (cm)	Depth (mbsf)	pH	Alk. (mM)	Sal. (g/kg)	Cl (mM)	Mg (mM)	Ca (mM)	SO <sub>4</sub> (mM)	NH <sub>4</sub> (μM)	NO <sub>2</sub> (μM)	H <sub>4</sub> SiO <sub>4</sub> (μM)	K (mM)	Li (μM)	Na (mM)	Sr (μM)	Mn (μM)	Mg/Ca (mol ratio)
145-881A-																	
1H-1, 145-150	5.45	7.68	3.65	36.0	554	50.45	10.90	28.23	40	0	854	12.23	21.1	491	85.0	87.8	4.63
1H-3, 145-150	8.45	7.63	3.55	35.1	561	49.75	10.95	27.80	92	0	803	12.97	19.9	487	86.1	43.9	4.54
1H-6, 145-150	12.95	7.82	4.01	35.1	563	49.82	11.20	27.48	159	0	857	13.19	18.1	500	85.7	70.6	4.45
145-881C-																	
1H-1, 145-150	1.45	7.70	3.19	35.0	562	51.41	10.91	27.90	0	0	691	10.95	27.2	496	83.6	44.2	4.71
2H-4, 145-150	9.75	7.56	3.57	35.0	572	51.10	11.22	27.13	101	0	717	11.98	19.0	484	85.8	70.6	4.56
3H-3, 145-150	17.75	7.49	3.95	35.5	571	51.28	11.20	26.91	159	n.m.	691	11.64	17.6	483	87.5	39.8	4.58
4H-4, 145-150	28.75	7.73	5.17	35.5	568	49.73	12.51	25.58	349	n.m.	703	11.81	19.2	485	88.4	23.1	3.98
5H-4, 145-150	38.25	7.78	5.81	35.5	576	49.90	12.66	25.00	557	n.m.	740	10.66	18.7	488	89.4	21.7	3.94
6H-5, 145-150	49.25	7.57	6.42	35.5	569	48.54	13.13	24.19	510	n.m.	752	10.73	19.3	492	83.8	16.3	3.70
8H-5, 145-150	68.25	7.59	7.11	35.5	566	47.78	13.49	24.15	585	n.m.	752	10.50	22.6	493	89.2	15.6	3.54
10H-4, 145-150	85.80	7.84	7.58	35.5	565	47.08	13.93	24.10	744	n.m.	880	9.72	22.4	496	100.3	13.5	3.38
12H-4, 145-150	104.75	7.69	7.58	35.0	562	46.05	14.23	23.70	660	n.m.	887	9.72	24.4	492	103.7	13.4	3.24
14H-4, 145-150	123.75	7.85	8.03	35.0	563	46.21	13.83	24.37	772	n.m.	985	9.56	28.9	472	96.7	16.3	3.34
16H-4, 145-150	142.75	7.95	7.69	35.0	567	45.21	13.46	23.47	952	n.m.	892	11.55	31.7	488	97.1	8.6	3.36
21H-4, 145-150	187.65	7.65	7.08	35.0	566	47.11	13.26	23.68	628	n.m.	980	10.31	44.6	484	100.6	17.6	3.55
23X-4, 145-150	206.55	7.67	6.78	35.0	570	47.70	13.14	23.49	614	n.m.	1141	9.93	49.3	508	109.5	19.7	3.63
25X-2, 145-150	221.95	7.41	6.25	35.0	559	47.41	13.20	23.40	597	n.m.	1059	9.24	52.3	489	111.4	19.5	3.59
29X-2, 135-140	260.55	7.63	5.46	35.0	562	47.14	13.14	23.97	499	n.m.	1106	9.52	67.1	494	110.3	18.7	3.59
32X-1, 135-140	287.95	7.76	4.42	35.0	560	47.34	12.78	23.68	514	n.m.	1043	8.46	71.2	483	109.6	19.5	3.71
35X-4, 145-150	321.35	7.32	4.07	34.8	566	46.79	13.00	23.10	457	n.m.	1055	8.80	83.2	488	111.3	27.7	3.60

n.m. = not measured. Alk. = alkalinity; Sal. = salinity.

from the Quad combination tool string are shown in Figures 31A and 31B. The open-hole conditions encountered during the Quad run were good; essentially no hole fill was encountered after the pre-logging wiper trip, and no tools stuck during logging. A relatively constant borehole diameter was indicated by the virtual absence of cycle skipping within the sonic velocity log. Logging data presented in this section have not been corrected for environmental or other factors, nor have the data been depth-shifted to match drilling depth.

The data from the natural gamma-ray spectrometry tool (NGT) shown in Figure 31A were recorded at 1800 ft/hr, the logging speed of a Quad run, which is faster than the recommended logging speed for this tool string. Better counting statistics normally are obtained from the slow logging speed of the geochemical run, which was not obtained at this site. The total gamma-ray (SGR) curve shown is of good quality, but the high-resolution variation of the spectral components of K, Th, and U is less reliable.

Figure 31B presents data from the resistivity, sonic, and density tools. The quality of data from the dual induction tool (DIT) and digital sonic tool (SDT) is excellent. The damaged eccentricizing caliper on the lithodensity tool (HLDT) allowed for tool "standoff" in sections of the hole. For most of the logged section, the data are of good quality, as indicated by close agreement with core-based bulk density measurements (see "Physical Properties" section, this chapter). Below 180 mbsf, however, a number of spikes in the density log indicate poor contact of the tool with the borehole wall and, hence, unreliable data quality. The baseline bulk density shows a sharp increase between 250 and 275 mbsf, while a similar trend is seen in the core-based measurements, the amplitude of this increase is considered unreliable.

## Results

The logs from the Quad tool string are shown and compared to the core-based lithologic descriptions in Figures 31A and 31B. The dominant feature apparent in the log responses is the marked change near 175 mbsf. The increased gamma-ray, bulk density, and resistivity values above this level indicate relative increases in terrigenous content. Smear slide analyses demonstrate that this zone marks the transition between diatom ooze below (lithologic Subunit IB) and clayey diatom ooze above (lithologic Subunit IA). This parallel increases in the K and Th logs, and the relatively flat profile of the U log demonstrates that the SGR log dominantly reflects variations in

clay content, as K and Th typically are concentrated in clays and other terrigenous minerals.

Curiously, the sonic log indicates a velocity decrease above this transition. Although burial compaction often acts to increase velocity with depth, the increased opal content below 175 mbsf was expected to exhibit lower velocities because of the associated increase in porosity and decrease in density. The opal-rich sediments are more rigid than the clay-rich sediments and thus have higher velocities.

The logging data indicate that the transition from lithologic Subunit IA to Subunit IB occurs at ~175 mbsf. Smear slide analyses of the core material in Hole 881B placed this boundary at 164.5 mbsf; however, the absence of any recovered material in Cores 145-881C-19X and -20X (162.3–181.7 mbsf) precluded the accurate placement of this boundary in Hole 881C, based on core data alone.

The increase in concentrations of terrigenous sediment above 175 mbsf is also associated with an increase in very coarse detrital material; the most likely source of this coarse fraction is from ice-rafting of poorly sorted glacial debris. Chronostratigraphic data at Site 881 place the Subunits IA/IB boundary just above the Matuyama/Gauss polarity transition at 2.6 Ma. The timing of this transition coincides with the first abundant appearance of IRD in North Atlantic (Shackleton et al., 1984) and North Pacific (Rea and Schrader, 1985) sediments, marking the onset of large-scale Northern Hemisphere glaciation. Studies of North Atlantic sediments demonstrated that the supply of ice-rafted sediment has varied coherently with the oxygen isotopic record of continental ice volume variability since the late Pliocene (Ruddiman et al., 1989).

Inspection of the tension log (an instantaneous monitor of weight on cable) demonstrates that the tool string experienced considerable vertical motion, even though the wireline heave compensator was engaged (Fig. 32). Uncompensated vertical tool motion can be misinterpreted in terms of downhole lithologic variability, which in turn may be misinterpreted as a paleoclimate signal. To examine the possible effect of ship's heave on the logging data, we used spectral analysis to estimate the dominant depth-domain periodicity within the tension and SGR logs. The tension and SGR logs from 175 to 125 mbsf were selected for analysis (approximately 2.6–1.7 Ma); these logs and their corresponding power spectra are shown in Figure 32. The tension log indicates a sharp, central periodicity near 1.25 m, which corresponds to a wave period of ~8 s. The absence of this periodicity within the SGR power spectra suggests that ship's heave does not significantly affect the SGR log. In fact, the SGR log over

**Table 12. Results of headspace gas analyses from Holes 881A, 881B, 881C, and 881D.**

Core, section, interval (cm)	Depth (mbsf)	C <sub>1</sub> (ppm)	C <sub>2</sub> (ppm)	C <sub>3</sub> (ppm)
145-881A-1H-4, 0-3	8.5	2.83	0.00	0.00
145-881B-1H-3, 0-3	3.0	2.44	0.00	0.00
2H-4, 0-3	10.0	2.21	0.00	0.00
3H-3, 0-3	18.0	3.39	0.00	0.00
4H-4, 0-3	29.0	3.44	0.00	0.00
5H-4, 0-3	38.5	3.00	0.00	0.00
6H-4, 0-3	48.0	2.35	0.00	0.00
7H-4, 0-3	57.5	4.06	0.00	0.00
8H-4, 0-3	67.0	3.62	0.00	0.00
9H-4, 0-3	76.5	13.99	0.00	0.00
10H-4, 0-3	86.0	6.39	0.00	0.00
11H-4, 0-3	95.5	5.08	0.00	0.00
12H-4, 0-3	105.0	4.64	0.00	0.00
13H-4, 0-3	114.5	9.05	0.00	0.00
14H-4, 0-3	124.0	15.76	0.00	0.00
15H-4, 0-3	133.5	15.73	0.00	0.00
16H-5, 0-3	144.5	10.65	0.00	0.00
17H-4, 0-3	152.5	13.84	0.00	0.00
18H-4, 0-3	162.0	16.13	0.00	0.00
145-881C-1H-1, 0-3	1.5	2.12	0.00	0.00
2H-5, 0-3	9.8	2.77	0.00	0.00
3H-4, 0-3	17.8	2.96	0.00	0.00
4H-5, 0-3	28.8	4.56	0.00	0.00
5H-5, 0-3	38.3	4.16	0.00	0.00
6H-6, 0-3	49.3	10.20	0.00	0.00
7H-5, 0-3	57.3	5.55	0.00	0.00
8H-6, 0-3	68.3	5.57	0.00	0.00
9H-5, 0-3	76.3	5.76	0.00	0.00
10H-5, 0-3	85.8	8.95	0.00	0.00
11H-4, 0-3	93.8	5.74	0.00	0.00
12H-5, 0-3	104.8	7.67	0.00	0.00
13H-4, 0-3	112.8	11.11	0.00	0.00
14H-5, 0-3	123.8	12.63	0.00	0.00
15H-4, 0-3	131.8	14.31	0.00	0.00
16H-5, 0-3	142.8	10.60	0.00	0.00
17H-4, 0-3	150.8	28.08	0.00	0.00
18X-2, 0-3	157.3	8.95	0.00	0.00
21X-5, 0-3	187.7	17.82	0.00	0.00
23X-5, 0-3	206.6	7.03	0.00	0.00
25X-3, 0-3	222	9.60	0.00	0.00
27X-5, 0-3	244.3	16.99	0.00	0.00
29X-2, 0-3	260.5	20.19	0.00	0.00
30X-4, 0-3	271.7	18.84	0.00	0.00
32X-2, 0-3	288	13.61	0.00	0.00
35X-5, 0-3	321.4	15.17	0.00	0.00
36X-5, 0-3	331.1	17.72	0.00	0.00
145-881D-1H-4, 0-3	159.5	12.15	0.00	0.00
2H-4, 0-3	169.0	19.23	0.00	0.00
3H-4, 0-3	178.5	22.35	0.00	0.00
4H-4, 0-3	188.0	23.06	0.00	0.00
5H-5, 0-3	199.0	8.65	0.00	0.00
6H-5, 0-3	208.5	9.09	0.00	0.00

C<sub>1</sub> = methane, C<sub>2</sub> = ethane, and C<sub>3</sub> = propane; all samples were headspace samples.

this interval is dominated by central periodicities near 11.3, 4.2–3.1, 1.8, and 0.8 m. Using the Pliocene–Pleistocene average sedimentation rate at Site 881 (~8.4 cm/k.y.; see “Sedimentation Rates and Fluxes” section, this chapter), these depth-domain periodicities correspond to time-domain periodicities near 136, 50–37, 21, and 10 k.y.. The 50–37 and 21-k.y. periodicities may correspond to dominant orbital tilt (41 k.y.) and precession (23–19 k.y.) periodicities within the global ice volume and North Atlantic Ocean IRD signals for the late Pliocene (e.g., Ruddiman et al., 1989).

A tentative comparison of the Site 881 SGR data with the benthic foraminiferal oxygen isotopic record from Site 677 (eastern equatorial Pacific Ocean) is shown in Figure 33 (Shackleton et al., 1990). The single down-going log and two up-going logs were depth-shifted and averaged to produce a shorter, but better defined, SGR curve (Fig. 33). While several gross similarities can be seen between the oxygen

isotopic record (as a record of global variability in ice volume) and the SGR log (as a record of variability in terrigenous content), initial correspondence between the two records is not great.

## SEISMIC-LITHOLOGIC CORRELATION

All the Leg 145 drilling locations were surveyed in order to drop the beacon at the proper pre-selected location. In each case, the surveys were run in the figure of the number 4, with the long leg duplicating the site-survey track line used to select the site and the cross-leg being as nearly orthogonal as practical. The shipboard air-gun seismic reflection profiling system was used for all the surveys, except for Site 883, when it was inoperable; the 3.5-kHz profiling system was used to locate that drill site.

The underway geophysical surveys were positioned with uncorrected realtime GPS navigation and used digital single-channel seismic-reflection profiling, high-resolution 3.5- and 12-kHz echo sounders and a magnetometer. The seismic data were generated using 200 and 80 in.<sup>3</sup> water guns towed 24 m astern and fired simultaneously, and a Teledyne hydrophone array having a 91.44-m active section and a 500-m tow leader, although less than the total length was paid out. Analog records were displayed with kronhite filter settings of 30 and 150 Hz. Nominally, 10-s record lengths were digitized (depending on water depth and the cycle time of the recording system). Data were recorded at either 1, 2, or 0.5 ms (depending on the profile and total sediment section thickness), on 9-track tape in SEG-Y format. Most lines were run at about 6 kt, with a firing rate of about 11 s between shots. The survey geometry of the ship was constant, and because of the placement of the sounder arrays, GPS antennas, water guns, and eels, the following lay-back corrections apply. For a given time, the survey geometry places the high-resolution echo sounder and sub-bottom 3.5 kHz traces 20.6 m in advance, and the single-channel seismic trace 100 to 350 m behind the GPS fix. Data from most surveys fit onto a single 9-track tape.

Seismic sections were processed on board the ship during the cruise with a UNIX-based Masscomp computer using the SIOSEIS processing software and were displayed on a Versatec plotter. Most sections received runstreams involving: mute to water bottom, a single filter passing 25–250 Hz (or less) to enhance the shallow stratigraphy, with mild AGC windows of 300 to 350 ms or average amplitude trace scaling. Thicker sections received time-varying filters that dropped the high frequencies cut off to as low as 50 Hz at the level of the basement reflectors. Some sections and the panels of traces compared to synthetics received predictive (spiking) deconvolution using short design window lengths to correct for source- and geometry-related reverberation. For sections without deconvolution, the upper 50 ms of record is severely overprinted by the source tail related to overly deep deployment for the guns or the streamer. Most “horizontal reflectors” above this level are purely artifacts of collection geometry. By using spiking deconvolution with 200- to 300-ms design windows hung from the water bottom, most of this effect is removed and reflector packages are better resolved. This processing sequence served to enhance deeper reflectors, reduce reverberation, and provided good correlation to synthetics generated from physical property and related density/velocity data.

The seismic reflection record crossing Site 881 (Fig. 34) shows approximately 0.5 s (two-way time), 385 m, of sediment overlying acoustic basement. Figure 34 shows a strong basement reflector at about 8.05 s. Overlying sediment conforms to basement attitude up to about 7.65 s, dipping gently north; shallower sediments are horizontal. This change in attitude from pelagic drape to horizontal bedding is an indication of onset of current mediated deposition and coincides with the boundary between lithologic Subunit IB, the more nearly pure diatom ooze, and Subunit IA, the clayey diatom ooze with ash and dropstones.

Site 881 lies 0.8 km south of a normal fault and on the downthrown side. The horizontally bedded Subunit IA fills the fault-caused low,

Table 13. Results of geochemical analyses from Holes 881B, 881C, and 881D.

Core, section, interval (cm)	Depth (mbsf)	TC	IC	TOC	CaCO <sub>3</sub>	TN	TS
145-881B-							
1H-1, 112-113	1.12	0.31	0.00	0.31	0.00	0.06	0.00
1H-2, 113-114	2.63	0.18	0.00	0.18	0.00	0.06	0.00
1H-3, 107-108	4.07	0.00	0.00				
2H-1, 100-101	6.50	0.39	0.00	0.39	0.00	0.08	0.09
2H-2, 108-109	8.08	0.00	0.00				
2H-3, 109-110	9.59	0.00	0.00				
2H-4, 111-112	11.11	0.28	0.00	0.28	0.00	0.05	0.00
2H-5, 106-107	12.56	0.11	0.00	0.11	0.00	0.02	0.09
2H-6, 107-108	14.07	0.00	0.00				
3H-1, 108-109	16.08	0.25	0.00	0.25	0.00	0.08	0.07
3H-2, 108-109	17.58	0.00	0.00				
3H-3, 108-109	19.08	0.00	0.00				
3H-4, 108-109	20.58	0.25	0.00	0.25	0.00	0.05	0.07
3H-5, 105-106	22.05	0.25	0.00	0.25	0.00	0.05	0.05
3H-6, 101-102	23.51	0.00	0.00				
4H-1, 112-113	25.62	0.28	0.00	0.28	0.00	0.05	0.02
4H-2, 112-113	27.12	0.00	0.00				
4H-3, 119-120	28.69	0.00	0.00				
4H-4, 115-116	30.15	0.18	0.00	0.18	0.00	0.04	0.00
4H-5, 112-113	31.62	0.22	0.00	0.22	0.00	0.05	0.04
4H-6, 112-113	33.12	0.00	0.00				
5H-1, 112-113	35.12	0.16	0.00	0.16	0.00	0.04	0.06
5H-2, 111-112	36.61	0.00	0.00				
5H-3, 122-123	38.22	0.00	0.00				
5H-4, 112-113	39.62	0.11	0.00	0.11	0.00	0.03	0.00
5H-5, 112-113	41.12	0.17	0.00	0.17	0.00	0.05	0.01
5H-6, 17-18	41.67	4.81	4.80	0.01	40.00	0.04	0.00
5H-6, 107-108	42.57	0.00	0.00				
6H-1, 113-114	44.63	0.25	0.00	0.25	0.00	0.05	0.00
6H-2, 125-126	46.25	0.00	0.00				
6H-3, 113-114	47.63	0.00	0.00				
6H-4, 112-113	49.12	0.34	0.00	0.34	0.00	0.06	0.00
6H-5, 111-112	50.61	0.22	0.00	0.22	0.00	0.04	0.00
6H-6, 100-101	52.00	0.00	0.00				
7H-1, 114-115	54.14	0.16	0.00	0.16	0.00	0.03	0.00
7H-2, 113-114	55.63	0.00	0.00				
7H-3, 113-114	57.13	0.00	0.00				
7H-4, 113-114	58.63	0.34	0.00	0.34	0.00	0.05	0.00
7H-5, 38-39	59.38	0.16	0.00	0.16	0.00	0.05	0.00
7H-6, 98-99	61.48	0.00	0.00				
8H-1, 112-113	63.62	0.13	0.00	0.13	0.00	0.04	0.00
8H-2, 112-113	65.12	0.00	0.00				
8H-3, 112-113	66.62	0.00	0.00				
8H-4, 111-112	68.11	0.13	0.00	0.13	0.00	0.06	0.00
8H-5, 112-113	69.62	0.24	0.00	0.24	0.00	0.05	0.00
8H-6, 112-113	71.12	0.00	0.00				
9H-1, 113-114	73.13	0.24	0.00	0.24	0.00	0.05	0.00
9H-2, 113-114	74.63	0.00	0.00				
9H-3, 113-114	76.13	0.00	0.00				
9H-4, 113-114	77.63	0.13	0.00	0.13	0.00	0.05	0.00
9H-5, 113-114	79.13	0.19	0.00	0.19	0.00	0.04	0.00
9H-6, 113-114	80.63	0.00	0.00				
10H-1, 117-118	82.67	0.27	0.00	0.27	0.00	0.06	0.00
10H-2, 105-106	84.05	0.00	0.00				
10H-3, 122-123	85.72	0.00	0.00				
10H-4, 116-117	87.16	0.11	0.00	0.11	0.00	0.03	0.00
10H-5, 117-118	88.67	0.15	0.00	0.15	0.00	0.04	0.00
10H-6, 117-118	90.17	0.00	0.00				
11H-1, 116-117	92.16	0.19	0.00	0.19	0.00	0.05	0.00
11H-2, 112-113	93.62	0.00	0.00				
11H-3, 115-116	95.15	0.00	0.00				
11H-4, 112-113	96.62	0.13	0.00	0.13	0.00	0.04	0.00
11H-5, 117-118	98.17	0.17	0.00	0.17	0.00	0.04	0.00
11H-6, 115-116	99.65	0.00	0.00				
12H-1, 113-114	101.63	0.16	0.00	0.16	0.00	0.04	0.00
12H-2, 113-114	103.13	0.00	0.00				
12H-3, 116-117	104.66	0.00	0.00				
12H-4, 111-112	106.11	0.23	0.00	0.23	0.00	0.04	0.00
12H-5, 116-117	107.66	0.10	0.00	0.10	0.00	0.04	0.00
12H-6, 116-117	109.16	0.12	0.00	0.12	0.00	0.04	0.00
13H-1, 118-119	111.18	0.00	0.00				
13H-2, 106-107	112.56	0.00	0.00				
13H-3, 112-113	114.12	0.00	0.00				
13H-4, 115-116	115.65	0.16	0.00	0.16	0.00	0.03	0.00
13H-5, 108-109	117.08	0.18	0.00	0.18	0.00	0.03	0.00
14H-1, 113-114	120.63	0.00	0.00				
14H-2, 109-110	122.09	0.19	0.00	0.19	0.00	0.04	0.00
14H-3, 109-110	123.59	0.00	0.00				
14H-4, 109-110	125.09	0.10	0.00	0.10	0.00	0.04	0.00
14H-5, 106-107	126.56	0.00	0.00				
15H-1, 113-114	130.13	0.13	0.00	0.13	0.00	0.03	0.00
15H-2, 111-112	131.61	0.00	0.00				
15H-3, 113-114	133.13	0.00	0.00				
15H-4, 111-112	134.61	0.28	0.00	0.28	0.00	0.03	0.00

Table 13 continued.

Core, section, interval (cm)	Depth (mbsf)	TC	IC	TOC	CaCO <sub>3</sub>	TN	TS
15H-5, 111-112	136.11	0.06	0.00	0.06	0.00		
15H-6, 111-112	137.61	0.00	0.00				
16H-1, 111-112	139.61	0.30	0.00	0.30	0.00	0.04	0.00
16H-2, 112-113	141.12	0.00	0.00				
16H-3, 108-109	142.58	0.00	0.00				
16H-4, 112-113	144.12	0.14	0.00	0.14	0.00	0.03	0.00
16H-5, 112-113	145.62	0.28	0.00	0.28	0.00	0.04	0.00
16H-6, 102-103	147.02	0.00	0.00				
17H-1, 111-112	149.11	0.17	0.00	0.17	0.00	0.01	0.00
17H-2, 111-112	150.61	0.00	0.00				
17H-3, 123-124	152.23	0.00	0.00				
17H-4, 113-114	153.63	0.44	0.00	0.44	0.00	0.01	0.00
17H-5, 122-123	155.22	1.25	0.88	0.37	7.30	0.04	0.00
17H-6, 130-131	156.8	0.00	0.00				
18H-1, 113-114	158.63	0.00	0.00				
18H-2, 76-77	159.76	5.74	5.54	0.20	46.10	0.03	0.00
18H-2, 86-87	159.86	0.08	0.00	0.08	0.00	0.03	0.00
18H-2, 112-113	160.12	0.50	0.00	0.50	0.00	0.04	0.00
18H-3, 112-113	161.62	0.00	0.00				
18H-4, 111-112	163.11	0.39	0.00	0.39	0.00	0.06	0.00
18H-5, 106-107	164.56	0.17	0.00	0.17	0.00	0.03	0.00
18H-6, 113-114	166.13	0.00	0.00				
145-881C-							
18X-1, 77-78	156.57	0.16	0.00	0.16	0.00	0.03	0.00
18X-2, 72-73	158.02	0.00	0.00				
18X-3, 39-40	159.19	0.00	0.00				
21H-1, 77-78	182.47	0.19	0.00	0.19	0.00	0.04	0.00
21H-2, 77-78	183.97	0.00	0.00				
21H-3, 77-78	185.47	0.14	0.00	0.14	0.00	0.00	0.00
21H-4, 76-77	186.96	0.00	0.00				
21H-5, 76-77	188.46	0.00	0.00				
21H-6, 81-82	190.01	0.00	0.00				
21H-7, 16-17	190.86	0.00	0.00				
23X-1, 77-78	201.37	0.92	0.48	0.44	4.00	0.04	0.00
23X-1, 98-99	201.58	6.33	6.15	0.18	51.20		
23X-2, 77-78	202.87	0.00	0.00				
23X-3, 97-98	204.57	0.00	0.00				
23X-4, 78-79	205.88	0.00	0.00				
23X-5, 77-78	207.37	0.29	0.00	0.29	0.00	0.03	0.00
23X-5, 140-141	208.00	6.81	6.40	0.41	53.30		
23X-6, 78-79	208.88	0.00	0.00				
23X-7, 23-24	209.33	0.00	0.00				
25X-1, 77-78	219.77	0.00	0.00				
25X-2, 73-74	221.23	0.00	0.00				
25X-3, 77-78	222.77	0.00	0.00				
25X-4, 31-32	223.81	0.24	0.00	0.24	0.00	0.00	0.00
27X-1, 92-93	239.22	0.45	0.00	0.45	0.00	0.03	0.00
27X-2, 92-93	240.72	0.00	0.00				
27X-3, 92-93	242.22	0.00	0.00				
27X-4, 92-93	243.72	0.38	0.00	0.38	0.00	0.00	0.00
27X-5, 92-93	245.22	0.39	0.00	0.39	0.00	0.02	0.00
27X-6, 61-62	246.41	0.00	0.00				
29X-1, 92-93	258.52	0.18	0.00	0.18	0.00	0.02	0.00
29X-2, 92-93	260.02	0.00	0.00				
29X-3, 92-93	261.42	0.36	0.00	0.36	0.00	0.03	0.00
30X-1, 91-92	268.11	0.21	0.00	0.21	0.00	0.00	0.00
30X-2, 91-92	269.61	0.00	0.00				
30X-3, 92-93	271.12	0.00	0.00				
30X-4, 91-92	272.61	0.22	0.00	0.22	0.00	0.00	0.00
30X-5, 91-92	274.11	0.30	0.00	0.30	0.00	0.00	0.00
30X-5, 107-108	274.27	5.78	5.38	0.40	44.80		
30X-6, 91-92	275.61	0.00	0.00				
32X-1, 93-94	287.43	0.00	0.00				
32X-2, 97-98	288.97	0.00	0.00				
35X-1, 92-93	316.32	0.00	0.00				
35X-3, 97-98	319.37	0.00	0.00				
35X-4, 92-93	320.82	0.00	0.00				
35X-5, 93-94	322.33	0.00	0.00				
36X-1, 92-93	326.02	0.00	0.00				
36X-2, 92-93	327.52	0.00	0.00				
36X-3, 92-93	329.02	0.00	0.00				
36X-4, 92-93	330.52	0.00	0.00				
36X-5, 92-93	332.02	0.00	0.00				
36X-6, 92-93	333.52	0.00	0.00				
145-881D-							
2H-1, 56-57	165.06	0.00	0.00				
2H-3, 56-57	168.06	0.10	0.00	0.10	0.00		
3H-1, 61-62	174.61	0.00	0.00				
3H-3, 61-62	177.61	0.41	0.00	0.41	0.00		
3H-5, 61-62	180.61	0.00	0.00				
4H-1, 58-59	184.08	0.00	0.00				
4H-3, 58-59	187.08	0.46	0.00	0.46	0.00		
4H-5, 58-59	190.08	0.00	0.00				
5H-1, 62-63	193.62	0.00	0.00				

Table 13 continued.

Core, section, interval (cm)	Depth (mbsf)	TC	IC	TOC	CaCO <sub>3</sub>	TN	TS
5H-3, 26-27	196.26	0.00	0.00				
5H-3, 62-63	196.62	0.27	0.00	0.27	0.00		
5H-5, 62-63	199.62	0.23	0.00	0.23	0.00		

TC = total carbon, IC = inorganic carbon, TOC = total organic carbon, TN = total nitrogen, and TS = total sulfur. All samples are carbonates. All results are given in weight percent of bulk sediment.

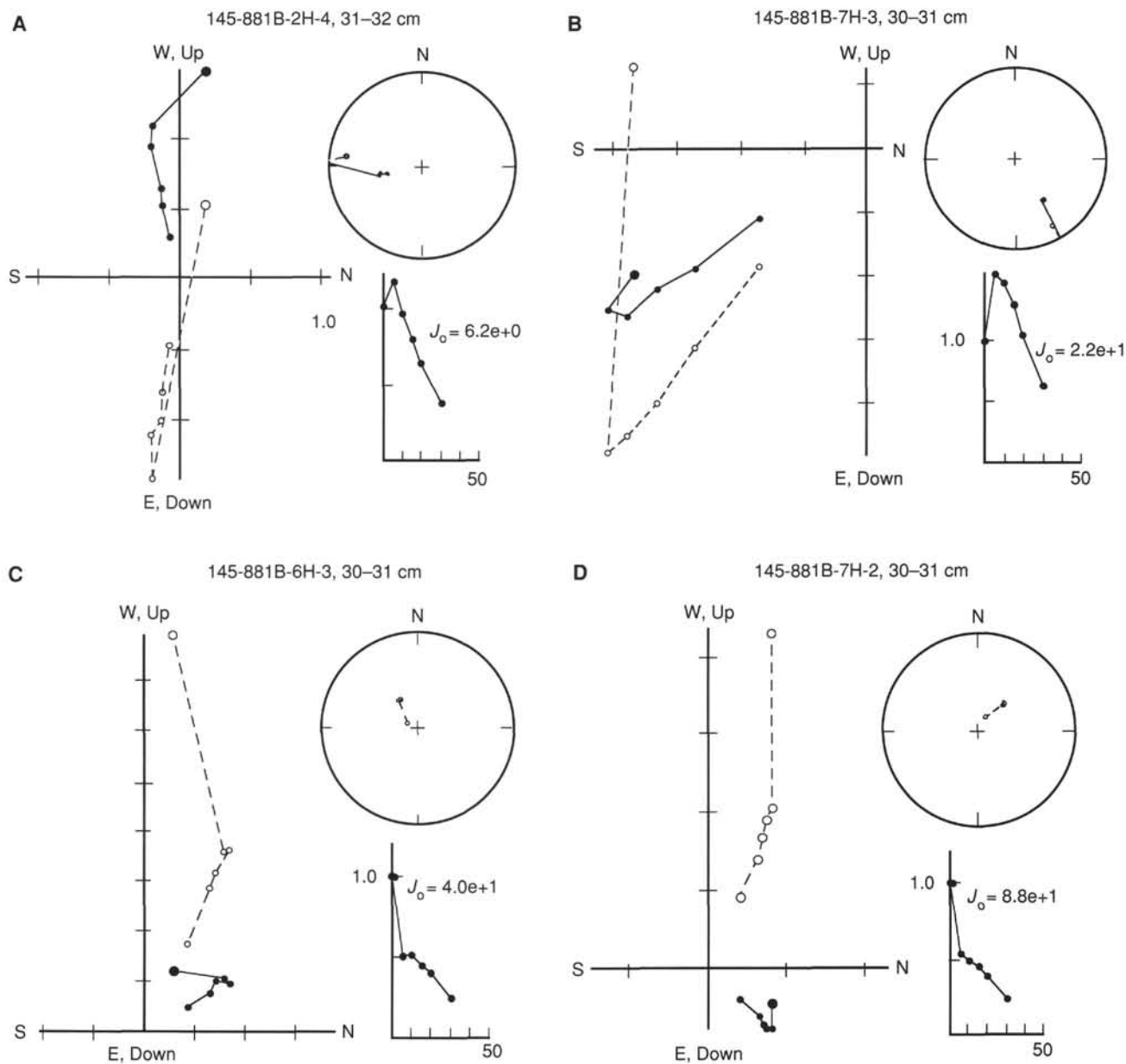


Figure 13. Representative Zijderveld plots from discrete-sample demagnetizations. Examples of normal-polarity samples (A, 145-881B-2H-4, 31-32 cm; B, 145-881B-7H-3, 30-31 cm). Examples of reversed-polarity samples (C, 145-881B-6H-3, 30-31 cm; D, 145-881B-7H-2, 30-31 cm).

**Table 14. Summary of physical properties measurements, Site 881.**

	Hole 881A	Hole 881B	Hole 881C	Hole 881D
Shear strength motorized vane	x	x	x	x
Compressional wave velocity P-wave logger	x	x	x	x
Digital sediment velocimeter	x	x	x	x
Index properties shipboard analysis	x	x	x	x
Thermal conductivity needle probe	-	x	x	-

and sedimentation rates determined for this unit will be perhaps twice the regional value.

## SUMMARY AND CONCLUSIONS

### Geologic Record

A total of 465.2 m of upper Miocene through Pleistocene ooze was recovered at Site 881 in four holes. Deepest penetration was in Hole 881C, an APC/XCB hole that reached 363.8 mbsf. All the sediments at Site 881 are diatom ooze that can be divided into upper and lower portions based on the presence of clay and ash in the upper part of the section. Lithologic Subunit IA is a clayey diatom ooze, well-bioturbated, that contains ash layers, dropstones, and rhodochrosite/dolomite concretions. Radiolarians, sponge spicules, quartz, and feldspar occur in accessory amounts within Subunit IA. Volcanic ash occurs as both light-colored layers of unaltered glass that are commonly tens of centimeters thick and reach thicknesses of up to 1 m, and as brown to dark brown layers up to tens of centimeters thick that are somewhat altered. All ash layers more than a few centimeters thick have a sharp lower boundary, gradational or bioturbated upper boundary, and the thicker ones show size gradation. Dropstones are common; the predominant lithologies are pyroxene basalt and felsic tuff. The size of the dropstones ranges from sand-sized to several centimeters in diameter. [The presence of so many pebbles in the sediment caused a problem for the APC/XCB bit. At the end of the time on site, the drilling crew removed about half a coffee-cup full of pebbles from the bit after it arrived on deck.] The rhodochrosite/dolomite occurs as concretions and as burrow fillings, often near (in conjunction with?) ash layers. Pore-water geochemistry is consistent with the authigenic formation of both rhodochrosite and dolomite.

Lithologic Subunit IB is dominated by diatom ooze and has accessory clay and radiolarians. Dropstones occur rarely and are of the same lithologies as in the overlying unit; the oldest one occurs 243.5 mbsf in lower Pliocene sediments, about 4.7 Ma. Minor amounts of ash occur. Rhodochrosite/dolomite concretions are fewer than in Subunit IA. A distinct 18-cm thick layer of this carbonate occurs at 158 mbsf in both Holes 881C and 881D, implying moderate lateral continuity for this unexpected (at 5542 m depth) lithology.

Physical properties of the formation measured both in the borehole and in the laboratory show distinct differences between Subunits IA and IB. The upper, relatively clay- and ash-rich unit has lower porosity and water content and greater bulk density and sonic velocity than the lower, more pure diatom ooze. The several transitions occur in the range of 160 to 180 mbsf and help to demonstrate the gradational nature of the boundary between the subunits. The seismic reflection profiles collected during the pre-site survey show four distinct acoustic units: (1) a lowermost unit having strong reflectors; (2) a nearly transparent unit; (3) a unit having continuous reflectors showing aspects of pelagic drape; and (4) an uppermost unit that displays aspects of bottom-current mediation of depositional processes. This uppermost acoustic unit thins over highs, thickens in lows, and displays onlapping relationships onto the sides of the lows. Site 881 was positioned to recover a complete section of this unit and to avoid any brief, local hiatuses that might occur. The boundary between

lithologic Subunits IA and IB approximates the position where the seismic profiles indicate a change from pelagic drape to current-controlled deposition.

Throughout this section, siliceous microfossils are moderately to well preserved. Foraminifers are entirely absent, except for a few samples, and nannofossils are rare. The presence of a good magnetostratigraphy back to the Gauss/Gilbert boundary may allow modification of zonal boundaries for the subarctic siliceous organisms.

Calculation of the mass accumulation rate or flux of the major sediment components permits insight into the depositional history of Site 881. Two important changes are apparent. The first occurs at the Pliocene/Miocene boundary, 5.4 Ma in Cande and Kent's (1992) time scale. At that time, a three-fold increase occurred in the mass accumulation rate of diatoms, from about  $0.4 \text{ g}(\text{cm}^2 \cdot \text{k.y.})^{-1}$  during the latest Miocene to in excess of  $1.2 \text{ g}(\text{cm}^2 \cdot \text{k.y.})^{-1}$  in the early Pliocene. Opal flux in the form of diatoms remained high,  $1.2$  to  $1.5 \text{ g}(\text{cm}^2 \cdot \text{k.y.})^{-1}$  throughout the entire Pliocene and Pleistocene. Values for organic carbon also appeared to have increased at the Pliocene/Miocene boundary and remained within a factor of two or three throughout the Pliocene and Pleistocene.

The fluxes of volcanogenic and terrigenous materials increased markedly during the middle of the late Pliocene, at the time of the Matuyama/Gauss reversal boundary, approximately 2.6 Ma. Clay fluxes, which are reasonably well constrained, increased by an order of magnitude from less than  $0.1$  to about  $0.8 \text{ g}(\text{cm}^2 \cdot \text{k.y.})^{-1}$ . Quartz flux may have increased by even greater amounts, from not measurable during the mid-Pliocene to  $0.2$  to  $0.3 \text{ g}(\text{cm}^2 \cdot \text{k.y.})^{-1}$  in the later Pliocene and Pleistocene. The influx of volcanic ash also increased 10- to 20-fold at this time.

### Paleoceanography and Paleoclimatology

Opal-rich pelagic sediments accumulated in the northwestern Pacific Ocean during the late Miocene at a rate of  $15 \text{ m/m.y.}$  ( $0.7 \text{ g}(\text{cm}^2 \cdot \text{k.y.})^{-1}$ ). Volcanic glass and clay accumulated along with opal, suggesting a moderate volcanogenic influx and the deposition of some continentally derived clays. At the close of Miocene time, biologic productivity (specifically silica productivity) increased several-fold and has remained high ever since. Investigation of the causes of increased late Neogene silica productivity in the North Pacific Ocean was one of the important objectives of Leg 145.

Additional striking changes occurred at 2.6 Ma. The deposition of volcanogenic material increased by more than an order of magnitude. This increase during ash deposition in the latest Pliocene in the North Pacific has been known for many years (Kennett and Thunell, 1975; Kennett et al., 1977), but Site 881 provides a much better dated sequence for determining the timing of onset of the northwestern Pacific Ocean portion of this oceanwide volcanic episode than has been available previously. Examination of the individual ash layers should reveal geochemical trends in Kuril-Kamchatka volcanism.

The first occurrence of IRD in Site 881 (early Pliocene age, at about 4.7 Ma) is evidence of local glaciers that reached sea level somewhere along the North Pacific rim. This age is older than the late Pliocene age of the oldest dropstones found in the Leg 86 drill sites several hundred miles to the south (Krissek et al., 1985). The sudden, large increase in dropstone abundance occurs at the time of the Matuyama/Gauss boundary at 2.6 Ma and is a clear demonstration of large-scale glacial activity around the North Pacific region and has been clearly identified from the Deep Sea Drilling Project drill sites. (von Huene et al., 1976; Rea and Schrader, 1985; Krissek et al., 1985). As in the case of the volcanic activity, results of coring at Site 881 provide the best dated record of North Pacific Ocean IRD.

The same climatic deterioration that resulted in glaciers and IRD probably enhanced the erosion of and runoff from the continents, especially Asia, resulting in the great influx of clays to the North Pacific. The clayey oozes of Subunit IA are most likely hemipelagic deposits, based on their closeness to land, very high sedimentation

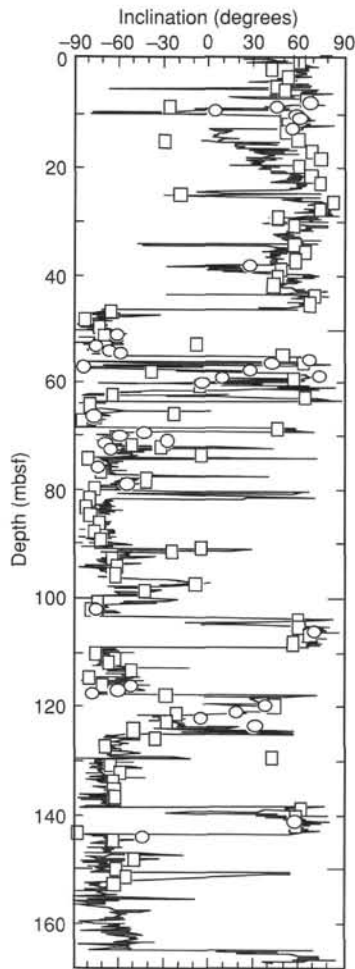


Figure 14. **A.** NRM intensity after demagnetization at 15 mT, Hole 881B. **B.** Anhyseretic remanent magnetization (ARM) and low-field susceptibility plotted on log scales so that their relative variation can be observed.

rates (also seen in the Leg 86 cores—Site 578, Janecek, 1985), and acoustic character. Dating the transition between the sediments of Subunits IA and IB establishes the beginning of relatively strong bottom current activity in the North Pacific to coincide with the onset of Northern Hemisphere glaciation at 2.6 Ma. This determination is the major new paleoceanographic discovery of Site 881; surficial effects of bottom current activity have been mapped in the region from seismic profiles (Damuth et al., 1983), but the geologic history of this activity has been unknown previously.

Quartz flux into the sediments also increases by more than an order of magnitude at 2.6 Ma. Much of this increased quartz flux may be associated with the increased hemipelagic influx, but quartz also is considered to be transported by eolian processes (Leinen and Heath, 1981). Other workers have shown a large increase in the flux of eolian dust into the North Pacific at the time of onset of extensive Northern Hemisphere glaciation, a flux that corresponds to the initiation of the vast Asian loess deposits (Janecek and Rea, 1983; Janecek, 1985; Rea et al., 1985). Increased quartz fluxes in the late Pliocene sediments of Site 881 may be recording these eolian processes.

In summary, Site 881 provides a well-dated paleoceanographic record of the past 7.2 m.y. Opal fluxes, low during the late Miocene, increased suddenly at the Miocene/Pliocene boundary and have remained high ever since. A number of important changes occur in conjunction with the late Pliocene onset of Northern Hemisphere glaciation. Dropstones become common, having been present but rare in lowermost Pliocene sediments. The mass accumulation rate of

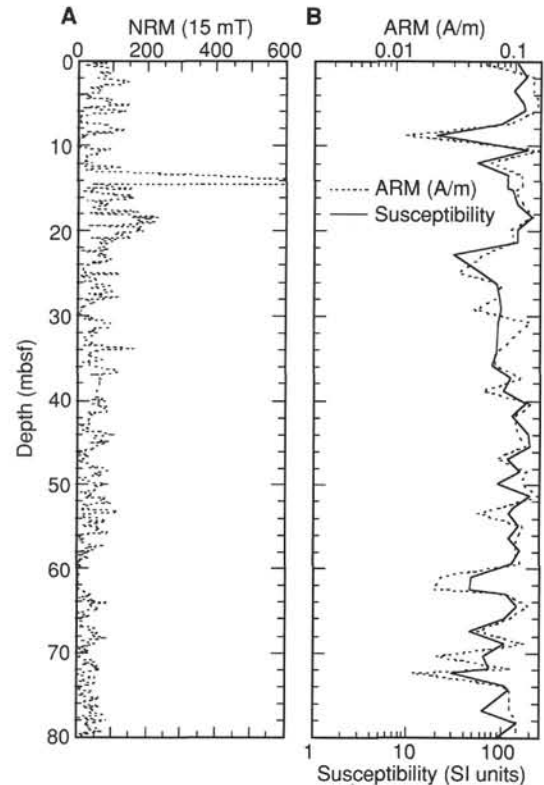


Figure 15. Comparison of whole-core measurements of inclinations, after 15 mT demagnetization, from Holes 881B and 881C. Discrete-sample data after 30 mT demagnetization are shown (open circles are from the Molspin spinner; open squares from the Japanese spinner) for Hole 881B for comparison with whole-core data.

the clay and quartz components of the sediments increases sharply, indicating increased terrigenous influx to the deep sea. Bottom-current mediation of the depositional process becomes dominant at 2.6 Ma, implying a vigorous circulation of Pacific Ocean Deep Water since that time. And, coincident with all these paleoceanographic and paleoclimatic changes, volcanism in the Kuril-Kamchatka arc began a period of heightened activity.

## REFERENCES\*

- Abelmann, A., 1992. Early to middle Miocene radiolarian stratigraphy of the Kerguelen Plateau, Leg 120. In Wise, S.W., Jr., Schlich, R., et al., *Proc. ODP, Sci. Results*, 120: College Station, TX (Ocean Drilling Program), 757–783.
- Barron, J.A., 1980. Lower Miocene to Quaternary diatom biostratigraphy of Leg 57, off northeastern Japan, Deep Sea Drilling Project. In von Huene, R., Nasu, N., et al., *Init. Repts. DSDP*, 56, 57 (Pt. 2): Washington (U.S. Govt. Printing Office), 641–686.
- , 1992. Neogene diatom datum levels in the equatorial and North Pacific. In Saito, T., and Ishizaki, K. (Eds.), *The Centenary of Japanese Micropaleontology*: Tokyo (Tokyo Univ. Press), 413–425.
- Berggren, W.A., Kent, D.V., and Van Couvering, J.A., 1985. The Neogene: Part 2. Neogene geochronology and chronostratigraphy. In Snelling, N.J. (Ed.), *The Chronology of the Geological Record*. Geol. Soc. London Mem., 10:211–260.
- Bischoff, J.L., Greer, R.E., and Luistro, A.O., 1970. Composition of interstitial waters of marine sediments: temperature of squeezing effect. *Science*, 167:1245–1246.
- Boyce, R.E., 1976. Definitions and laboratory techniques of compressional sound velocity parameters and wet-water content, wet-bulk density, and

\* Abbreviations for names of organizations and publication titles in ODP reference lists follow the style given in *Chemical Abstracts Service Source Index* (published by American Chemical Society).

- porosity parameters by gravimetric and gamma ray attenuation techniques. *In* Schlanger, S.O., Jackson, E.D., et al., *Init. Repts. DSDP*, 33: Washington (U.S. Govt. Printing Office), 931–958.
- Cande, S.C., and Kent, D.V., 1992. A new geomagnetic polarity timescale for the Late Cretaceous and Cenozoic. *J. Geophys. Res.*, 97:13917–13951.
- Chen, P.H., 1975. Antarctic radiolaria. *In* Hayes, D.E., Frakes, L.A., et al., *Init. Repts. DSDP*, 28: Washington (U.S. Govt. Printing Office), 437–513.
- Damuth, J.E., Jacobi, R.D., and Hayes, D.E., 1983. Sedimentation processes in the northwest Pacific Basin revealed by the echo-character mapping studies. *Geol. Soc. Am. Bull.*, 94:381–395.
- Foreman, H.P., 1975. Radiolaria from the North Pacific, Deep Sea Drilling Project, Leg 32. *In* Larson, R.L., Moberly, R., et al., *Init. Repts. DSDP*, 32: Washington (U.S. Govt. Printing Office), 579–676.
- Froelich, P.N., Klinkhammer, G.P., Bender, M.L., Luedtke, N.A., Heath, G.R., Cullen, D., Dauphin, P., Hartman, B., Hammond, D., and Maynard, V., 1979. Early oxidation of organic matter in pelagic sediments of the eastern Equatorial Atlantic: suboxic diagenesis. *Geochim. Cosmochim. Acta*, 43:1075–1090.
- Gieskes, J.M., 1981. Deep-sea drilling interstitial water studies: implications for chemical alteration of the oceanic crust, layers I and II. *In* Warne, J.E., Douglas, R.G., and Winterer, E.L. (Eds.), *The Deep Sea Drilling Project: A Decade of Progress*. Spec. Publ.—Soc. Econ. Paleontol. Mineral., 32:149–167.
- Hays, J.D., 1970. Stratigraphy and evolutionary trends of radiolaria in North Pacific deep sea sediments. *In* Hays, J.D. (Ed.), *Geological Investigations of the North Pacific*. Mem.—Geol. Soc. Am., 126:185–218.
- Hays, J.D., and Shackleton, N.J., 1976. Globally synchronous extinction of radiolarian *Stylatractus universus*. *Geology*, 4:649–652.
- Heath, G.R., Burckle, L.H., et al., 1985. *Init. Repts. DSDP*, 86: Washington (U.S. Govt. Printing Office).
- Hurd, D.C., and Theyer, F., 1975. Changes in the physical and chemical properties of biogenic silica from the central equatorial Pacific. I: Solubility, specific surface area, and solution rate constants of acid-cleaned samples. *In* Gibbs, T.R.P., Jr. (Ed.), *Analytical Methods in Oceanography*, Am. Chem. Soc., Advances in Chemistry Ser., 147:211–230.
- Janecek, T.R., 1985. Eolian sedimentation in the Northwest Pacific Ocean: a preliminary examination of the data from Deep Sea Drilling Project Sites 576 and 578. *In* Heath, G.R., Burckle, L.H., et al., *Init. Repts. DSDP*, 86: Washington (U.S. Govt. Printing Office), 589–603.
- Janecek, T.R., and Rea, D.K., 1983. Eolian deposition in the Northeast Pacific Ocean: Cenozoic history of atmospheric circulation. *Geol. Soc. Am. Bull.*, 94:730–738.
- Keigwin, L.D., Jones, G.A., and Froelich, N.P., 1993. A 15,000-year paleoenvironmental record from Meiji seamount, far northwestern Pacific. *Earth Planet Sci. Lett.*, 111:425–440.
- Kennett, J.P., McBirney, A.R., and Thunell, R.C., 1977. Episodes of Cenozoic volcanism in the Circum-Pacific region. *J. Volcanol. Geotherm. Res.*, 2:145–163.
- Kennett, J.P., and Thunell, R.C., 1975. Global increase in Quaternary explosive volcanism. *Science*, 187:497–503.
- Kling, S.A., 1973. Radiolaria from the eastern North Pacific, Deep Sea Drilling Project Leg 18. *In* Kulm, L.D., von Huene, R., et al., *Init. Repts. DSDP*, 18: Washington (U.S. Govt. Printing Office), 617–671.
- Koizumi, I., 1992. Diatom biostratigraphy of the Japan Sea: Leg 127. *In* Pisciotto, K.A., Ingle, J.C., Jr., von Breyman, M.T., Barron, J., et al., *Proc. ODP, Sci. Results*, 127/128 (Pt. 1): College Station, TX (Ocean Drilling Program), 249–289.
- Krissek, L.A., Morley, J.J., and Lofland, D.K., 1985. The occurrence, abundance, and composition of ice-rafted debris in sediments from Deep Sea Drilling Project Sites 579 and 580, northwest Pacific. *In* Heath, G.R., Burckle, L.H., et al., *Init. Repts. DSDP*, 86: Washington (U.S. Govt. Printing Office), 647–655.
- Leinen, M., and Heath, G.R., 1981. Sedimentary indicators of atmospheric circulation in the Northern Hemisphere during the Cenozoic. *Palaeogeogr. Palaeoclimatol., Palaeoecol.*, 36:1–21.
- Ling, H.Y., 1973. Radiolaria: Leg 19 of the Deep Sea Drilling Project. *In* Creager, J.S., Scholl, D.W., et al., *Init. Repts. DSDP*, 19: Washington (U.S. Govt. Printing Office), 777–797.
- Mammerickx, J., and Sharman, G.F., 1988. Tectonic evolution of the North Pacific during the Cretaceous quiet period. *J. Geophys. Res.*, 93:3009–3024.
- Mangelsdorf, P.C., Wilson, T.R.S., and Daniel, E., 1969. Potassium enrichments in interstitial waters of recent marine sediments. *Science*, 165:171–174.
- McDuff, R.E., 1985. The chemistry of interstitial waters, Deep Sea Drilling Project, Leg 86. *In* Heath, G.R., Burckle, L.H., et al., *Init. Repts. DSDP*, 86: Washington (U.S. Govt. Printing Office), 675–687.
- McDuff, R.E., and Gieskes, J.M., 1976. Calcium and magnesium profiles in DSDP interstitial waters: diffusion or reaction? *Earth Planet. Sci. Lett.*, 33:1–10.
- Morley, J.J., 1985. Radiolarians from the Northwest Pacific, Deep Sea Drilling Project Leg 86. *In* Heath, G.R., Burckle, L.H., et al., *Init. Repts. DSDP*, 86: Washington (U.S. Govt. Printing Office), 399–422.
- Morley, J.J., and Shackleton, N.J., 1978. Extension of the radiolarian *Stylatractus universus* as a biostratigraphic datum to the Atlantic Ocean. *Geology*, 6:309–311.
- Rea, D.K., Leinen, M., and Janecek, T.R., 1985. A geological approach to the long-term history of atmospheric circulation. *Science*, 227:721–725.
- Rea, D.K., and Schrader, H., 1985. Late Pliocene onset of glaciation: ice rafting and diatom stratigraphy of North Pacific DSDP cores. *Palaeogeogr. Palaeoclimatol., Palaeoecol.*, 49:313–325.
- Renkin, M.L., and Sclater, J.G., 1988. Depth and age in the North Pacific. *J. Geophys. Res.*, 93:2919–2935.
- Reynolds, R.A., 1980. Radiolarians from the western North Pacific, Leg 57, Deep Sea Drilling Project. *In* von Huene, R., Nasu, N., et al., *Init. Repts. DSDP*, 56, 57 (Pt. 2): Washington (U.S. Govt. Printing Office), 735–769.
- Riedel, W.R., and Sanfilippo, A., 1970. Radiolaria, Leg 4, Deep Sea Drilling Project. *In* Bader, R.G., Gerard, R.D., et al., *Init. Repts. DSDP*, 4: Washington (U.S. Govt. Printing Office), 503–575.
- , 1978. Stratigraphy and evolution of tropical Cenozoic radiolarians. *Micropaleontology*, 24:61–96.
- Ruddiman, W.F., Raymo, M.E., Martinson, D.G., Clement, B.M., and Backman, J., 1989. Pleistocene evolution: Northern Hemisphere ice sheets and North Atlantic Ocean. *Paleoceanography*, 4:353–412.
- Shackleton, N.J., Backman, J., Zimmerman, H., Kent, D.V., Hall, M.A., Roberts, D.G., Schnitker, D., Baldauf, J., Desprairies, A., Homrighausen, R., Huddleston, P., Keene, J.B., Kaltenback, A.J., Krumsiek, K.A.O., Morton, A.C., Murray, J.W., and Westberg-Smith, J., 1984. Oxygen isotope calibration of the onset of ice-rafting in DSDP Site 552A: history of glaciation in the North Atlantic region. *Nature*, 307:620–623.
- Shackleton, N.J., Berger, A., and Peltier, W.R., 1990. An alternative astronomical calibration of the lower Pleistocene timescale based on ODP Site 677. *Trans. R. Soc. Edinburgh, Earth Sci.*, 81:251–261.
- von Huene, R., Crouch, J., and Larson, E., 1976. Glacial advance in the Gulf of Alaska area implied by ice rafted material. *In* Cline, R.M., and Hays, J.D. (Eds.), *Investigation of Late Quaternary Paleooceanography and Paleoclimatology*. Mem.—Geol. Soc. Am., 145:411–422.
- Wolfart, R., 1981. Neogene radiolarians from the eastern North Pacific (off Alta and Baja California), Deep Sea Drilling Project Leg 63. *In* Yeats, R.S., Haq, B.U., et al., *Init. Repts. DSDP*, 63: Washington (U.S. Govt. Printing Office), 473–506.

## Ms 145IR-105

**NOTE: For all sites drilled, core-description forms (“barrel sheets”) and core photographs can be found in Section 3, beginning on page 395. Forms containing smear-slide data can be found in Section 4, beginning on page 985. Conventional log data can be found in CD-ROM form (back pocket).**

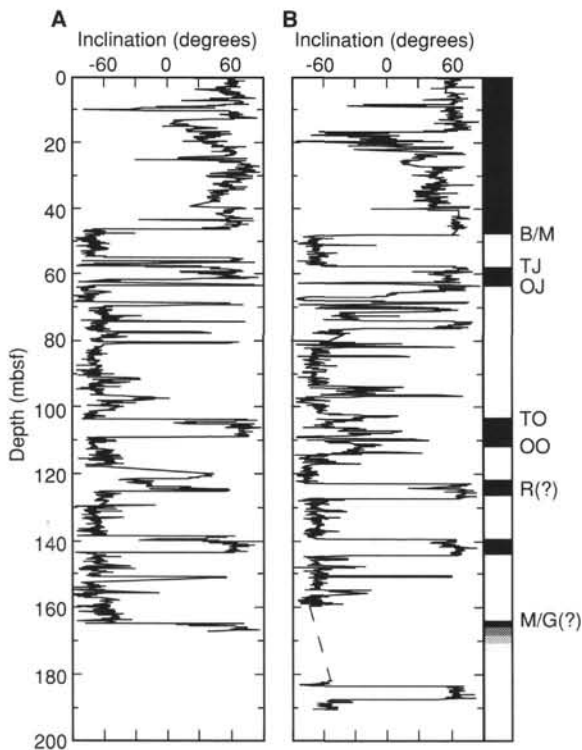


Figure 16. Magnetic inclination from whole-core measurements after 15 mT. A. Hole 881D. B. Hole 881C. Magnetostratigraphic interpretation also shown.

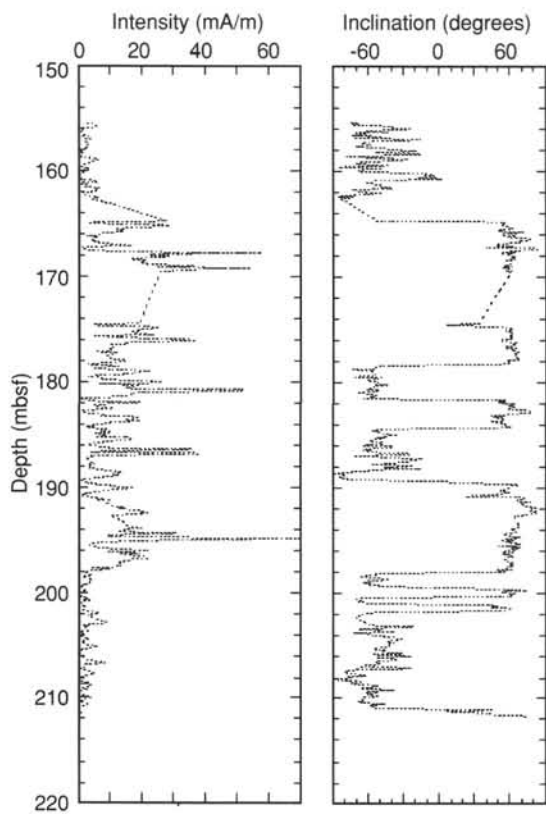


Figure 17. Magnetic intensity and inclination from whole-core measurements at Hole 881D after 15 mT demagnetization.

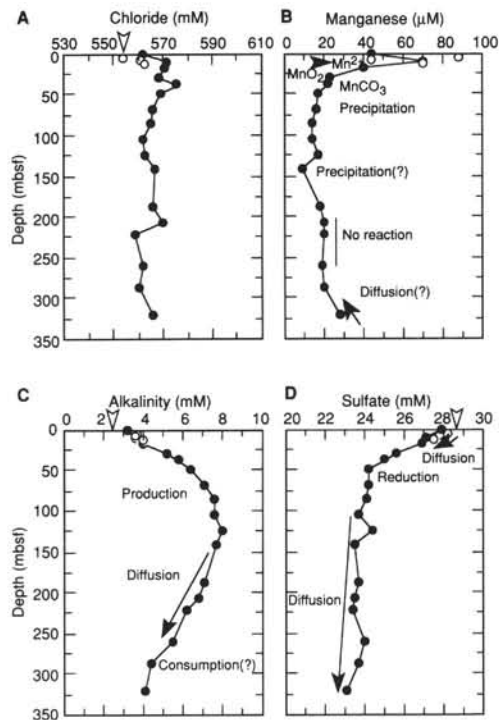


Figure 18. A. Chloride. B. Manganese. C. Alkalinity. D. Sulfate. Concentrations plotted vs. depth in interstitial waters at Site 881. Open circles indicate samples from Hole 881A; filled circles indicate samples from Hole 881C. Open arrowhead indicates the concentration in modern seawater.

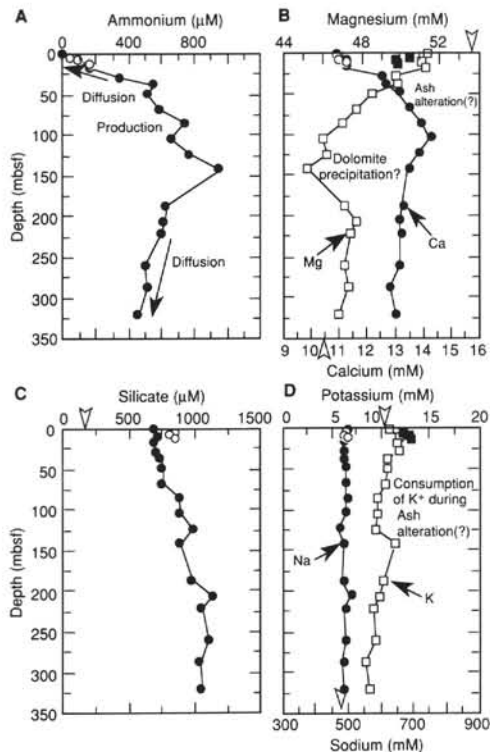


Figure 19. A. Ammonium. B. Calcium and magnesium. C. Silicate. D. Potassium and sodium. Concentrations plotted vs. depth in interstitial waters at Site 881. Open circles indicate samples from Hole 881A; filled circles indicate samples from Hole 881C. Open arrowhead indicates the concentration in modern seawater.

Table 15. Index properties data from Hole 881B.

Core, section, interval (cm)	Depth (mbsf)	Wet-bulk density <sub>s</sub> (g/cm <sup>3</sup> )	Dry-bulk density <sub>s</sub> (g/cm <sup>3</sup> )	Grain density <sub>s</sub> (g/cm <sup>3</sup> )	Wet porosity (%)	Dry porosity (%)	Wet water content (%)	Dry water content (%)	Void ratio 1	Void ratio 2
145-881B-										
1H-1, 37.0	0.37	1.39	0.55	3.12	82.1	82.6	60.5	153.4	4.58	4.67
1H-1, 109.0	1.09	1.41	0.64	2.60	75.0	75.6	54.6	120.1	3.00	3.05
1H-2, 53.0	2.03	1.37	0.55	2.83	80.3	80.9	60.1	150.8	4.08	4.16
1H-2, 110.0	2.60	1.36	0.59	2.44	75.5	76.1	56.8	131.5	3.09	3.13
1H-3, 39.0	3.39	1.43	0.67	2.64	74.3	74.8	53.1	113.3	2.88	2.92
1H-3, 103.0	4.03	1.42	0.64	2.73	76.3	76.9	55.0	122.4	3.22	3.27
1H-4, 39.0	4.89	1.50	0.80	2.56	68.5	69.0	46.8	87.9	2.17	2.20
2H-1, 39.0	5.89	1.44	0.68	2.66	74.2	74.8	52.9	112.4	2.88	2.92
2H-1, 102.0	6.52	1.38	0.56	2.77	79.2	79.8	59.0	143.7	3.81	3.88
2H-2, 39.0	7.39	1.44	0.66	2.75	75.5	76.1	53.9	116.7	3.09	3.13
2H-2, 110.0	8.10	1.38	0.59	2.62	77.0	77.6	57.0	132.7	3.34	3.40
2H-3, 39.0	8.89	1.51	0.84	2.45	65.4	65.9	44.4	79.8	1.89	1.91
2H-3, 110.0	9.60	1.34	0.51	2.73	80.9	81.5	61.8	161.8	4.23	4.32
2H-4, 39.0	10.39	1.34	0.53	2.55	78.7	79.3	60.2	151.2	3.70	3.76
2H-4, 113.0	11.13	1.47	0.72	2.70	73.1	73.7	51.1	104.3	2.72	2.75
2H-5, 39.0	11.89	1.27	0.42	2.62	83.8	84.4	67.4	206.7	5.16	5.28
2H-5, 108.0	12.58	1.41	0.62	2.68	76.5	77.0	55.7	126.0	3.25	3.30
2H-6, 39.0	13.39	1.44	0.67	2.77	75.5	76.1	53.6	115.7	3.08	3.13
2H-6, 109.0	14.09	1.40	0.60	2.76	77.9	78.5	57.1	133.1	3.53	3.58
2H-7, 39.0	14.89	1.44	0.67	2.76	75.3	75.9	53.5	115.1	3.05	3.09
3H-1, 45.0	15.45	1.39	0.58	2.86	79.4	79.9	58.4	140.2	3.85	3.92
3H-1, 109.0	16.09	1.44	0.68	2.69	74.5	75.1	53.0	112.8	2.92	2.96
3H-2, 39.0	16.89	1.38	0.58	2.72	78.2	78.8	57.9	137.5	3.59	3.65
3H-2, 109.0	17.59	1.46	0.71	2.63	72.6	73.2	51.1	104.7	2.65	2.69
3H-3, 44.0	18.44	1.41	0.63	2.67	76.0	76.5	55.2	123.0	3.16	3.21
3H-3, 109.0	19.09	1.33	0.49	2.68	81.2	81.8	62.8	168.7	4.33	4.42
3H-4, 39.0	19.89	1.46	0.72	2.63	72.1	72.7	50.5	101.9	2.59	2.62
3H-4, 109.0	20.59	1.41	0.64	2.67	75.8	76.4	55.0	122.0	3.14	3.18
3H-5, 39.0	21.39	1.44	0.69	2.61	73.2	73.8	52.1	108.8	2.74	2.77
3H-5, 106.0	22.06	1.49	0.68	3.41	79.8	80.3	54.8	121.0	3.95	4.03
3H-6, 41.0	22.91	1.24	0.39	2.36	83.1	83.8	68.6	219.0	4.92	5.04
4H-1, 49.0	24.99	1.51	0.80	2.67	69.9	70.4	47.4	90.1	2.32	2.35
4H-1, 109.0	25.59	1.44	0.69	2.65	73.6	74.1	52.2	109.2	2.79	2.82
4H-2, 39.0	26.39	1.38	0.59	2.58	76.8	77.4	57.2	133.6	3.31	3.36
4H-2, 109.0	27.09	1.30	0.49	2.39	79.0	79.6	62.1	164.1	3.76	3.83
4H-3, 32.0	27.82	1.49	0.78	2.55	69.3	69.8	47.8	91.5	2.26	2.28
4H-3, 117.0	28.67	1.46	0.71	2.63	72.5	73.1	51.0	104.0	2.64	2.67
4H-4, 39.0	29.39	1.46	0.72	2.64	72.4	72.9	50.8	103.2	2.62	2.66
4H-4, 112.0	30.12	1.49	0.78	2.56	69.4	69.9	47.8	91.5	2.27	2.29
4H-5, 39.0	30.89	1.33	0.50	2.69	81.1	81.7	62.5	166.4	4.29	4.38
4H-5, 109.0	31.59	1.51	0.77	2.88	73.1	73.6	49.4	97.7	2.71	2.75
4H-6, 39.0	32.39	1.41	0.61	2.84	78.3	78.8	56.9	131.9	3.60	3.66
4H-6, 109.0	33.09	1.44	0.67	2.76	75.3	75.9	53.5	114.9	3.05	3.10
4H-7, 39.0	33.89	1.44	0.67	2.74	75.1	75.6	53.3	114.3	3.01	3.05
5H-1, 39.0	34.39	1.37	0.58	2.62	77.5	78.1	57.8	137.2	3.45	3.50
5H-1, 109.0	35.09	1.47	0.75	2.58	70.8	71.3	49.3	97.2	2.42	2.45
5H-2, 39.0	35.89	1.35	0.57	2.49	76.9	77.5	58.1	138.9	3.33	3.38
5H-2, 109.0	36.59	1.38	0.61	2.45	74.6	75.2	55.5	124.6	2.94	2.98
5H-3, 39.0	37.39	1.39	0.60	2.62	76.8	77.4	56.8	131.3	3.31	3.36
5H-3, 119.0	38.19	1.52	0.81	2.64	68.9	69.4	46.5	86.8	2.21	2.24
5H-4, 39.0	38.89	1.50	0.80	2.58	68.7	69.2	46.9	88.2	2.20	2.22
5H-4, 109.0	39.59	1.41	0.65	2.54	73.9	74.4	53.7	115.8	2.83	2.87
5H-5, 39.0	40.39	1.48	0.75	2.63	71.2	71.7	49.3	97.2	2.47	2.50
5H-5, 109.0	41.09	1.46	0.70	2.70	73.7	74.2	51.8	107.4	2.80	2.84
5H-6, 39.0	41.89	1.24	0.46	1.97	76.3	77.1	63.0	169.9	3.23	3.27
5H-6, 104.0	42.54	1.48	0.73	2.73	72.9	73.4	50.4	101.8	2.68	2.72
5H-7, 39.0	43.39	1.35	0.56	2.49	77.3	77.9	58.7	142.2	3.40	3.45
6H-1, 45.0	43.95	1.44	0.67	2.78	75.6	76.2	53.7	115.8	3.10	3.15
6H-1, 109.0	44.59	1.44	0.71	2.55	72.0	72.5	51.1	104.5	2.57	2.60
6H-2, 39.0	45.39	1.53	0.80	2.78	71.0	71.5	47.6	90.9	2.44	2.47
6H-2, 117.0	46.17	1.44	0.66	2.75	75.7	76.2	54.0	117.5	3.11	3.16
6H-3, 47.0	46.97	1.44	0.67	2.75	75.4	75.9	53.7	115.8	3.06	3.10
6H-3, 111.0	47.61	1.50	0.78	2.61	69.7	70.2	47.7	91.4	2.30	2.32
6H-4, 39.0	48.39	1.39	0.63	2.47	74.3	74.9	54.9	121.6	2.90	2.94
6H-4, 109.0	49.09	1.48	0.76	2.52	69.4	69.9	48.2	92.9	2.27	2.29
6H-5, 39.0	49.89	1.36	0.61	2.32	73.6	74.2	55.5	124.5	2.78	2.82
6H-5, 109.0	50.59	1.41	0.69	2.36	70.3	70.9	50.9	103.7	2.37	2.39
6H-6, 39.0	51.39	1.47	0.75	2.62	71.2	71.7	49.5	97.8	2.47	2.50
6H-6, 97.0	51.97	1.41	0.67	2.46	72.6	73.1	52.7	111.5	2.64	2.68
6H-7, 39.0	52.89	1.46	0.71	2.66	73.0	73.5	51.3	105.5	2.70	2.74
7H-1, 36.0	53.36	1.53	0.82	2.67	68.9	69.4	46.2	85.9	2.21	2.24
7H-1, 111.0	54.11	1.40	0.61	2.74	77.4	77.9	56.5	129.9	3.42	3.47
7H-2, 44.0	54.94	1.38	0.59	2.60	76.8	77.4	56.9	132.2	3.31	3.36
7H-2, 110.0	55.60	1.45	0.68	2.79	75.1	75.7	53.0	112.7	3.02	3.07
7H-3, 114.0	57.14	1.34	0.55	2.38	76.4	77.0	58.6	141.6	3.24	3.29
7H-4, 44.0	57.94	1.36	0.57	2.52	77.2	77.7	58.2	139.5	3.38	3.43
7H-4, 109.0	58.59	1.49	0.78	2.54	68.8	69.3	47.3	89.8	2.20	2.23
7H-5, 39.0	59.39	1.44	0.70	2.57	72.4	73.0	51.5	106.1	2.63	2.66
7H-5, 101.0	60.01	1.46	0.73	2.59	71.7	72.2	50.3	101.3	2.53	2.56
7H-6, 39.0	60.89	1.49	0.78	2.62	70.0	70.5	48.0	92.3	2.33	2.36
7H-6, 94.0	61.44	1.45	0.72	2.55	71.3	71.8	50.2	100.9	2.48	2.51
7H-7, 39.0	62.39	1.53	0.87	2.46	64.2	64.7	42.9	75.2	1.79	1.81
8H-1, 39.0	62.89	1.46	0.70	2.73	74.1	74.6	52.1	108.6	2.86	2.89

Table 15 continued.

Core, section, interval (cm)	Depth (mbsf)	Wet-bulk density (g/cm <sup>3</sup> )	Dry-bulk density (g/cm <sup>3</sup> )	Grain density (g/cm <sup>3</sup> )	Wet porosity (%)	Dry porosity (%)	Wet water content (%)	Dry water content (%)	Void ratio 1	Void ratio 2
8H-1, 109.0	63.59	1.31	0.47	2.56	81.1	81.8	63.7	175.4	4.30	4.39
8H-2, 39.0	64.39	1.56	0.87	2.72	67.8	68.3	44.4	80.0	2.10	2.12
8H-2, 109.0	65.09	1.63	1.06	2.43	56.2	56.6	35.2	54.4	1.28	1.29
8H-3, 39.0	65.89	1.52	0.80	2.72	70.4	70.9	47.5	90.4	2.37	2.40
8H-3, 109.0	66.59	1.57	0.87	2.76	68.3	68.8	44.7	80.8	2.15	2.17
8H-4, 39.0	67.39	1.37	0.58	2.52	76.7	77.2	57.5	135.3	3.28	3.33
8H-4, 109.0	68.09	1.31	0.50	2.47	79.6	80.2	62.2	164.7	3.90	3.97
8H-5, 39.0	68.89	1.53	0.82	2.73	69.7	70.2	46.5	87.0	2.30	2.32
8H-5, 109.0	69.59	1.56	0.87	2.69	67.4	67.9	44.3	79.5	2.07	2.09
8H-6, 39.0	70.39	1.53	0.86	2.49	65.4	65.9	43.9	78.3	1.89	1.91
8H-6, 109.0	71.09	1.43	0.72	2.41	69.7	70.3	49.8	99.2	2.30	2.33
8H-7, 39.0	71.89	1.33	0.52	2.50	78.7	79.4	60.7	154.7	3.71	3.77
9H-1, 39.0	72.39	1.66	1.14	2.34	51.0	51.5	31.4	45.8	1.04	1.05
9H-1, 109.0	73.09	1.48	0.75	2.66	71.6	72.2	49.6	98.3	2.53	2.55
9H-2, 39.0	73.89	1.29	0.49	2.33	78.7	79.4	62.3	165.6	3.70	3.77
9H-2, 109.0	74.59	1.45	0.68	2.76	75.1	75.6	53.2	113.6	3.01	3.06
9H-3, 39.0	75.39	1.52	0.80	2.76	70.8	71.4	47.7	91.3	2.43	2.46
9H-3, 109.0	76.09	1.50	0.79	2.61	69.4	69.9	47.3	89.9	2.27	2.29
9H-4, 39.0	76.89	1.31	0.48	2.61	81.4	82.0	63.7	175.2	4.38	4.46
9H-4, 109.0	77.59	1.34	0.53	2.56	78.9	79.5	60.4	152.4	3.74	3.81
9H-5, 109.0	79.09	1.56	0.90	2.56	64.3	64.8	42.2	72.9	1.80	1.82
9H-6, 39.0	79.89	1.40	0.62	2.63	76.1	76.7	55.8	126.1	3.19	3.24
9H-6, 109.0	80.59	1.47	0.74	2.63	71.4	72.0	49.7	98.7	2.50	2.53
9H-7, 29.0	81.29	1.52	0.81	2.71	69.9	70.4	47.0	88.6	2.32	2.34
10H-1, 35.0	81.85	1.59	0.93	2.65	64.8	65.2	41.7	71.6	1.84	1.85
10H-1, 114.0	82.64	1.47	0.76	2.46	68.7	69.2	48.0	92.1	2.19	2.22
10H-2, 39.0	83.39	1.48	0.76	2.60	70.7	71.2	48.9	95.9	2.41	2.44
10H-2, 102.0	84.02	1.44	0.71	2.48	71.2	71.8	50.8	103.3	2.48	2.51
10H-3, 39.0	84.89	1.53	0.86	2.52	65.4	65.9	43.7	77.7	1.89	1.91
10H-3, 119.0	85.69	1.46	0.73	2.56	71.0	71.5	49.8	99.0	2.44	2.47
10H-4, 39.0	86.39	1.38	0.71	2.10	66.1	66.7	49.0	96.0	1.95	1.96
10H-4, 114.0	87.14	1.44	0.68	2.66	74.0	74.5	52.6	110.9	2.84	2.88
10H-5, 39.0	87.89	1.43	0.69	2.54	72.5	73.0	51.8	107.6	2.63	2.66
10H-5, 114.0	88.64	1.40	0.63	2.65	76.1	76.6	55.5	124.6	3.18	3.23
10H-6, 39.0	89.39	1.49	0.77	2.64	70.6	71.1	48.5	94.0	2.40	2.42
10H-6, 114.0	90.14	1.33	0.55	2.40	76.9	77.5	59.1	144.2	3.33	3.38
10H-7, 45.0	90.95	1.43	0.68	2.52	72.6	73.2	52.2	109.2	2.66	2.69
11H-1, 39.0	91.39	1.48	0.76	2.57	70.1	70.6	48.5	94.2	2.34	2.37
11H-1, 113.0	92.13	1.41	0.66	2.53	73.7	74.3	53.5	115.0	2.80	2.84
11H-2, 39.0	92.89	1.45	0.71	2.56	71.9	72.4	50.9	103.7	2.56	2.59
11H-2, 109.0	93.59	1.53	0.87	2.44	64.1	64.6	43.1	75.6	1.79	1.80
11H-3, 39.0	94.39	1.40	0.63	2.50	74.3	74.9	54.6	120.1	2.89	2.93
11H-3, 112.0	95.12	1.38	0.60	2.51	75.5	76.1	56.1	128.0	3.09	3.13
11H-4, 39.0	95.89	1.44	0.69	2.58	72.8	73.4	51.9	107.8	2.68	2.71
11H-4, 109.0	96.59	1.41	0.64	2.58	74.8	75.4	54.5	119.7	2.97	3.01
11H-5, 39.0	97.39	1.38	0.60	2.54	75.9	76.5	56.2	128.5	3.15	3.19
11H-5, 114.0	98.14	1.41	0.65	2.57	74.5	75.1	54.2	118.4	2.93	2.96
11H-6, 39.0	98.89	1.39	0.63	2.43	73.6	74.2	54.4	119.2	2.80	2.83
11H-6, 111.0	99.61	1.44	0.71	2.47	70.9	71.5	50.6	102.3	2.44	2.47
11H-7, 19.0	100.19	1.39	0.60	2.64	77.0	77.5	56.8	131.6	3.34	3.39
12H-1, 39.0	100.89	1.56	0.88	2.65	66.5	67.0	43.7	77.6	1.99	2.00
12H-1, 114.0	101.64	1.40	0.63	2.58	75.3	75.9	55.1	122.8	3.05	3.10
12H-2, 41.0	102.41	1.38	0.61	2.54	75.6	76.2	56.0	127.1	3.11	3.15
12H-2, 109.0	103.09	1.44	0.70	2.52	71.8	72.3	51.1	104.6	2.54	2.57
12H-3, 39.0	103.89	1.47	0.75	2.55	70.1	70.7	48.8	95.2	2.35	2.37
12H-3, 114.0	104.64	1.46	0.74	2.50	70.1	70.7	49.3	97.2	2.35	2.37
12H-4, 39.0	105.39	1.36	0.58	2.48	76.1	76.7	57.2	133.4	3.18	3.23
12H-4, 109.0	106.09	1.34	0.56	2.38	76.2	76.8	58.3	139.9	3.20	3.24
12H-5, 39.0	106.89	1.41	0.65	2.56	74.3	74.8	54.0	117.3	2.89	2.92
12H-5, 114.0	107.64	1.41	0.63	2.60	75.3	75.9	54.9	121.7	3.05	3.09
12H-6, 39.0	108.39	1.35	0.56	2.51	77.4	78.0	58.7	142.3	3.43	3.48
12H-6, 114.0	109.14	1.47	0.73	2.63	71.8	72.4	50.1	100.5	2.55	2.58
12H-7, 39.0	109.89	1.44	0.72	2.43	69.9	70.5	49.8	99.3	2.33	2.35
13H-1, 39.0	110.39	1.40	0.61	2.67	76.8	77.4	56.4	129.1	3.32	3.37
13H-1, 119.0	111.19	1.36	0.60	2.36	74.4	75.0	56.1	127.8	2.91	2.95
13H-2, 40.0	111.90	1.49	0.81	2.44	66.3	66.9	45.5	83.6	1.97	1.99
13H-2, 108.0	112.58	1.46	0.73	2.53	70.7	71.2	49.6	98.6	2.41	2.44
13H-3, 39.0	113.39	1.41	0.64	2.58	74.9	75.5	54.6	120.4	2.99	3.03
13H-3, 115.0	114.15	1.38	0.60	2.58	76.6	77.1	56.8	131.6	3.27	3.32
13H-4, 39.0	114.89	1.47	0.76	2.52	69.6	70.1	48.4	93.9	2.28	2.31
13H-4, 119.0	115.69	1.47	0.74	2.61	71.5	72.0	49.9	99.6	2.51	2.54
13H-5, 36.0	116.36	1.48	0.78	2.51	68.7	69.2	47.5	90.4	2.19	2.22
13H-5, 109.0	117.09	1.49	0.79	2.53	68.7	69.2	47.2	89.5	2.19	2.21
13H-6, 38.0	117.88	1.42	0.67	2.58	73.8	74.4	53.1	113.3	2.82	2.86
14H-1, 39.0	119.89	1.36	0.56	2.57	77.8	78.4	58.7	142.3	3.51	3.57
14H-1, 114.0	120.64	1.48	0.77	2.51	68.9	69.4	47.7	91.4	2.22	2.24
14H-2, 39.0	121.39	1.39	0.63	2.49	74.4	75.0	54.8	121.4	2.91	2.95
14H-2, 109.0	122.09	1.44	0.71	2.48	71.0	71.6	50.6	102.3	2.45	2.48
14H-3, 39.0	122.89	1.42	0.67	2.53	73.2	73.7	52.9	112.1	2.73	2.76
14H-3, 109.0	123.59	1.38	0.62	2.43	74.1	74.7	55.1	122.5	2.87	2.91
14H-4, 39.0	124.39	1.44	0.68	2.66	74.0	74.5	52.5	110.7	2.84	2.88
14H-4, 109.0	125.09	1.35	0.58	2.37	75.1	75.7	56.9	132.2	3.02	3.06
14H-5, 39.0	125.89	1.52	0.83	2.52	66.6	67.1	45.1	82.0	2.00	2.01
14H-5, 107.0	126.57	1.45	0.70	2.61	72.9	73.4	51.6	106.8	2.69	2.72
14H-6, 39.0	127.39	1.38	0.58	2.64	77.5	78.1	57.6	135.9	3.45	3.51

Table 15 continued.

Core, section, interval (cm)	Depth (mbsf)	Wet-bulk density (g/cm <sup>3</sup> )	Dry-bulk density (g/cm <sup>3</sup> )	Grain density (g/cm <sup>3</sup> )	Wet porosity (%)	Dry porosity (%)	Wet water content (%)	Dry water content (%)	Void ratio 1	Void ratio 2
14H-7, 39.0	128.39	1.50	0.80	2.56	68.3	68.8	46.5	87.0	2.15	2.17
15H-1, 39.0	129.39	1.50	0.81	2.51	67.5	68.1	46.1	85.6	2.08	2.10
15H-1, 115.0	130.15	1.52	0.82	2.57	67.8	68.3	45.8	84.5	2.10	2.12
15H-2, 39.0	130.89	1.48	0.76	2.55	69.7	70.3	48.3	93.5	2.31	2.33
15H-2, 109.0	131.59	1.34	0.55	2.45	77.1	77.7	58.8	142.7	3.36	3.42
15H-3, 39.0	132.39	1.41	0.65	2.60	74.8	75.3	54.2	118.4	2.96	3.00
15H-3, 114.0	133.14	1.38	0.59	2.61	76.9	77.5	57.0	132.6	3.33	3.38
15H-4, 39.0	133.89	1.50	0.69	3.31	78.7	79.3	53.9	116.7	3.70	3.77
15H-4, 109.0	134.59	1.47	0.74	2.58	70.9	71.4	49.4	97.5	2.43	2.46
15H-5, 39.0	135.39	1.44	0.71	2.48	70.9	71.5	50.4	101.7	2.44	2.46
15H-5, 109.0	136.09	1.51	0.82	2.57	67.9	68.4	45.9	85.0	2.11	2.13
15H-6, 39.0	136.89	1.53	0.80	2.83	71.3	71.8	47.6	90.8	2.48	2.51
15H-6, 109.0	137.59	1.43	0.67	2.69	74.9	75.4	53.5	114.9	2.98	3.02
16H-1, 39.0	138.89	1.50	0.77	2.73	71.3	71.8	48.6	94.4	2.49	2.52
16H-1, 109.0	139.59	1.37	0.60	2.48	75.6	76.2	56.6	130.2	3.10	3.15
16H-2, 39.0	140.39	1.43	0.68	2.58	73.5	74.0	52.7	111.2	2.77	2.80
16H-2, 109.0	141.09	1.42	0.67	2.58	73.8	74.4	53.1	113.3	2.82	2.86
16H-3, 39.0	141.89	1.42	0.66	2.61	74.3	74.9	53.5	115.0	2.90	2.93
16H-3, 114.0	142.64	1.53	0.82	2.66	68.7	69.2	46.1	85.5	2.20	2.22
16H-4, 39.0	143.39	1.38	0.61	2.50	75.1	75.6	55.6	125.1	3.01	3.05
16H-4, 109.0	144.09	1.55	0.86	2.69	67.8	68.3	44.7	81.0	2.11	2.13
16H-5, 39.0	144.89	1.40	0.68	2.34	70.8	71.3	51.7	107.1	2.42	2.45
16H-5, 109.0	145.59	1.42	0.66	2.60	74.1	74.7	53.4	114.6	2.87	2.91
16H-6, 39.0	146.39	1.44	0.72	2.49	70.7	71.3	50.1	100.6	2.41	2.44
16H-6, 103.0	147.03	1.49	0.76	2.63	70.7	71.2	48.7	95.0	2.41	2.44
16H-7, 39.0	147.89	1.49	0.76	2.64	70.9	71.4	48.8	95.5	2.43	2.46
17H-1, 42.0	148.42	1.53	0.81	2.74	70.2	70.7	47.1	89.0	2.36	2.38
17H-2, 39.0	149.89	1.48	0.75	2.67	71.7	72.3	49.6	98.4	2.54	2.57
17H-2, 109.0	150.59	1.40	0.66	2.42	72.6	73.2	53.2	113.6	2.65	2.69
17H-3, 39.0	151.39	1.42	0.66	2.53	73.4	74.0	53.1	113.2	2.76	2.80
17H-3, 124.0	152.24	1.48	0.77	2.50	68.8	69.4	47.8	91.4	2.21	2.23
17H-4, 39.0	152.89	1.36	0.60	2.29	73.3	73.9	55.4	124.4	2.75	2.79
17H-4, 109.0	153.59	1.38	0.59	2.56	76.6	77.2	57.0	132.8	3.27	3.32
17H-5, 39.0	154.39	1.38	0.60	2.55	76.2	76.8	56.6	130.4	3.20	3.25
17H-5, 119.0	155.19	1.34	0.55	2.44	77.2	77.8	59.0	144.0	3.38	3.43
17H-6, 39.0	155.89	1.39	0.65	2.37	72.2	72.7	53.1	113.3	2.59	2.62
17H-6, 127.0	156.77	1.47	0.75	2.57	70.5	71.0	49.1	96.4	2.39	2.41
17H-7, 29.0	157.29	1.38	0.63	2.41	73.5	74.1	54.4	119.4	2.77	2.81
18H-1, 39.0	157.89	1.28	0.48	2.28	78.7	79.4	62.9	169.4	3.70	3.77
18H-1, 114.0	158.64	1.31	0.50	2.39	78.6	79.2	61.5	159.6	3.66	3.73
18H-2, 39.0	159.39	1.32	0.53	2.37	77.2	77.8	59.7	148.4	3.38	3.44
18H-2, 109.0	160.09	1.45	0.75	2.44	69.2	69.7	48.7	95.1	2.24	2.26
18H-3, 39.0	160.89	1.31	0.51	2.39	78.3	78.9	61.1	157.3	3.60	3.66
18H-3, 109.0	161.59	1.36	0.60	2.30	73.4	74.0	55.5	124.5	2.77	2.80
18H-4, 39.0	162.39	1.45	0.72	2.59	71.9	72.5	50.6	102.6	2.56	2.59
18H-4, 109.0	163.09	1.34	0.56	2.41	76.3	76.9	58.1	138.7	3.21	3.26
18H-5, 39.0	163.89	1.33	0.54	2.34	76.4	77.0	59.0	143.9	3.23	3.28
18H-5, 104.0	164.54	1.32	0.53	2.37	77.2	77.8	59.9	149.1	3.39	3.44
18H-6, 39.0	165.39	1.34	0.57	2.31	75.1	75.7	57.5	135.2	3.01	3.05
18H-6, 109.0	166.09	1.32	0.54	2.27	76.1	76.7	59.3	145.5	3.18	3.23
18H-7, 39.0	166.89	1.32	0.53	2.38	77.5	78.2	60.1	150.8	3.45	3.51

Table 16. Vane shear strength data from Hole 881B.

Core, section, interval (cm)	Depth (mbsf)	Shear strength (kPa)
145-881B-		
2H-2, 110.0	8.10	18.0
2H-3, 110.0	9.60	3.7
2H-4, 40.0	10.40	14.2
2H-5, 40.0	11.90	10.6
2H-5, 109.0	12.59	21.1
2H-6, 40.0	13.40	20.4
2H-7, 40.0	14.90	22.9
3H-1, 56.0	15.56	7.6
3H-1, 110.0	16.10	15.0
3H-2, 40.0	16.90	18.5
3H-2, 110.0	17.60	14.6
3H-3, 45.0	18.45	9.9
3H-3, 110.0	19.10	16.0
3H-4, 40.0	19.90	30.8
3H-4, 110.0	20.60	16.2
3H-5, 40.0	21.40	17.3
3H-5, 107.0	22.07	25.0
3H-6, 42.0	22.92	18.5
4H-1, 50.0	25.00	21.3
4H-1, 110.0	25.60	22.2
4H-2, 40.0	26.40	9.7
4H-2, 110.0	27.10	29.4
4H-3, 33.0	27.83	32.4
4H-3, 118.0	28.68	28.2
4H-4, 40.0	29.40	25.9
4H-4, 113.0	30.13	33.8
4H-5, 40.0	30.90	36.8
4H-5, 110.0	31.60	39.1
4H-6, 40.0	32.40	31.7
4H-6, 110.0	33.10	22.9
4H-7, 40.0	33.90	25.5
5H-1, 40.0	34.40	17.6
5H-1, 110.0	35.10	27.3
5H-2, 40.0	35.90	20.1
5H-2, 110.0	36.60	22.2
5H-3, 40.0	37.40	40.5
5H-3, 120.0	38.20	38.0
5H-4, 40.0	38.90	41.7
5H-4, 110.0	39.60	37.1
5H-5, 110.0	41.10	34.5
5H-6, 105.0	42.55	20.4
5H-7, 40.0	43.40	33.1
6H-1, 52.0	44.02	32.0
6H-1, 110.0	44.60	34.0
6H-2, 40.0	45.40	34.7
6H-2, 118.0	46.18	36.6
6H-3, 112.0	47.62	31.5
6H-4, 110.0	49.10	46.9
6H-5, 110.0	50.60	44.9
6H-6, 98.0	51.98	44.0
6H-7, 40.0	52.90	43.1
7H-1, 111.0	54.11	35.7
7H-2, 111.0	55.61	35.0
7H-3, 115.0	57.15	47.0
7H-4, 110.0	58.60	30.5
7H-5, 102.0	60.02	47.3
7H-6, 95.0	61.45	40.1
7H-7, 40.0	62.40	3.3
8H-1, 117.0	63.67	30.5
8H-2, 90.0	64.90	56.5
8H-3, 40.0	65.90	45.7
8H-3, 110.0	66.60	61.6
8H-4, 40.0	67.40	53.2
8H-5, 40.0	68.90	87.8
8H-6, 110.0	71.10	60.7
8H-7, 40.0	71.90	71.2
9H-1, 110.0	73.10	63.0
9H-2, 110.0	74.60	82.5
9H-3, 110.0	76.10	56.2
9H-4, 110.0	77.60	73.9
9H-5, 110.0	79.10	148.5
9H-6, 110.0	80.60	69.0
9H-7, 30.0	81.30	52.1
10H-1, 110.0	82.60	62.6
10H-2, 105.0	84.05	53.2
10H-3, 110.0	85.60	72.7
10H-4, 110.0	87.10	90.8
10H-5, 110.0	88.60	81.8
10H-6, 105.0	90.05	90.8
10H-7, 46.0	90.96	81.8
11H-1, 105.0	92.05	66.0
11H-2, 110.0	93.60	36.7
11H-3, 105.0	95.05	66.7
11H-4, 110.0	96.60	105.8

Table 16 continued.

Core, section, interval (cm)	Depth (mbsf)	Shear strength (kPa)
11H-5, 110.0	98.10	84.8
11H-6, 112.0	99.62	84.8
12H-1, 110.0	101.60	60.7
12H-2, 110.0	103.10	45.0
12H-3, 105.0	104.55	71.2
12H-4, 110.0	106.10	94.5
12H-5, 110.0	107.60	111.0
12H-6, 110.0	109.10	.5
13H-1, 115.0	111.15	106.5
13H-2, 108.0	112.58	132.0
13H-3, 112.0	114.12	21.0
13H-4, 115.0	115.65	94.5
13H-5, 110.0	117.10	91.5
13H-6, 35.0	117.85	125.3
14H-1, 110.0	120.60	102.0
14H-2, 110.0	122.10	60.7
14H-5, 108.0	126.58	105.8
14H-6, 80.0	127.80	87.8
15H-1, 116.0	130.16	67.5
15H-3, 110.0	133.10	63.7
15H-5, 110.0	136.10	190.6
16H-1, 110.0	139.60	91.5
16H-3, 110.0	142.60	193.6
16H-5, 110.0	145.60	112.5
17H-1, 110.0	149.10	86.3
17H-3, 120.0	152.20	75.7
17H-5, 120.0	155.20	102.8
18H-1, 115.0	158.65	75.7
18H-3, 120.0	161.70	87.8
18H-5, 105.0	164.55	141.0

Table 17. Index properties data from Hole 881C.

Core, section, interval (cm)	Depth (mbsf)	Wet-bulk density (g/cm <sup>3</sup> )	Dry-bulk density (g/cm <sup>3</sup> )	Grain density (g/cm <sup>3</sup> )	Wet porosity (%)	Dry porosity (%)	Wet water content (%)	Dry water content (%)	Void ratio 1	Void ratio 2
145-881C-										
1H-1, 74.0	0.74	1.39	0.58	2.84	79.07	79.63	58.11	138.73	3.78	3.84
1H-2, 74.0	2.24	1.39	0.60	2.65	77.04	77.61	56.87	131.86	3.36	3.41
1H-3, 49.0	3.49	1.37	0.60	2.50	75.82	76.40	56.61	130.44	3.14	3.18
2H-1, 74.0	4.54	1.43	0.66	2.65	74.67	75.22	53.61	115.55	2.95	2.99
2H-2, 74.0	6.04	1.35	0.55	2.54	78.15	78.74	59.48	146.77	3.58	3.64
2H-3, 79.0	7.59	1.40	0.61	2.71	77.19	77.75	56.51	129.94	3.38	3.44
2H-4, 74.0	9.04	1.49	0.74	2.80	73.18	73.70	50.27	101.07	2.73	2.76
2H-5, 74.0	10.54	1.43	0.67	2.68	74.61	75.16	53.27	114.00	2.94	2.98
2H-6, 74.0	12.04	1.35	0.54	2.64	79.16	79.74	60.03	150.20	3.80	3.86
2H-7, 24.0	12.54	1.39	0.62	2.58	75.66	76.23	55.59	125.16	3.11	3.15
3H-1, 74.0	14.04	1.43	0.65	2.74	76.00	76.55	54.55	120.04	3.17	3.21
3H-2, 74.0	15.54	1.35	0.53	2.70	79.88	80.46	60.55	153.49	3.97	4.04
3H-3, 74.0	17.04	1.35	0.57	2.40	76.09	76.69	57.95	137.81	3.18	3.23
3H-4, 74.0	18.54	1.38	0.59	2.59	77.02	77.60	57.38	134.62	3.35	3.40
3H-5, 74.0	20.04	1.37	0.57	2.58	77.33	77.91	57.95	137.79	3.41	3.46
3H-6, 74.0	21.46	1.36	0.55	2.71	79.34	79.91	59.66	147.91	3.84	3.91
3H-CC, 2.0	23.54	1.37	0.58	2.60	77.42	78.00	57.86	137.29	3.43	3.48
4H-1, 74.0	25.04	1.48	0.72	2.83	74.18	74.70	51.27	105.20	2.87	2.91
4H-2, 74.0	26.54	1.48	0.74	2.65	71.70	72.23	49.80	99.20	2.53	2.56
4H-3, 74.0	28.04	1.43	0.67	2.64	74.18	74.73	53.04	112.94	2.87	2.91
4H-4, 74.0	29.54	1.46	0.71	2.75	73.94	74.47	51.71	107.09	2.84	2.87
4H-5, 74.0	31.04	1.41	0.64	2.61	75.25	75.81	54.75	121.02	3.04	3.08
4H-6, 74.0	32.30	1.41	0.65	2.54	74.13	74.70	53.95	117.14	2.87	2.90
4H-7, 50.0	33.04	1.37	0.58	2.57	76.87	77.45	57.39	134.66	3.32	3.37
5H-1, 74.0	34.54	1.44	0.66	2.83	76.38	76.92	54.28	118.72	3.23	3.28
5H-2, 74.0	36.04	1.53	0.83	2.62	68.03	68.53	45.62	83.89	2.13	2.15
5H-3, 74.0	37.54	1.32	0.51	2.44	78.89	79.50	61.43	159.30	3.74	3.80
5H-4, 74.0	39.04	1.43	0.68	2.59	73.49	74.05	52.60	110.97	2.77	2.81
5H-5, 74.0	40.29	1.44	0.69	2.64	73.58	74.13	52.27	109.51	2.79	2.82
5H-6, 49.0	40.72	1.51	0.80	2.60	68.82	69.33	46.77	87.87	2.21	2.23
5H-7, 19.0	42.54	1.32	0.50	2.53	79.83	80.43	62.02	163.30	3.96	4.03
6H-1, 74.0	44.09	1.50	0.77	2.71	71.15	71.67	48.53	94.28	2.47	2.49
6H-2, 79.0	45.64	1.17	0.35	1.78	79.96	80.82	70.06	234.05	3.99	4.06
6H-3, 84.0	47.04	1.42	0.66	2.56	73.91	74.47	53.43	114.71	2.83	2.87
6H-4, 74.0	48.54	1.47	0.75	2.58	70.55	71.08	49.06	96.30	2.40	2.42
6H-5, 74.0	50.04	1.48	0.76	2.58	70.23	70.76	48.64	94.69	2.36	2.38
6H-6, 74.0	51.29	1.42	0.66	2.62	74.61	75.17	53.85	116.68	2.94	2.98
6H-7, 49.0	52.09	1.40	0.63	2.59	75.25	75.81	54.91	121.78	3.04	3.08
7H-1, 79.0	53.54	1.45	0.70	2.59	72.55	73.09	51.41	105.79	2.64	2.67
7H-2, 74.0	55.09	1.43	0.66	2.69	75.15	75.70	53.88	116.82	3.02	3.07
7H-3, 79.0	56.54	1.28	0.44	2.48	81.80	82.43	65.49	189.76	4.49	4.59
7H-4, 74.0	58.04	1.50	0.79	2.55	68.65	69.17	47.02	88.74	2.19	2.21
7H-5, 74.0	59.54	1.49	0.74	2.78	73.16	73.69	50.45	101.82	2.73	2.76
7H-6, 74.0	60.40	1.48	0.75	2.68	71.66	72.19	49.48	97.92	2.53	2.56
7H-7, 19.0	61.54	1.41	0.64	2.63	75.38	75.93	54.71	120.81	3.06	3.10
8H-1, 74.0	63.04	1.46	0.71	2.65	72.97	73.51	51.36	105.60	2.70	2.73
8H-2, 74.0	64.59	1.46	0.74	2.54	70.50	71.03	49.37	97.52	2.39	2.42
8H-3, 79.0	66.04	1.42	0.65	2.60	74.66	75.22	54.01	117.45	2.95	2.99
8H-4, 74.0	67.54	1.50	0.76	2.79	72.31	72.83	49.25	97.05	2.61	2.64
8H-5, 74.0	69.04	1.52	0.80	2.73	70.34	70.85	47.36	89.96	2.37	2.40
8H-6, 74.0	70.34	1.54	0.84	2.68	68.23	68.73	45.32	82.88	2.15	2.17
8H-7, 54.0	71.04	1.36	0.56	2.60	77.98	78.56	58.62	141.66	3.54	3.60
9H-1, 74.0	72.54	1.31	0.48	2.61	81.32	81.93	63.59	174.62	4.35	4.44
9H-2, 74.0	74.09	1.42	0.67	2.54	73.26	73.81	52.79	111.80	2.74	2.77
9H-3, 79.0	75.54	1.59	0.87	3.00	70.75	71.23	45.49	83.44	2.42	2.45
9H-4, 74.0	77.09	1.60	0.93	2.72	65.62	66.10	42.02	72.47	1.91	1.93
9H-5, 79.0	78.09	1.50	0.77	2.69	70.90	71.42	48.42	93.87	2.44	2.46
9H-6, 29.0	80.54	1.43	0.69	2.55	72.63	73.18	51.94	108.05	2.65	2.69
10H-1, 74.0	82.04	1.52	0.83	2.52	66.75	67.26	45.13	82.26	2.01	2.03
10H-2, 74.0	83.59	1.46	0.74	2.57	71.04	71.57	49.70	98.79	2.45	2.48
10H-3, 79.0	85.04	1.39	0.62	2.58	75.80	76.37	55.76	126.02	3.13	3.18
10H-4, 74.0	86.54	1.56	0.88	2.63	66.29	66.78	43.61	77.33	1.97	1.98
10H-5, 74.0	88.04	1.47	0.72	2.73	73.12	73.65	50.83	103.36	2.72	2.75
10H-6, 74.0	90.04	1.54	0.82	2.76	69.82	70.33	46.46	86.77	2.31	2.34
11H-1, 74.0	91.54	1.37	0.58	2.54	76.87	77.45	57.61	135.88	3.32	3.37
11H-2, 74.0	92.99	1.57	0.87	2.77	68.17	68.66	44.49	80.14	2.14	2.16
11H-3, 69.0	94.59	1.41	0.66	2.54	73.74	74.31	53.48	114.97	2.81	2.84
11H-4, 79.0	96.04	1.47	0.73	2.70	72.84	73.37	50.72	102.91	2.68	2.71
11H-5, 74.0	97.54	1.46	0.73	2.56	71.22	71.76	50.06	100.23	2.47	2.50
11H-6, 74.0	99.49	1.44	0.68	2.61	73.50	74.05	52.42	110.19	2.77	2.81
12H-1, 69.0	101.04	1.41	0.65	2.51	73.63	74.20	53.56	115.31	2.79	2.83
12H-2, 74.0	102.64	1.35	0.55	2.58	78.19	78.78	59.18	144.97	3.59	3.64
12H-3, 84.0	104.04	1.40	0.67	2.35	71.02	71.59	51.88	107.80	2.45	2.48
12H-4, 74.0	105.59	1.54	0.88	2.52	64.97	65.46	43.20	76.05	1.85	1.87
12H-5, 79.0	107.04	1.41	0.66	2.52	73.56	74.12	53.38	114.49	2.78	2.82
12H-6, 74.0	108.19	1.47	0.77	2.49	68.65	69.18	47.69	91.18	2.19	2.21
12H-7, 39.0	108.99	1.47	0.73	2.68	72.30	72.83	50.26	101.03	2.61	2.64
13H-1, 69.0	110.54	1.48	0.76	2.54	69.61	70.14	48.31	93.46	2.29	2.32
13H-2, 74.0	112.09	1.41	0.64	2.59	74.91	75.47	54.46	119.60	2.99	3.03
13H-3, 79.0	113.54	1.41	0.63	2.65	75.85	76.42	55.22	123.31	3.14	3.19
13H-4, 74.0	115.04	1.40	0.61	2.70	76.86	77.42	56.18	128.21	3.32	3.37
13H-5, 74.0	116.54	1.47	0.75	2.53	70.14	70.68	48.97	95.98	2.35	2.37
13H-6, 74.0	118.54	1.49	0.77	2.63	70.17	70.69	48.13	92.77	2.35	2.38

Table 17 continued.

Core, section, interval (cm)	Depth (mbsf)	Wet-bulk density (g/cm <sup>3</sup> )	Dry-bulk density (g/cm <sup>3</sup> )	Grain density (g/cm <sup>3</sup> )	Wet porosity (%)	Dry porosity (%)	Wet water content (%)	Dry water content (%)	Void ratio 1	Void ratio 2
14H-1, 74.0	120.04	1.45	0.70	2.66	73.41	73.95	51.89	107.85	2.76	2.80
14H-2, 74.0	121.59	1.46	0.72	2.61	71.86	72.40	50.39	101.58	2.55	2.58
14H-3, 79.0	123.04	1.46	0.75	2.49	69.56	70.09	48.75	95.13	2.28	2.31
14H-4, 74.0	124.54	1.46	0.71	2.63	72.57	73.10	51.04	104.24	2.65	2.68
14H-5, 74.0	126.04	1.38	0.60	2.56	76.13	76.71	56.41	129.43	3.19	3.24
14H-6, 74.0	127.19	1.35	0.56	2.46	76.72	77.31	58.20	139.25	3.30	3.35
14H-7, 39.0	127.99	1.46	0.71	2.67	73.23	73.77	51.52	106.25	2.74	2.77
15H-1, 69.0	129.54	1.46	0.74	2.51	70.38	70.92	49.49	97.98	2.38	2.40
15H-2, 74.0	131.09	1.32	0.50	2.48	79.33	79.95	61.72	161.21	3.84	3.91
15H-3, 79.0	132.54	1.48	0.79	2.45	67.32	67.85	46.48	86.86	2.06	2.08
15H-4, 74.0	134.04	1.44	0.73	2.42	69.65	70.19	49.51	98.04	2.29	2.32
15H-5, 74.0	135.54	1.43	0.68	2.55	72.91	73.47	52.29	109.61	2.69	2.73
15H-6, 74.0	137.54	1.43	0.68	2.59	73.27	73.81	52.34	109.80	2.74	2.77
16H-1, 74.0	139.04	1.42	0.66	2.60	74.31	74.86	53.58	115.45	2.89	2.93
16H-2, 74.0	140.64	1.47	0.76	2.55	69.92	70.45	48.56	94.42	2.32	2.35
16H-3, 84.0	142.04	1.37	0.57	2.60	77.54	78.12	58.01	138.17	3.45	3.51
16H-4, 74.0	143.54	1.42	0.67	2.50	72.91	73.47	52.74	111.60	2.69	2.72
16H-5, 74.0	145.04	1.50	0.78	2.64	70.06	70.58	47.84	91.71	2.34	2.36
16H-6, 74.0	146.19	1.48	0.74	2.65	71.59	72.12	49.63	98.53	2.52	2.55
16H-7, 39.0	147.04	1.42	0.67	2.55	73.40	73.96	52.84	112.06	2.76	2.79
17H-1, 74.0	148.54	1.39	0.62	2.54	75.12	75.69	55.22	123.31	3.02	3.06
17H-2, 74.0	150.09	1.52	0.84	2.55	66.98	67.49	45.08	82.09	2.03	2.05
17H-3, 79.0	151.54	1.43	0.68	2.56	73.23	73.79	52.56	110.78	2.74	2.77
17H-4, 74.0	153.09	1.49	0.77	2.63	70.26	70.78	48.18	92.97	2.36	2.39
17H-5, 79.0	154.54	1.36	0.58	2.50	76.39	76.97	57.37	134.58	3.23	3.28
17H-6, 74.0	156.54	1.39	0.64	2.44	73.35	73.92	53.90	116.94	2.75	2.79
18X-1, 74.0	157.99	1.39	0.60	2.64	77.14	77.71	57.04	132.77	3.37	3.43
18X-2, 69.0	159.17	1.33	0.53	2.45	78.01	78.62	60.12	150.74	3.55	3.61
18X-3, 37.0	182.44	1.45	0.70	2.60	72.56	73.11	51.36	105.59	2.64	2.68
21H-1, 74.0	183.94	1.24	0.41	2.21	81.16	81.84	67.10	203.92	4.31	4.39
21H-2, 74.0	185.44	1.37	0.60	2.44	74.95	75.54	56.03	127.45	2.99	3.03
21H-3, 74.0	186.94	1.27	0.45	2.27	79.87	80.53	64.55	182.07	3.97	4.04
21H-4, 74.0	188.44	1.33	0.54	2.45	77.75	78.36	59.77	148.59	3.49	3.55
21H-5, 74.0	189.99	1.26	0.44	2.25	80.13	80.79	65.20	187.39	4.03	4.11
21H-6, 79.0	190.84	1.27	0.46	2.26	79.34	79.99	63.94	177.34	3.84	3.91
21H-7, 14.0	201.34	1.27	0.44	2.32	80.58	81.23	65.10	186.54	4.15	4.23
23X-1, 74.0	202.84	1.21	0.35	2.21	83.63	84.34	70.85	243.05	5.11	5.23
23X-2, 74.0	204.54	1.28	0.46	2.30	79.70	80.35	63.99	177.72	3.93	4.00
23X-3, 94.0	205.84	1.25	0.41	2.31	81.74	82.41	66.94	202.47	4.48	4.57
23X-4, 74.0	207.34	1.26	0.41	2.37	82.15	82.81	67.00	203.02	4.60	4.70
23X-5, 74.0	208.84	1.24	0.42	2.21	80.81	81.49	66.55	198.96	4.21	4.29
23X-6, 74.0	209.29	1.25	0.43	2.19	80.26	80.94	65.91	193.34	4.06	4.14
23X-7, 19.0	219.74	1.23	0.39	2.29	82.78	83.45	68.74	219.86	4.81	4.91
25X-1, 74.0	221.24	1.23	0.37	2.40	84.09	84.75	69.82	231.39	5.28	5.41
25X-2, 74.0	222.74	1.22	0.37	2.17	82.37	83.08	69.28	225.48	4.67	4.77
25X-3, 74.0	223.74	1.22	0.36	2.29	84.08	84.77	70.76	242.05	5.28	5.41
25X-4, 24.0	239.19	1.24	0.40	2.33	82.60	83.27	68.05	212.98	4.75	4.85
27X-1, 89.0	240.69	1.21	0.36	2.12	82.77	83.50	70.33	236.99	4.81	4.91
27X-2, 89.0	242.19	1.22	0.39	2.06	80.82	81.55	68.13	213.81	4.21	4.30
27X-3, 89.0	243.69	1.35	0.57	2.35	75.26	75.87	57.32	134.32	3.04	3.09
27X-4, 89.0	245.19	1.23	0.40	2.14	80.87	81.57	67.35	206.27	4.23	4.31
27X-5, 89.0	246.39	1.24	0.42	2.08	79.23	79.94	65.69	191.49	3.81	3.88
27X-6, 59.0	258.49	1.27	0.46	2.18	78.43	79.10	63.47	173.75	3.64	3.70
29X-1, 89.0	259.99	1.28	0.48	2.21	78.10	78.76	62.73	168.31	3.57	3.62
29X-2, 89.0	261.39	1.28	0.46	2.37	80.11	80.75	63.90	177.01	4.03	4.10
29X-3, 89.0	268.09	1.29	0.48	2.40	79.77	80.40	63.14	171.33	3.94	4.02
30X-1, 89.0	269.59	1.24	0.40	2.20	81.35	82.04	67.46	207.28	4.36	4.45
30X-2, 89.0	271.09	1.27	0.45	2.22	79.20	79.86	64.13	178.78	3.81	3.87
30X-3, 89.0	272.59	1.25	0.43	2.15	79.46	80.15	65.21	187.41	3.87	3.94
30X-4, 89.0	274.09	1.25	0.44	2.14	79.31	80.00	65.13	186.77	3.83	3.90
30X-5, 89.0	275.59	1.24	0.41	2.15	80.39	81.08	66.55	198.93	4.10	4.18
30X-6, 89.0	276.39	1.27	0.46	2.22	78.98	79.64	63.83	176.44	3.76	3.82
30X-7, 19.0	287.39	1.25	0.45	2.13	78.75	79.44	64.42	181.03	3.71	3.77
32X-1, 89.0	288.94	1.25	0.44	2.17	79.34	80.02	64.84	184.38	3.84	3.91
32X-2, 94.0	289.99	1.27	0.46	2.25	79.24	79.90	63.92	177.17	3.82	3.88
32X-3, 49.0	316.29	1.25	0.42	2.20	80.49	81.17	66.21	195.98	4.12	4.20
35X-1, 89.0	317.79	1.27	0.47	2.15	77.64	78.31	62.71	168.18	3.47	3.53
35X-2, 89.0	319.34	1.29	0.50	2.17	76.60	77.25	61.03	156.60	3.27	3.32
35X-3, 94.0	320.79	1.29	0.48	2.26	78.31	78.95	62.42	166.11	3.61	3.67
35X-4, 89.0	322.29	1.29	0.48	2.33	78.90	79.54	62.61	167.43	3.74	3.80
35X-5, 89.0	325.99	1.32	0.50	2.49	79.36	79.98	61.71	161.14	3.85	3.91
36X-1, 89.0	327.49	1.29	0.49	2.24	77.79	78.44	61.91	162.52	3.50	3.56
36X-2, 89.0	328.99	1.28	0.47	2.28	79.02	79.67	63.29	172.38	3.77	3.83
36X-3, 89.0	330.49	1.27	0.46	2.27	79.50	80.16	64.03	178.05	3.88	3.95
36X-4, 89.0	331.99	1.29	0.49	2.29	78.39	79.03	62.25	164.91	3.63	3.69
36X-5, 89.0	333.49	1.29	0.51	2.19	76.29	76.94	60.44	152.76	3.22	3.27
36X-6, 89.0	334.29	1.31	0.52	2.28	76.60	77.23	59.92	149.51	3.27	3.32
36X-7, 19.0		1.32	0.53	2.35	77.03	77.65	59.80	148.75	3.35	3.41

**Table 18. Vane shear strength data from Hole 881C.**

Core, section, interval (cm)	Depth (mbsf)	Shear strength (kPa)
145-881C-		
1H-2, 75.0	2.25	7.1
2H-3, 80.0	7.60	15.8
3H-3, 75.0	17.05	9.4
4H-3, 100.0	26.80	18.6
5H-3, 75.0	36.05	12.7
6H-3, 75.0	45.55	27.8
7H-3, 75.0	55.05	43.1
8H-3, 75.0	64.55	48.2
9H-3, 75.0	74.05	73.5
10H-3, 75.0	83.55	63.7
11H-3, 80.0	93.10	65.2
12H-3, 75.0	102.55	45.7
13H-3, 75.0	112.05	66.7
14H-3, 75.0	121.55	81.8
15H-3, 75.0	131.05	25.5
16H-3, 75.0	140.55	87.8
17H-3, 75.0	150.05	138.0
18X-2, 75.0	158.05	39.7
21H-3, 75.0	185.45	81.8
23X-3, 75.0	204.35	27.7
25X-2, 75.0	221.25	21.0
27X-3, 90.0	242.20	36.7
29X-2, 90.0	260.00	36.0
30X-3, 90.0	271.10	36.7
32X-2, 90.0	288.90	5.2
35X-3, 95.0	319.35	78.0
36X-3, 90.0	329.00	38.2
36X-6, 20.0	332.80	80.3
36X-6, 90.0	333.50	71.2

**Table 19. Index properties data from Hole 881D.**

Core, section, interval (cm)	Depth (mbsf)	Wet-bulk density (g/cm <sup>3</sup> )	Dry-bulk density (g/cm <sup>3</sup> )	Grain density (g/cm <sup>3</sup> )	Wet porosity (%)	Dry porosity (%)	Wet water content (%)	Dry water content (%)	Void ratio 1	Void ratio 2
145-881D-										
1H-1, 59.0	155.59	1.37	0.58	2.57	77.1	77.7	57.7	136.3	3.37	3.42
1H-3, 59.0	158.59	1.45	0.72	2.52	71.1	71.7	50.3	101.3	2.46	2.49
1H-5, 54.0	161.54	1.32	0.54	2.30	76.2	76.9	59.2	145.3	3.21	3.26
2H-1, 59.0	165.09	1.35	0.55	2.64	79.0	79.6	59.7	148.2	3.75	3.82
2H-3, 59.0	168.09	1.28	0.47	2.26	78.7	79.3	63.0	170.4	3.69	3.76
3H-1, 59.0	174.59	1.28	0.47	2.29	79.0	79.6	63.1	170.8	3.76	3.82
3H-3, 59.0	177.59	1.25	0.44	2.21	79.9	80.5	65.2	187.3	3.96	4.04
3H-5, 59.0	180.59	1.30	0.51	2.22	76.5	77.2	60.4	152.8	3.26	3.31
3H-7, 39.0	183.39	1.26	0.45	2.18	79.1	79.8	64.5	181.4	3.80	3.86
4H-1, 59.0	184.09	1.25	0.42	2.28	81.4	82.1	66.7	200.2	4.38	4.46
4H-3, 59.0	187.09	1.24	0.43	2.06	79.0	79.7	65.5	190.2	3.77	3.83
4H-5, 59.0	190.09	1.24	0.43	2.14	79.7	80.4	65.7	191.3	3.92	3.99
5H-1, 59.0	193.59	1.30	0.50	2.37	78.7	79.3	61.9	162.2	3.69	3.75
5H-3, 59.0	196.59	1.33	0.58	2.19	73.2	73.9	56.5	129.8	2.74	2.77
5H-5, 59.0	199.59	1.23	0.40	2.09	80.4	81.1	67.2	204.7	4.11	4.19
6H-1, 59.0	203.09	1.34	0.48	3.06	83.9	84.5	64.1	178.7	5.21	5.33
6H-3, 59.0	206.09	1.23	0.39	2.18	81.6	82.3	68.0	212.6	4.43	4.52
6H-5, 69.0	209.19	1.24	0.43	2.09	79.1	79.8	65.3	188.3	3.78	3.85

**Table 20. Wave shear strength data from Hole 881D.**

Core, section, interval (cm)	Depth (mbsf)	Shear strength (kPa)
145-881D-		
1H-2, 96.0	157.46	39.7
2H-2, 96.0	166.96	42.0
2H-5, 96.0	171.46	14.2
3H-4, 96.0	179.46	35.2
4H-4, 96.0	188.96	77.2
5H-4, 96.0	198.46	66.0
6H-4, 96.0	207.96	75.7

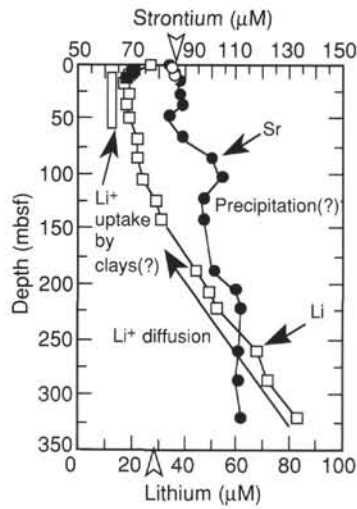


Figure 20. Plot of concentrations of lithium and strontium vs. depth in interstitial waters at Site 881. Open circles and filled squares indicate samples from Hole 881A; filled circles and open squares indicate samples from Hole 881C. Open arrowhead indicates the concentration in modern seawater.

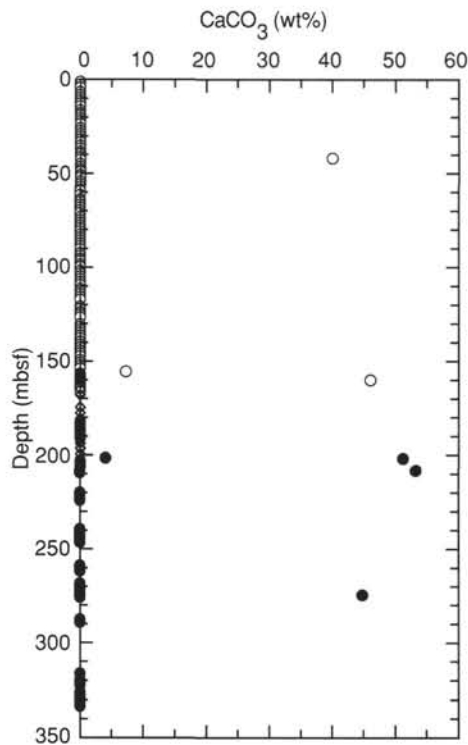


Figure 21. Plot of carbonate contents vs. depth at Site 881. Open circle = Hole 881B, solid circle = Hole 881C, and diamond = Hole 881D.

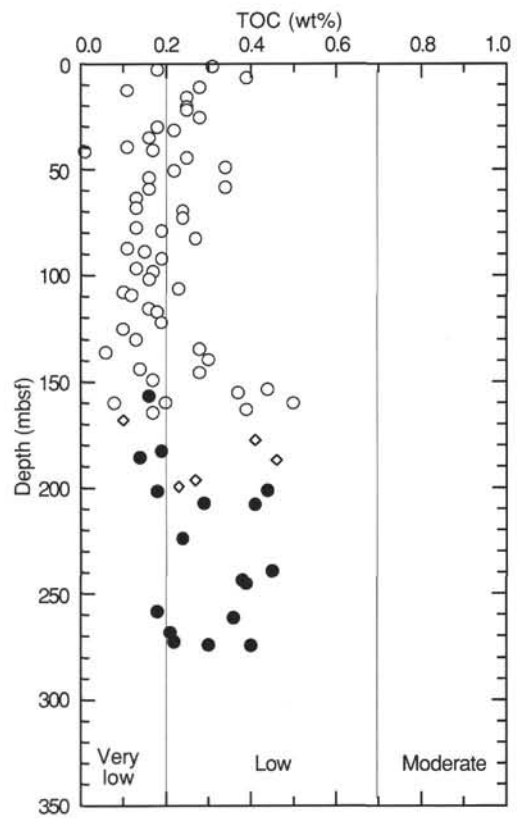


Figure 22. Plot of total organic carbon contents vs. depth, Site 881. Open circle = Hole 881B, solid circle = Hole 881C, and diamond = Hole 881D.

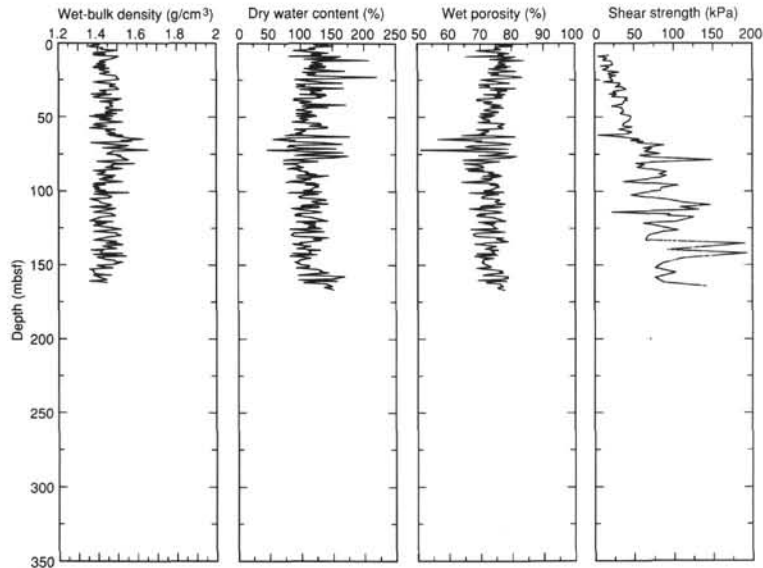


Figure 23. Index property data vs. depth for Hole 881B.

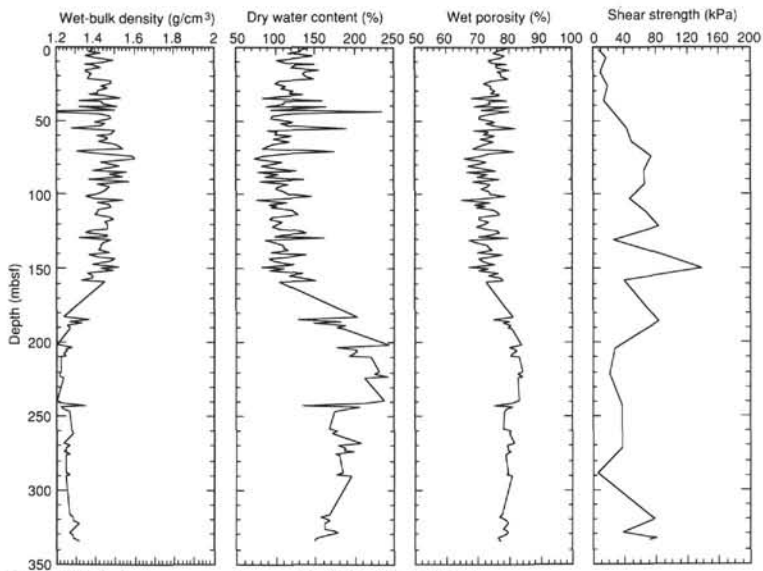


Figure 24. Index property data vs. depth for Hole 881C.

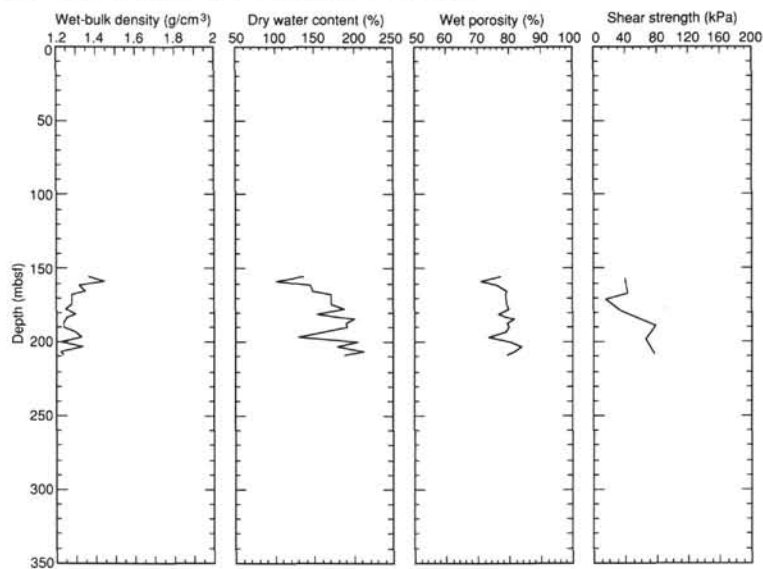


Figure 25. Index property data vs. depth for Hole 881D.

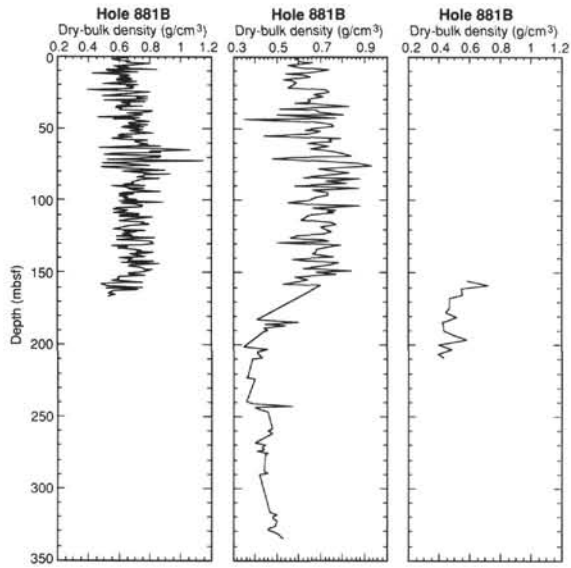


Figure 26. Dry-bulk density data vs. depth for Holes 881B, 881C, and 881D.

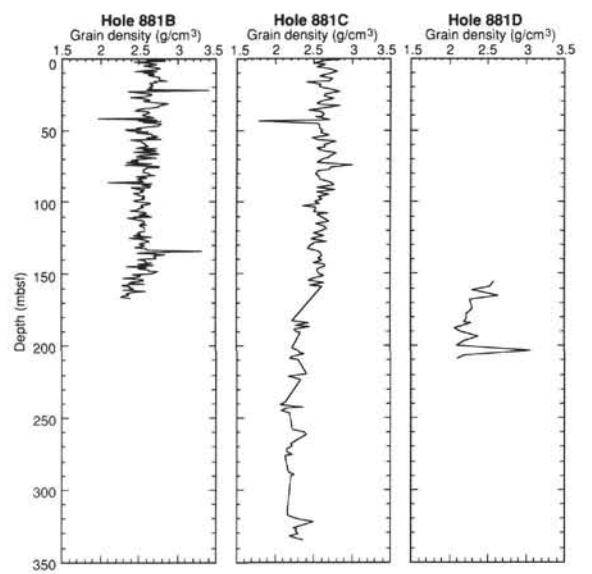


Figure 27. Grain density data vs. depth for Holes 881B, 881C, and 881D.

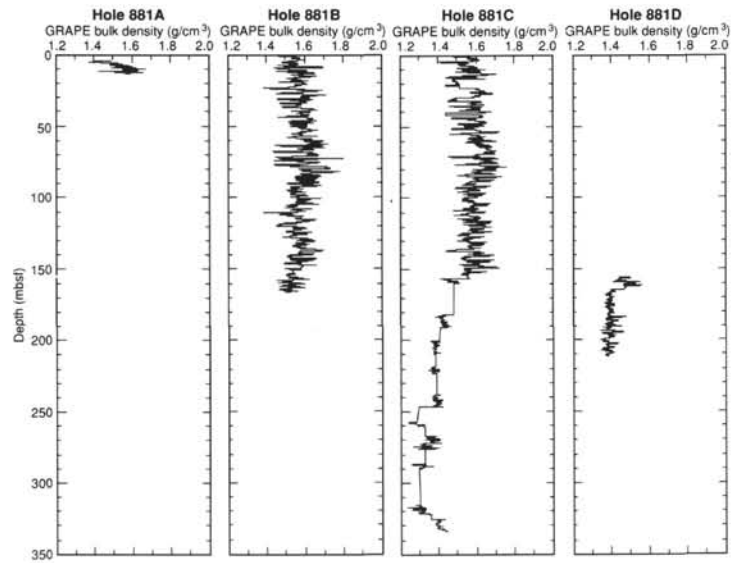


Figure 28. GRAPE bulk density data vs. depth for Holes 881A, 881B, 881C, and 881D.

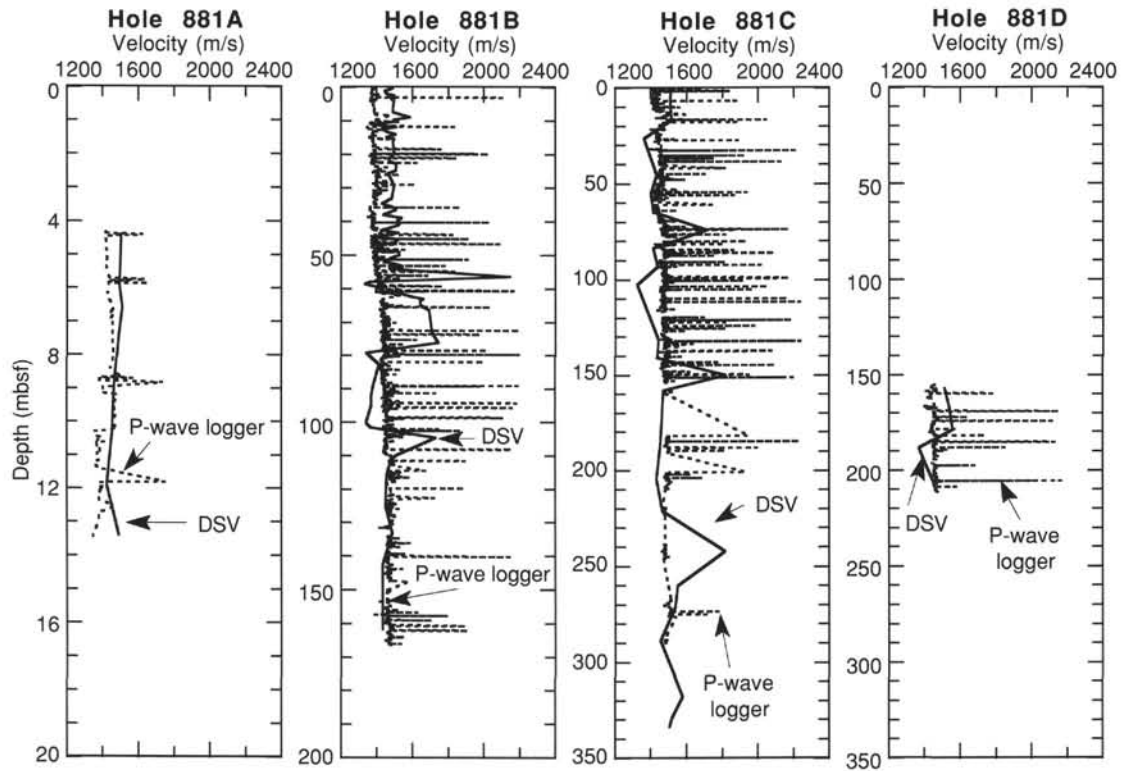


Figure 29. P-wave velocity data vs. depth for Holes 881A, 881B, 881C, and 881D.

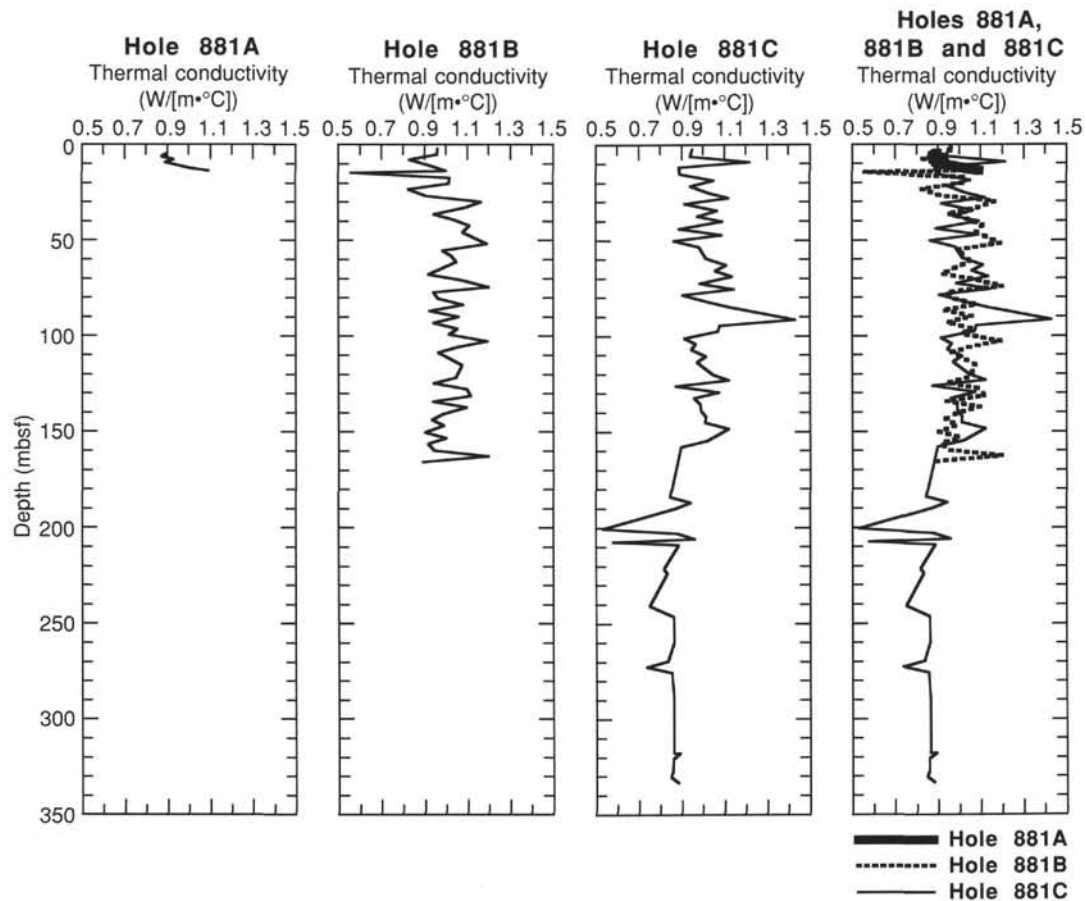


Figure 30. Thermal conductivity data vs. depth for Holes 881A, 881B, 881C, and 881D.

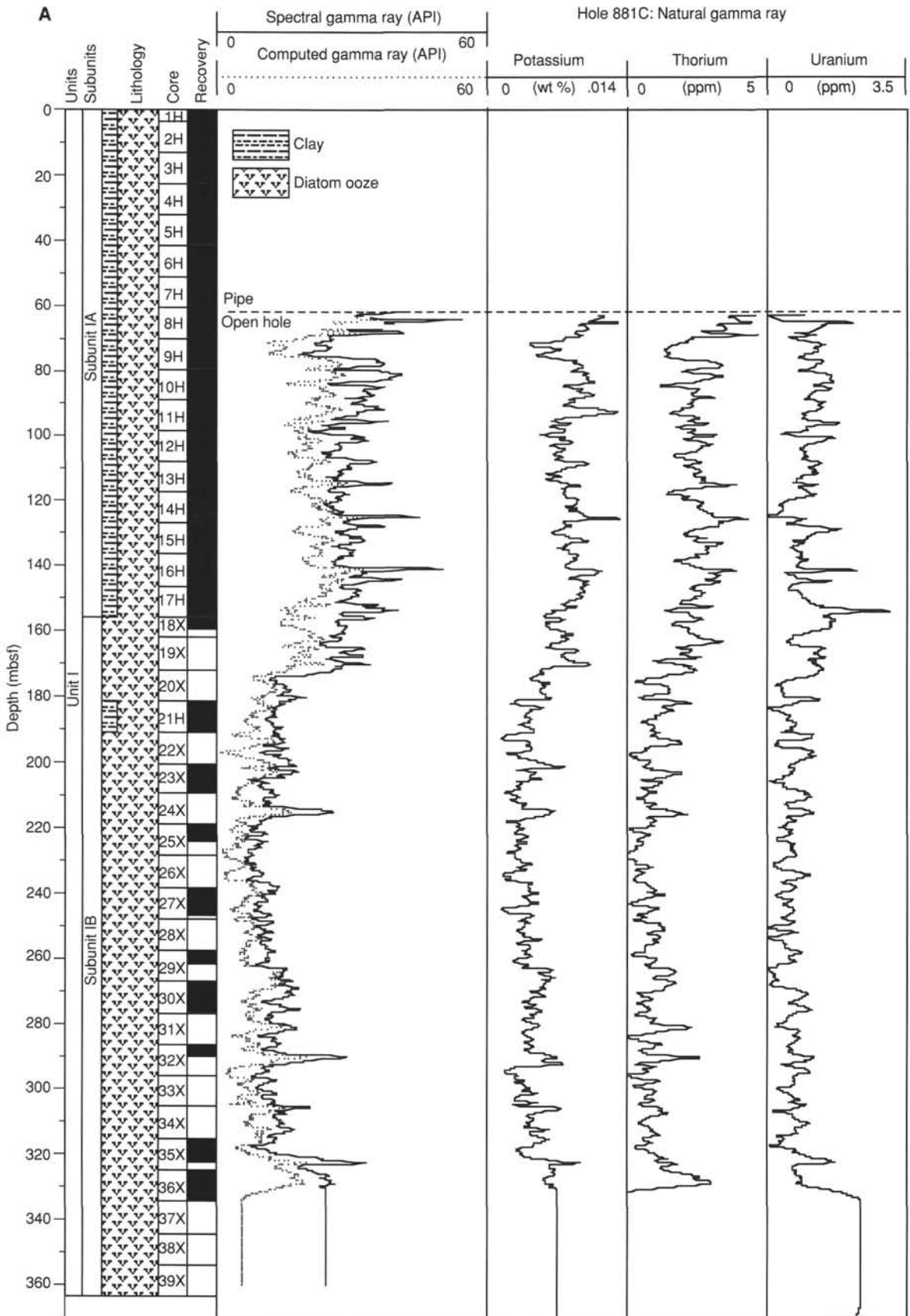


Figure 31. **A.** Data from the natural gamma-ray spectrometry tool (NGT), recorded on the Quad combination tool string. **B.** Data from the dual induction (DIT), sonic velocity (SDT), and lithodensity (HLDT) tools, recorded on the Quad combination tool string.

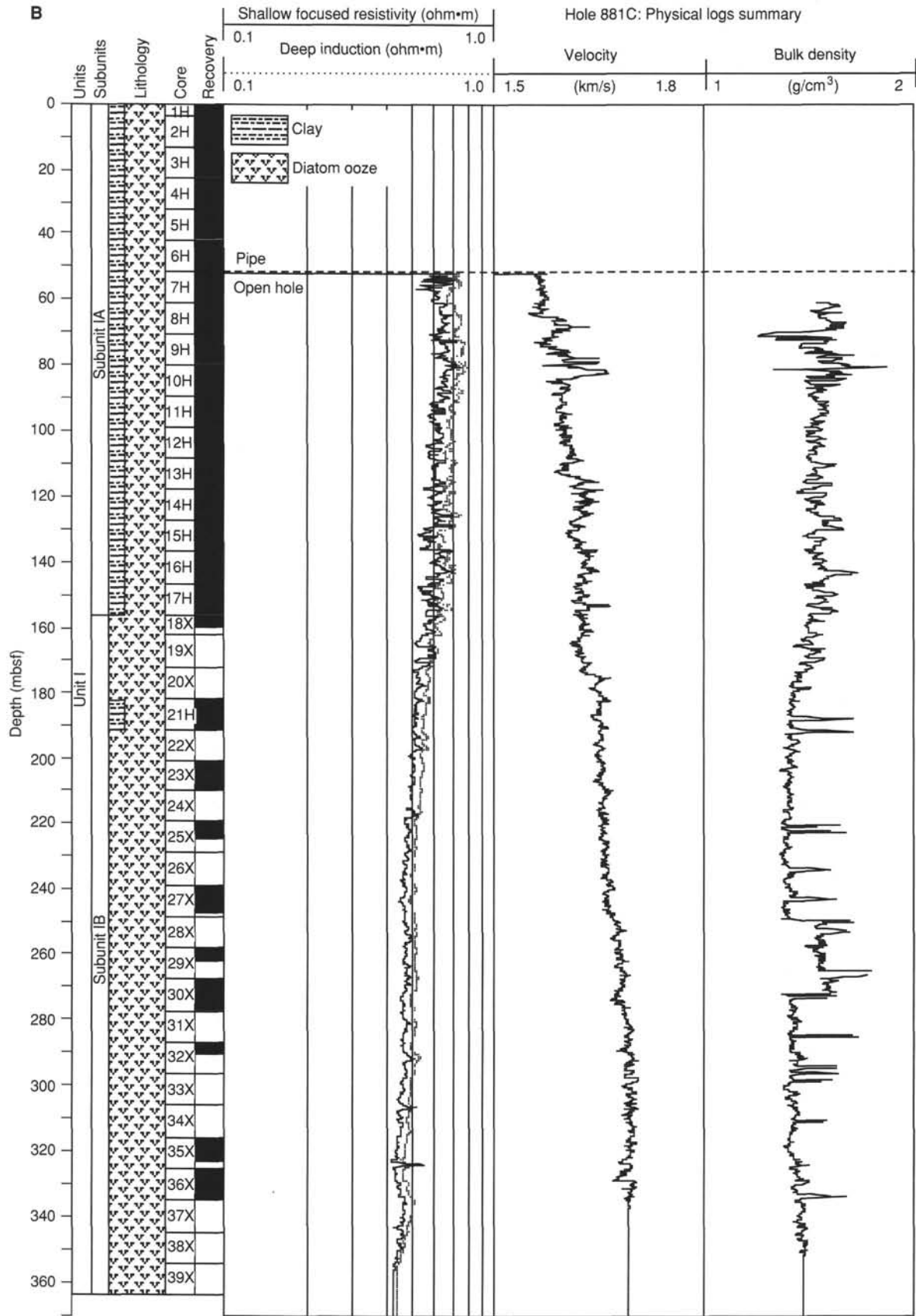


Figure 31 (continued).

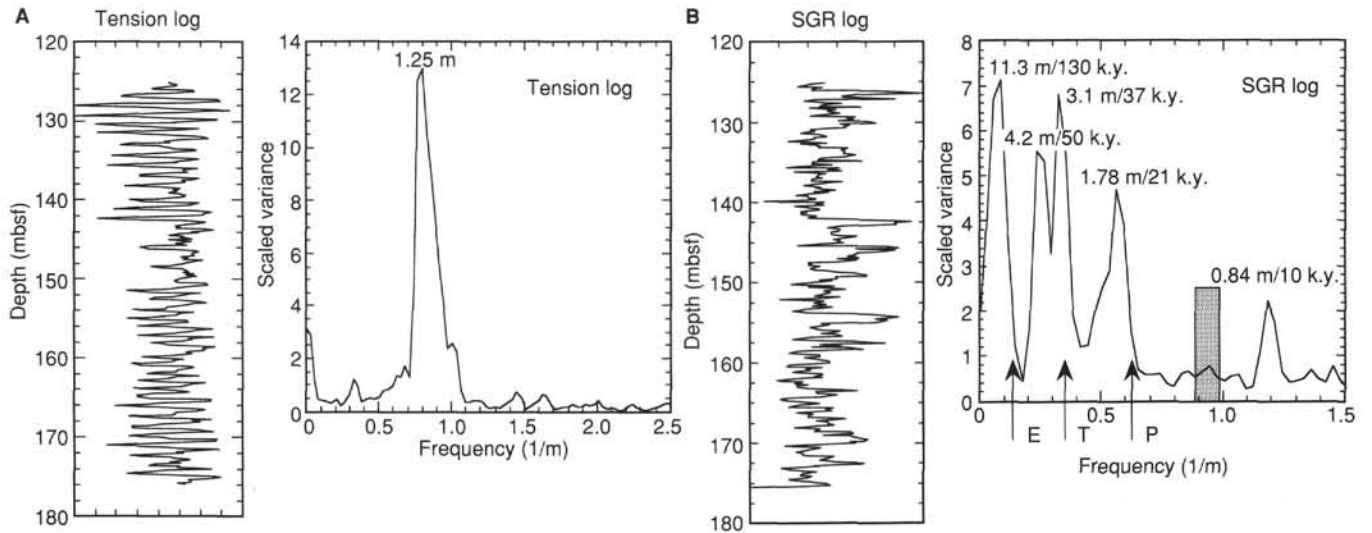


Figure 32. **A.** Plot of the tension log from Hole 881C (175–125 mbsf) and its corresponding power spectra. **B.** Plot of the SGR gamma-ray log from the same interval of Hole 881C and its corresponding power spectra. The absence of shared variance spectra between the two logs demonstrates that ship's heave did not significantly affect the log data. The SGR log does have dominant periodicities near 11.3, 4.2–3.1, 1.8, and 0.8 m, corresponding to temporal periodicities near 130, 50–37, 21, and 10 k.y., based on an average sedimentation rate of 8.4 cm/k.y.. The “E, T, P” symbols represent the approximate depth-domain frequencies corresponding with orbital eccentricity (100 k.y.), tilt (41 k.y.), and precession (23–19 k.y.).

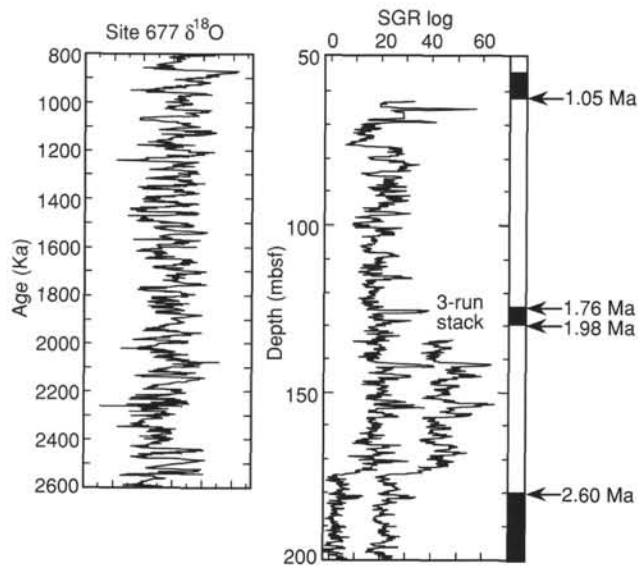


Figure 33. Plot of the Hole 881C SGR log compared to the Site 677 (eastern equatorial Pacific ocean) benthic oxygen isotopic record of global variability in ice volume (from Shackleton et al., 1990). The Hole 881C paleomagnetic reversal boundaries are shown on the right.

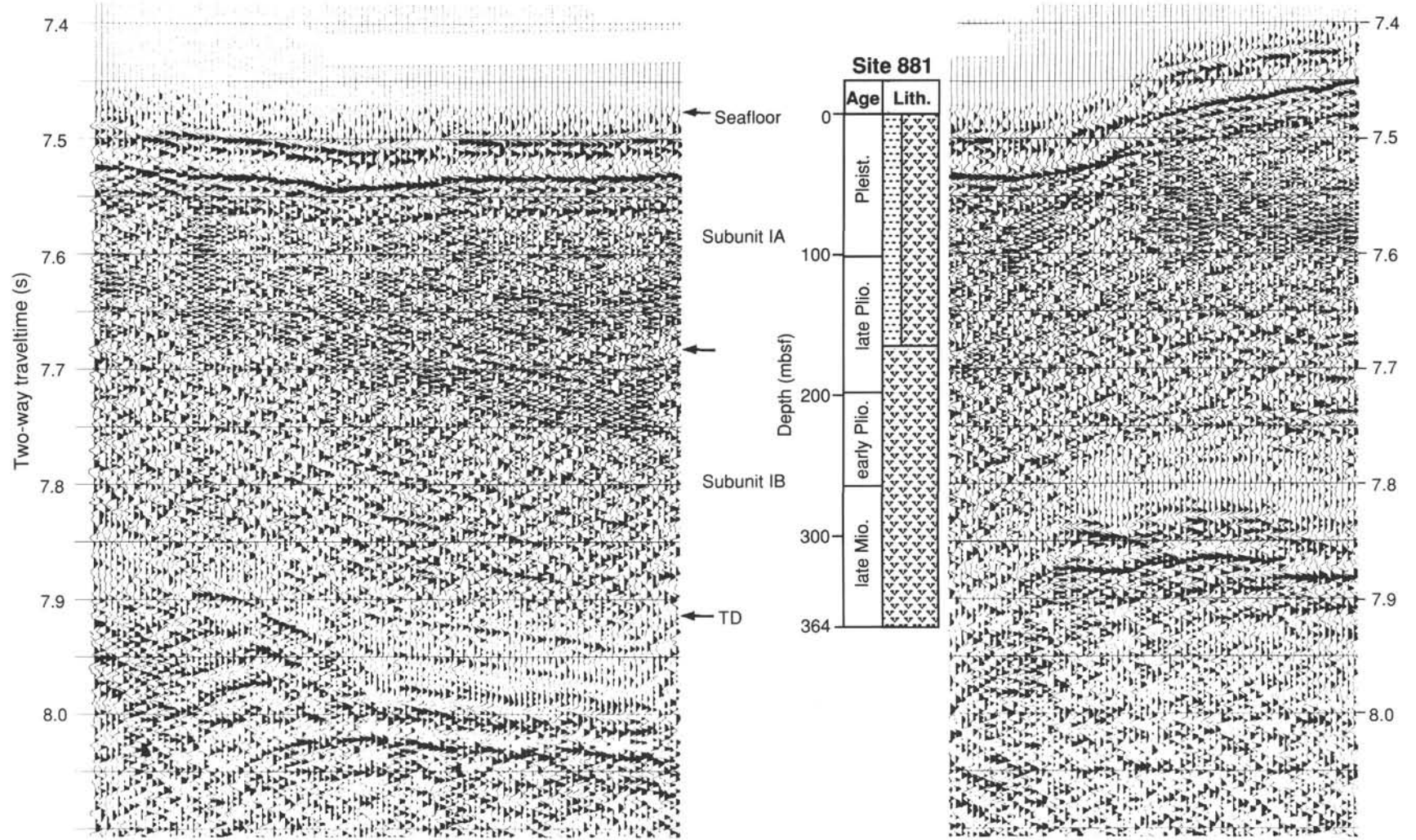
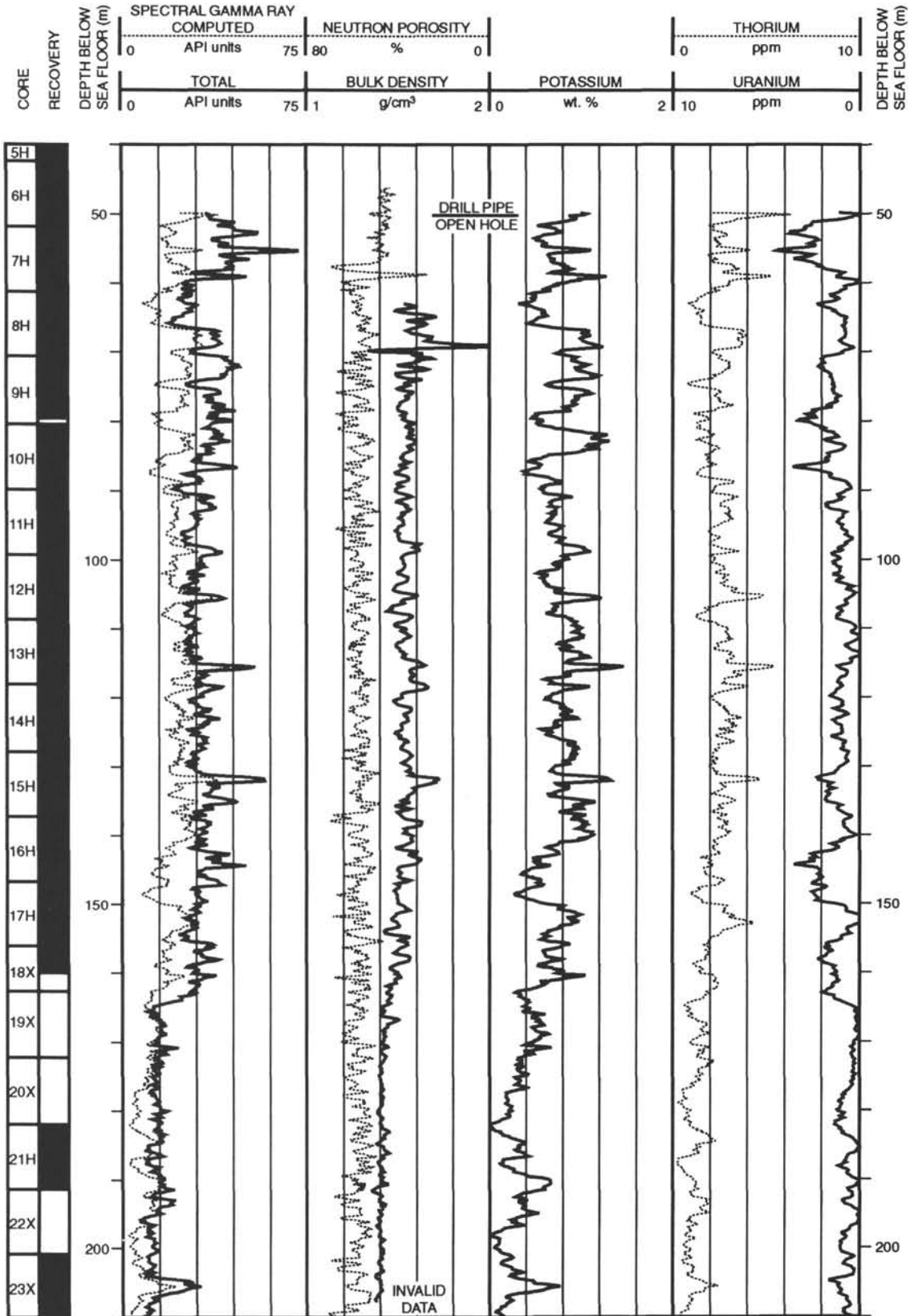
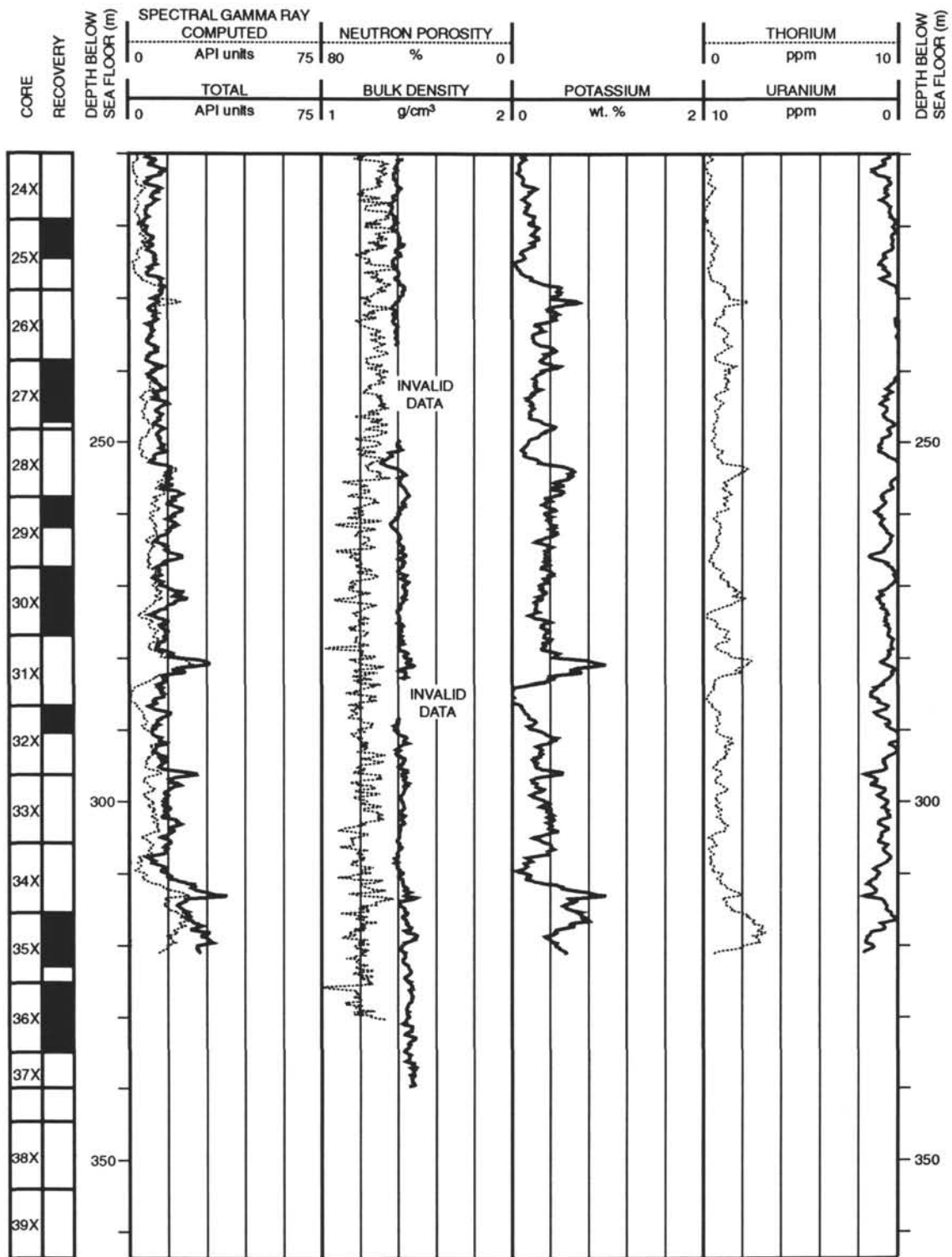


Figure 34. Processed seismic reflection profile crossing Site 881. Line trends north-northwesterly, north is to the right. The depth ranges of lithologic Subunits IA and IB are indicated on the profile inset.

Hole 881C: Density-Porosity-Natural Gamma Ray Log Summary



Hole 881C: Density-Positivity-Natural Gamma Ray Log Summary (continued)



Hole 881C: Resistivity-Velocity-Natural Gamma Ray Log Summary

